

대한비뇨생식기영상의학회 창립 30주년기념

제20회 정기학술대회

The 20th Annual Meeting
of the Korean Society of Urogenital Radiology



일시: 2023년 4월 22일 (토) - 4월 23 (일)

장소: 제주그랜드 하얏트 호텔

주최: 대한비뇨생식기영상의학회

후원: 대 한 영 상 의 학 회

대한비뇨생식기영상의학회 창립 30주년기념 제20회 정기학술대회

일시: 2022년 4월 22일 (토) – 4월 23일 (일)

장소: 제주그랜드 하얏트 호텔

2023년 4월 22일 토요일

09:00–09:50 등록

09:50–10:00 개회 개회사 오영택 (비영회장)
환영사 이정민 (대영회장)

10:00–11:00 Uroradiology 좌장: 오영택 (세브란스병원), 정성일 (건국대병원)

10:00–10:20 Management of tumors of kidney and urinary tract based on
radiological findings Jinzaki (Japan) 3
10:20–10:40 Recent advances in renal imaging 김찬교 (삼성서울병원) 4
10:40–11:00 Urolithiasis: basic and update 심영섭 (길병원) 23
11:00–11:20 Coffee break and 사진촬영

11:20–12:20 Gynecologic and Obstetric Imaging 좌장: 이은주 (아주대병원), 강병철 (세브란스병원)

11:20–11:40 Next Generation MRI in Gynecology Oncology Gigin Lin (Taiwan) 41
11:40–12:00 MRI approach for Adnexal Lesions 박계진 (서울아산병원) 42
12:00–12:20 Pregnancy-related Genitourinary Emergency 박성빈 (중앙대병원) 44
12:20–13:30 Lunch

13:30–14:00 Plenary lecture 좌장: 조정연 (서울대병원)

13:30–14:00 KSUR 30 Years, The International Path 김승협 (K영상클리닉) 53
14:00–14:20 Coffee break and 사진촬영

14:20–15:50 Scientific Session (I) 좌장: 이영준 (은평성모병원), 정대철 (세브란스병원)

15:50–16:00 Coffee break 71

16:00–17:00 Scientific Session (II) 좌장: 김시형 (경북대병원), 조범상 (충북대병원)

18:00–21:00 대한비뇨생식기영상의학회 30주년 기념행사 및 만찬 81

2023년 4월 23일 일요일

10:00 – 11:00	Prostate Imaging	좌장: 성득제 (고대안암병원), 윤성국 (동아대병원)
10:00–10:20	APIWG survey: what's now and next?	Li-jen Wang (Taiwan) 91
10:20–10:40	PI-RADS v 2.1: our institution experience	Chau Hung Lee (Singapore) 112
10:40–11:00	RADSs in urological imaging beyond PI-RADS: PI-RR, MET-RADS-p, and NODE-RADS	Satoru Takahashi (Japan) 113
11:00 – 12:00	Clinical Issues	좌장: 성창규 (보라매병원), 김경아 (고대구로병원)
11:00–11:20	Contrast Media guideline Update	이명석 (보라매병원) 119
11:20–11:40	Dose Optimization	김상윤 (서울대병원) 129
11:40–12:00	AI Applications in the prostate gland	황성일 (분당서울대병원) 131
12:00–12:10	폐회	

10:00 – 11:00 Uroradiology

좌장: 오영택 (세브란스병원)

정성일 (건국대병원)

Management of tumors of kidney and urinary tract based on radiological findings

Masahiro Jinzaki

Dept. of Radiology, Keio University

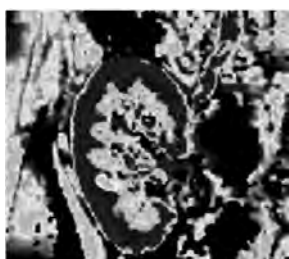
School of Medicine

First, I would like to give my warmest congratulations to KSUR for their 30th anniversary. These past 30 years have been an era of continuous progress in radiologic-pathologic correlation research. During that time, many novel diagnostic methods, such as MDCT, 3T MRI, and diffusion-weighted imaging have become available, and image quality has also improved drastically. Through these developments, we now know that many factors such as unenhanced CT values, T2WI signal intensity, contrast enhancement patterns, diffusion-weighted image signal intensity are all effective clues for differentiating benign from malignant pathology.

In this session, I would like to present a case study and ask everyone to think about the management of those cases. Through these case studies, I hope we can fully realize together just how much progress has been made in diagnosis over the past 30 years. I would also like to touch a little on the direction in which we are headed in the future.



Recent Advances in Renal Imaging



Chan Kyo Kim, MD

*Department of Radiology, Samsung Medical Center,
Sungkyunkwan University School of Medicine, Seoul, Korea*

Recent Advances in Renal Imaging

**Pathphysiological (functional & structural) changes
in renal ds at cellular/molecular levels**

- Renal perfusion
- Fibrosis
- Oxygenation
- Injury
- Metabolism
- Molecular expression

- Functional MRI
 - DCE, DWI, DTI, BOLD, ASL, MRE, MRS, MT, CEST
- US
 - Elastography, CEUS
- CT, PET



Recent Imaging Tools in Renal Ds

MRI techniques

Main applications

DCE	Perfusion, GFR, blood volume, vessel size, vascular reactivity
DWI, IVIM, DKI, DTI	Perfusion, tissue injury, fibrosis
BOLD	Oxygen delivery, vascular reactivity
Arterial spin labelling	Perfusion
MR elastography	Fibrosis
MR spectroscopy	Metabolism
Magnetic transfer	Cell death, urine retention, fibrosis
Chemical exchange saturation transfer	Metabolites, pH

US techniques

Elastography	Fibrosis
Contrast-enhanced	Perfusion



Recent Advances in Renal Imaging

Pathological (functional & structural) changes in renal diseases at cellular/molecular levels

- Renal perfusion
- Fibrosis
- Oxygenation
- Injury
- Metabolism
- Molecular expression

- Functional MRI
 - DCE, DWI, DTI, BOLD, ASL, MRE, MRS, MT, CEST
- US
 - Elastography, CEUS
- CT, PET

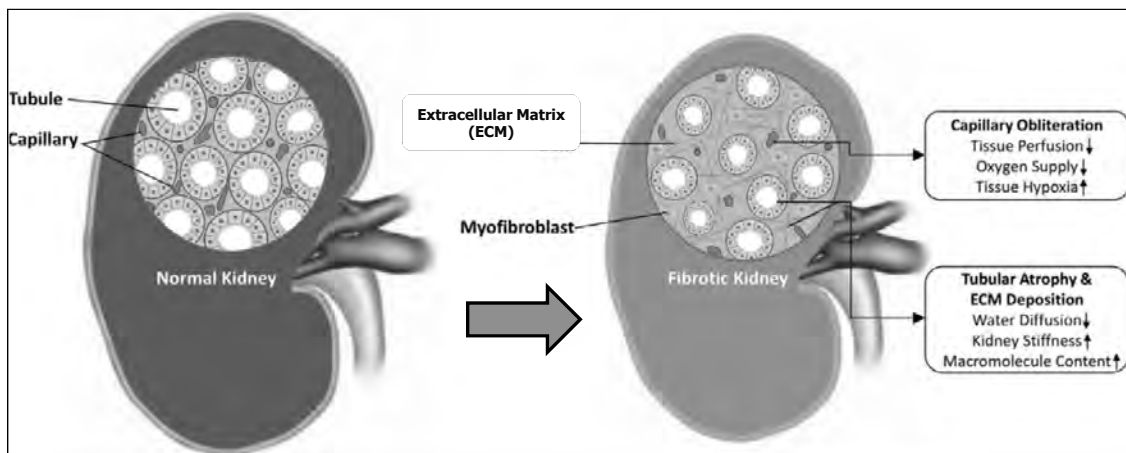


Renal Fibrosis

- Biomarker of renal ds diagnosis & guidance of therapeutic interventions of CKD
- Common pathological feature in CKD
- Gold standard – invasive tissue biopsy
- Often accompanies by vascular obliteration, tubular atrophy, & kidney shrinkage
→ Changes in functional, mechanical & molecular properties
- Useful noninvasive imaging techniques
 - DWI, MR elastography, magnetic transfer imaging (MTI)
 - US elastography



Renal Fibrogenesis & Injury



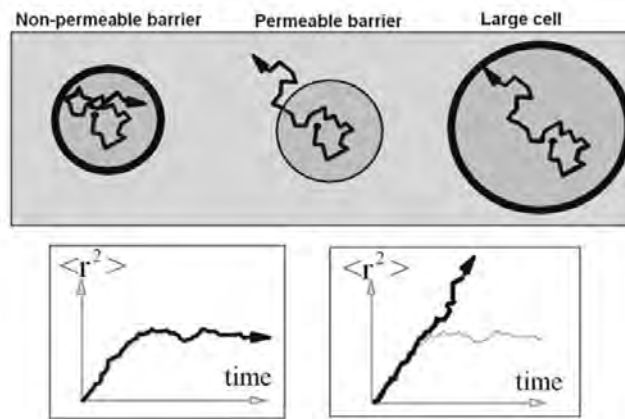
Healthy Kidney

- Healthy tubules
- Preserved capillary density
- Minimal interstitial extracellular matrix
- Minimal matrix cross-linking
- Soft extracellular matrix
- Minimal oxygen diffusion distance to tubular cells

*Translational Research 2019;209:105-120
Clin J Am Soc Nephrol 2017;12:1019-28*



Diffusion

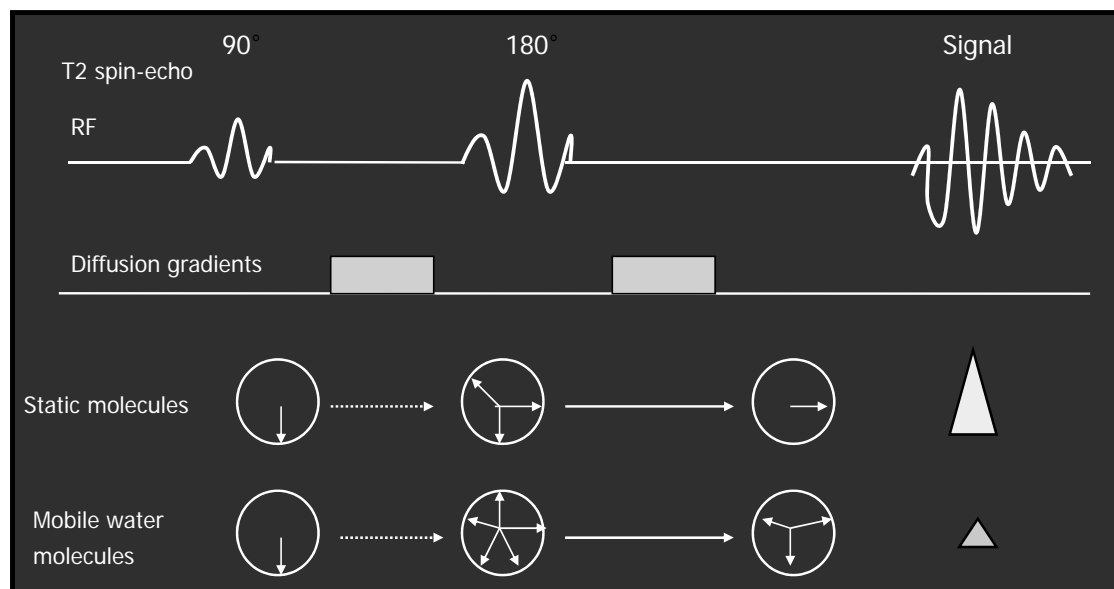


- Constant random Brownian motion (free diffusion) in container
- Restricted motion of water molecules in biologic tissues



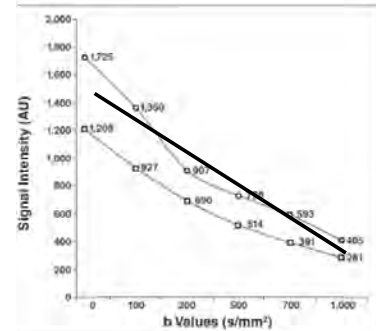
Diffusion-Weighted Imaging

- Typical pulse sequence



DWI

- Apparent diffusion coefficient (ADC)
 - $ADC = -\ln(S/S_0) / b$
- Measuring water motion (1-17 μm)
- Monoexponential model
 - $> 200 \text{ s/mm}^2$ for slow diffusion
- Renal fibrosis
 - Low ADC in renal allograft & native kidney dysfunction, unilateral ureteral obstruction
 - Good correlation betw ADC & histopathological score
 - d/t decreased renal perfusion & tubular flow



Assessment of early renal allograft dysfunction with blood oxygenation level-dependent MRI and diffusion-weighted imaging

Sung Yoon Park^b, Chan Kyo Kim^{a,*}, Byung Kwan Park^a, Sung Ju Kim^c, Sanghoon Lee^c, Wooseong Huh^d

^a Department of Radiology and Center for Imaging Science, Samsung Medical Center, Sungkyunkwan University School of Medicine, Seoul, Republic of Korea

^b Department of Radiology and Research Institute of Radiological Science, Severance Hospital, Yonsei University College of Medicine, Seoul, Republic of Korea

^c Department of Surgery, Samsung Medical Center, Sungkyunkwan University School of Medicine, Seoul, Republic of Korea

^d Department of Nephrology, Samsung Medical Center, Sungkyunkwan University School of Medicine, Seoul, Republic of Korea

R2* and ADC values of cortex and medulla in renal allografts with acute rejection (AR), acute tubular necrosis (ATN) and normal function.

Parameters	AR	ATN	Normal	P value ^a	P value ^b	P value ^c
R2* value (s ⁻¹)						
Cortex8 ^a	10.4 ± 2.4	10.7 ± 3.2	14.6 ± 2.4	0.001	0.016	1.000
Cortex16 ^a	13.4 ± 1.7	13.5 ± 1.3	15.4 ± 1.5	0.012	0.057	1.000
Medulla8 ^a	19.4 ± 2.4	20.6 ± 4.3	29.7 ± 3.0	<0.001	<0.001	1.000
Medulla16 ^a	21.4 ± 3.3	21.6 ± 4.1	26.9 ± 2.8	0.001	0.010	1.000
ADC value (10 ⁻³ mm ² /s)						
Cortex800 ^b	2.12 ± 0.18	2.17 ± 0.19	2.33 ± 0.14	0.022	0.190	1.000
Cortex800 ^c	1.92 ± 0.14	1.97 ± 0.17	2.10 ± 0.12	0.022	0.228	1.000
Medulla800 ^b	1.98 ± 0.18	1.95 ± 0.39	2.16 ± 0.16	0.259	0.237	1.000
Medulla800 ^c	1.84 ± 0.17	1.78 ± 0.26	1.99 ± 0.14	0.225	0.112	1.000

Relationship between R2* or ADC values and estimated glomerular filtration rate in all renal allografts.

Parameters	Correlation coefficient	P value
R2* value		
Cortex8 ^a	0.584	<0.001
Cortex16 ^a	0.403	0.018
Medulla8 ^a	0.672	<0.001
Medulla16 ^a	0.553	0.001
ADC value		
Cortex800 ^b	0.481	0.004
Cortex800 ^c	0.506	0.002
Medulla800 ^b	0.411	0.016
Medulla800 ^c	0.431	0.011

Note: Data are correlation coefficients and P-values of Spearman's correlation test.

^a Gradient echo of 8.

^b Gradient echo of 16.

^c b value = 500 s/mm².

^d b value = 800 s/mm².

- 34 pts (early dysfunction, 24; normal, 10)
- BOLD MRI & DWI may reflect early functional state of renal allografts, but may be limited in characterizing a cause of early renal allograft function

EJR 2014;83:2114-121

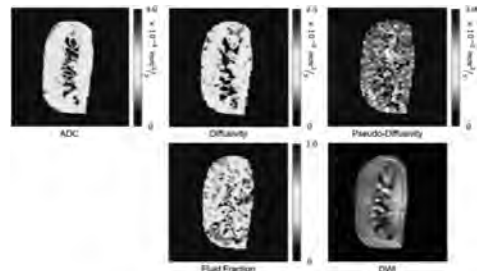


Intravoxel Incoherent Motion

- Pseudorandom for vascular & tubular flows, biased by organization of capillary network & renal tubules
- Bi-exponential equation by multiple b-values
 - True diffusivity(D), pseudodiffusivity(D*), perfusion fraction (f)

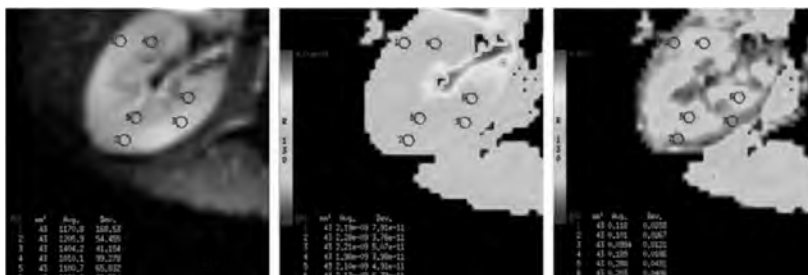
$$\frac{S(b)}{S(0)} = f \cdot \exp^{-D^*b} + (1-f) \cdot \exp^{-Db}$$

- Renal fibrosis
 - Decreased diffusion, lower perfusion in native kidney/allograft dysfunction
 - More accurate than ADC in distinguishing renal lesions
 - Conflicted results for assessing renal dysfunction
 - IVIM parameters negatively correlated well with renal fibrosis



Diffusion Tensor Imaging

- Preferential diffusion in certain direction in biological tissues or diffusion anisotropy reflects tissue microstructure
- Minimum 6 directions: mean diffusivity, FA (fractional anisotropy)
- FA – index for amount of diffusion asymmetry in a voxel
- Higher FA in medulla, relatively isotopically-structured cortex
- Good correlation betw medullary FA & eGFR
- Diffuse interstitial fibrosis, tubular atrophy, & cell infiltration alter water diffusion & correlate well with renal FA

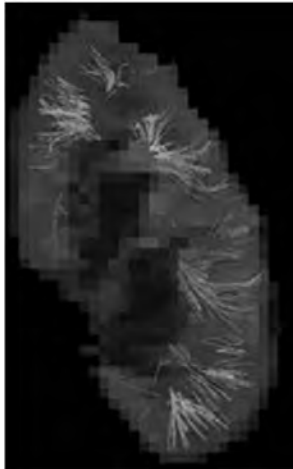


Clin Radiol 2019;74:116-22



DTI Tractography

Normal
eGFR = 120

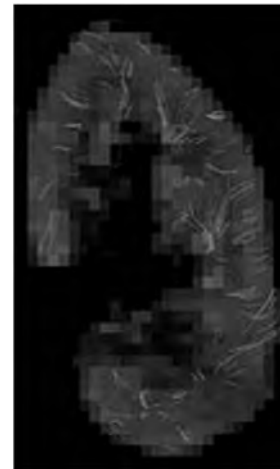


Track counts & lengths

DM-normoalbuminouria
eGFR = 84.1



DM-microalbuminouria
eGFR = 80.1



JMRI 2018;48:863-81



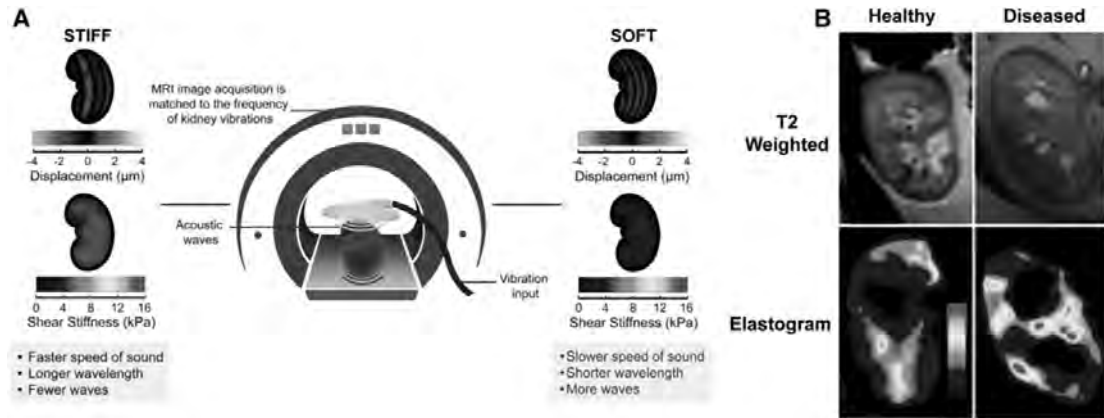
MR Elastography

- Accumulation of ECM during developing renal fibrosis hardening affected organs
- Tissue stiffness as biomarker of fibrosis
- Noninvasive measuring tissue stiffness by visualizing propagation of shear waves in tissue
 - Mechanical vibrations, 40-200 Hz, pneumatic driver
- Vibrating acoustic waves generating shear waves propagating in tissue, images by a phase contrast sequence
- Stiffer tissue causes faster propagating waves with longer wavelength
- RAS – correlation betw tissue stiffness & renal medullary fibrosis
- Good reproducibility & correlation with eGFR or fibrosis in human kidney

Clin J Am Soc Nephrol 2017;12:1019-28
Acad Radiol 2012;19:834-41



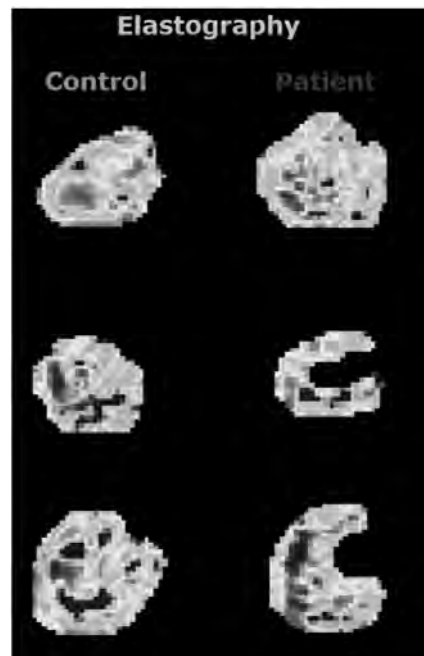
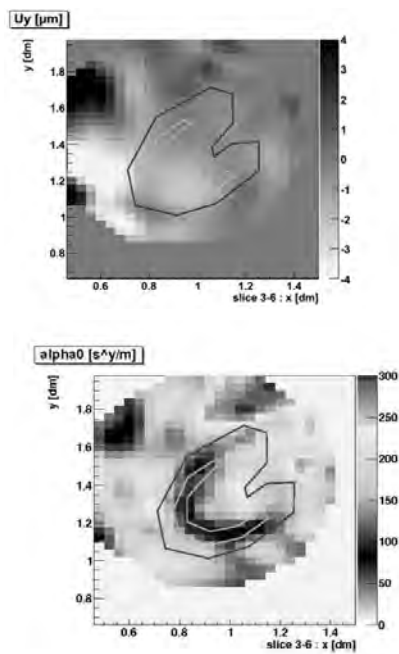
MRE



Clin J Am Soc Nephrol 2017;12:1019-28



MRE, SMC



US Elastography

- CKD

- ↓ shear wave velocity (SWV) associated with renal dysfunction
- Good correlation betw SWV & renal fibrosis
- Not predictable CKD stage or correlation with renal fibrosis

*BMC Nephrol 2015;16:119
Eur Radiol 2014;24:871-9*

- Allograft

- Conflicted results
- SWV correlated with renal fibrosis, not useful in distinguishing of different grades of fibrosis
- Stiffness is significantly decreased by reduction in renal perfusion
- Not reflective of cortical fibrosis, but associated with medullary fibrosis

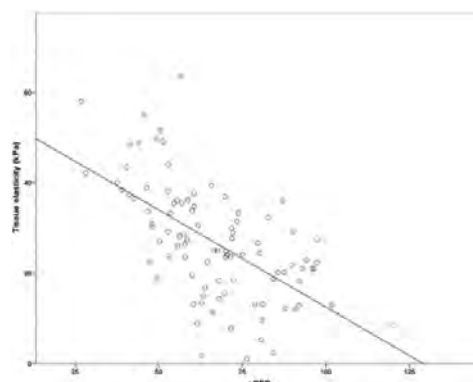
*Int J Urol 2018;25:450-5
Eur Radiol 2012;22:2138-46*



SWE: Subclinical Rejection

- Feasible in distinguishing btw patients with SCR & without SCR in stable functioning renal allografts

Variables	Stable renal allograft function (n = 95)		
	AR (n= 34)	No AR (n = 61)	P-value
Tissue elasticity (kPa)	31.0 ± 12.8	24.5 ± 12.2	0.016
RI	0.72 ± 0.06	0.70 ± 0.06	0.112
Age	52.2 ± 11.7	46.2 ± 11.3	0.017
Kidney size	11.3 ± 1.2	10.8 ± 1.1	0.048
Bun	20.1 ± 9.7	18.4 ± 5.5	0.262
Cr	1.27 ± 0.30	1.08 ± 0.30	0.003
eGFR	57.6 ± 13.5	71.5 ± 18.1	< 0.001



Moderate negative correlation btw kPa & eGFR (correlation coefficient = -0.604, $p < 0.001$)

Br J Radiol .2017;91(1081)



Recent Advances in Renal Imaging

Pathological (functional & structural) changes in renal diseases at cellular/molecular levels

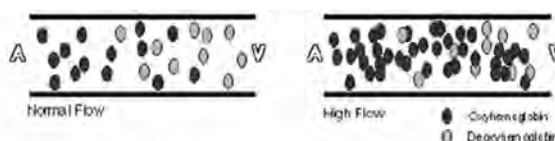
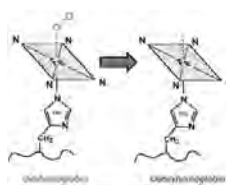
- Renal perfusion
- Fibrosis
- **Oxygenation**
- Injury
- Metabolism
- Molecular expression

- Functional MRI
 - DCE, DWI, DTI, BOLD, ASL, MRE, MRS, MT, CEST
- US
 - Elastography, CEUS
- CT, PET



Blood Oxygenation Level-Dependent

- OxyHb (diamagnetic)
- DeoxyHb (paramagnetic)
 - Shortening T2 & T2* signal
- Blood oxygenation level-dependent (BOLD)
 - Ogawa (1990) first demonstrated BOLD effect in vivo
 - DeoxyHb → reduction of signal by microscopic field gradient inhomogeneity
 - Blood flow ↑ (O2 demand ↑) in activated area → deoxyHb ↓ → local MR signal ↑

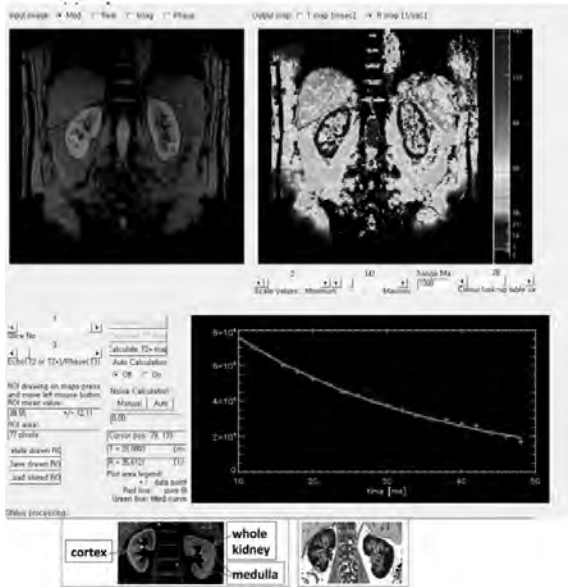


- Imaging of susceptibility differences in tissues



BOLD MRI

• Technique

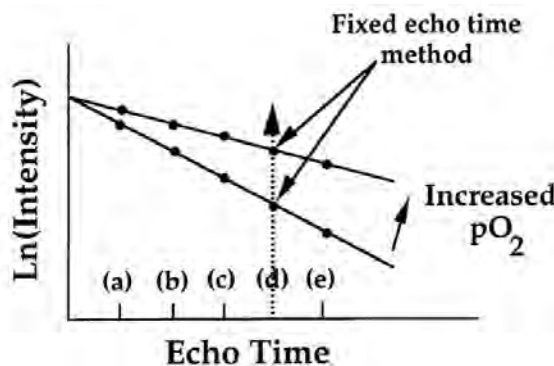


- 2D GRE c multiple TE
- Typically 8-16 TE
- Single breath hold
- Normal hydration (100ml water), 4h fasting from food
- Parametric images of $R2^*$ generated by fitting SI vs. TE data to a single decaying exponential fit or long-linear fit

MAGMA 2019 Nov



BOLD MRI



- $R2^*$ ($1/s$, $1/T2^*$) = slope ~ $\text{conc}(\text{deoxyHb}) \sim \text{blood } pO_2 \sim \text{tissue } pO_2$
- $\Delta R2^* = \ln(S(t)/S_0)/TE$

- $\uparrow R2^* = \uparrow \text{deoxyHb level} = \downarrow \text{oxygen bioavailability}$



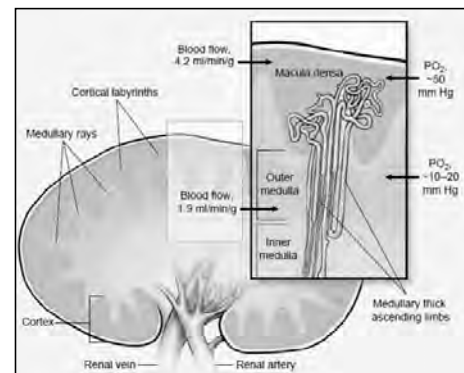
Potential Clinical Applications

- Functional renal disease
 - Renal artery stenosis, DM, HTN, unilateral ureteral obstruction
 - Chronic kidney disease
 - Acute rejection, acute tubular necrosis
- Oncology
 - Lesion characterization
 - Tumor hypoxia evaluation
 - Cervix, kidney, prostate, brain, breast
 - Surrogate predictors



Renal Medullary Hypoxia

- Low ambient pO₂ of medulla
 - Lower blood flow
 - Countercurrent arrangement of blood vessels (O₂ diffusion from arterial to vasa recta)
 - Medullary thick ascending limbs responsible for generation of osmotic gradient by active reabsorption of Na (↑O₂ demand) via Na⁺-K⁺-2Cl⁻ cotransporter



→ Vulnerable to hypoxic injury



Renal Medullary Hypoxia

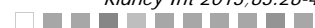
- Most cases of ARF d/t compromised renal perfusion (ischemic ARF) & nephrotoxins
 - Inadequate BF d/t RAS, occlusion or intrarenal small vessels lesions
 - Damage to endothelium or alternation in endothelial function resulting in \uparrow vasoconstrictive factors
- Nephrotoxicity d/t contrast or NSAID, initiation & progression of CKD
- Changes in oxygen saturation of Hb associated with changes in blood pO₂ are most marked at low levels of pO₂
 - BOLD MRI ideally suited for oxygenation measurements in renal medulla



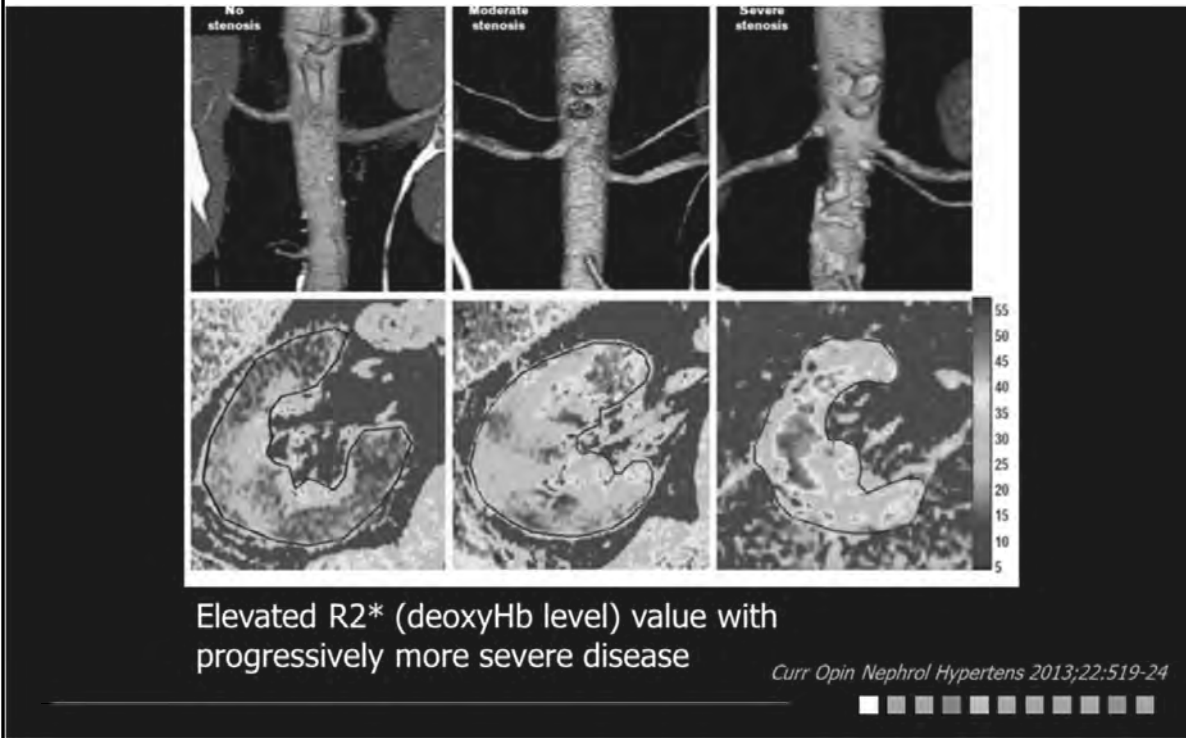
Renal Artery Stenosis

- \uparrow R2* relaxivity continuously & progressively in parallel with \downarrow in renal BF in response to increasing levels of stenosis
 - D/t \downarrow GFR & O₂-consuming tubular reabsorption of Na, surplus of oxygenated blood
 - Irreversible renal injury (functional loss, tissue fibrosis, ESRD)
- R2* returned to baseline values upon releasing occlusion
- Insights to changes in renal function prior to onset of irreversible renal injury & identifying reverse or repair disorders of tissue oxygenation

Curr Opin Nephrol Hypertens 2013;22:519-24
Am J Hypertens 2010;23:1159-69
Kidney Int 2013;83:28-40



Renal Artery Stenosis

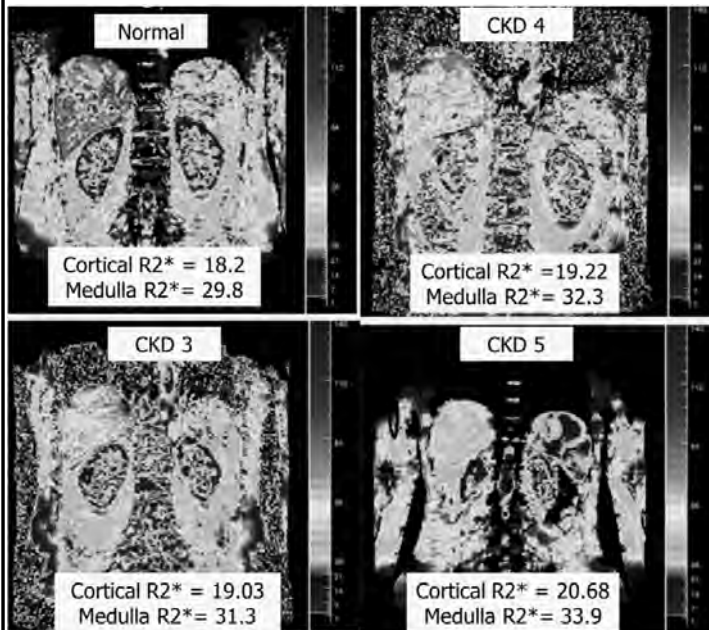


Chronic Kidney Ds

- Progressive loss of kidney function caused by chronic tubulointerstitial injury, which encompasses tubular atrophy & interstitial fibrosis
- ↓ Renal oxygenation → initiating & promoting fibrotic responses via various cytokine signaling pathways & cell-signaling events
- Major variables of CKD progression
 - Fibrosis, hypoxia
- Conflict results of BOLD MRI
 - Good correlation of R2* with eGFR
 - Moderate stenosis associated with medullary & cortical R2*
 - No differences in cortical or medullary R2* between different CKD stages

Kidney Int 2012;81:642
Am J Hypertens 2010;23:1159-69
Plos One 2014;23:95895

Chronic Kidney Ds



- 49 CKD & 11 healthy
- Cortical or medullary R2* of CKD was higher than that in healthy volunteers
- No differences among each CKD stage
- Good correlation of cortical & medullary R2* with eGFR

Bae JM, et al. ECR 2015



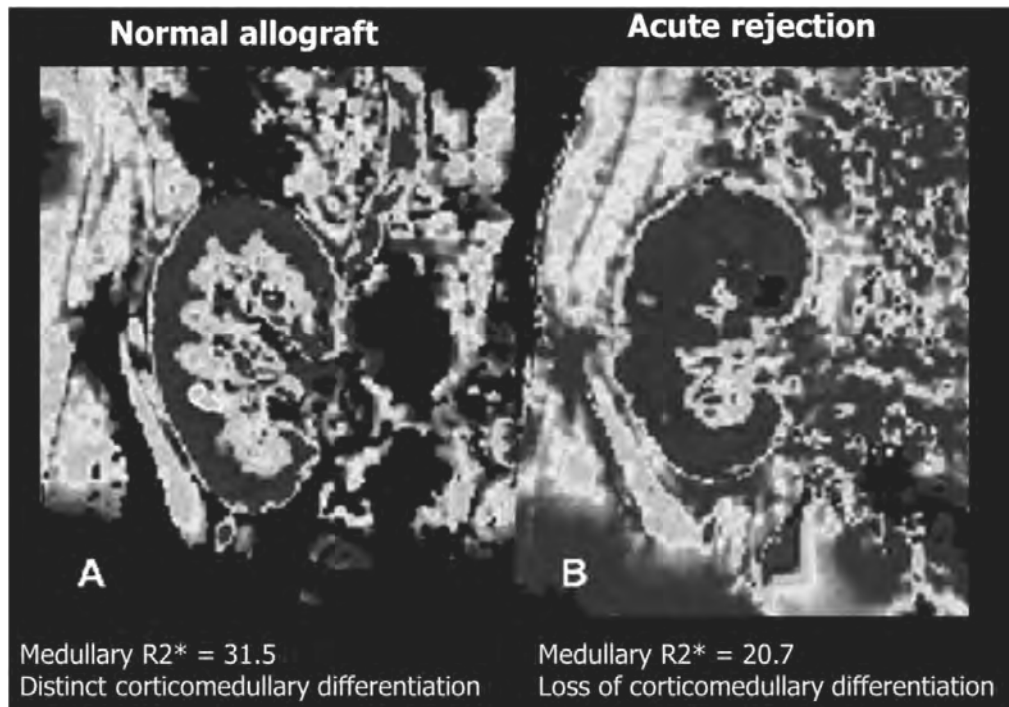
Renal Allograft

- Early dysfunction of renal allograft
 - Associated with poor long-term graft function or graft survival
 - Major causes: acute rejection & ATN
- Acute rejection or ATN
 - ↓ DeoxyHb → ↓ medullary or cortical R2* (↑ pO₂) d/t reduced tubular fractional reabsorption of Na
- Chronic allograft nephropathy
 - ↓ Cortical or medullary R2*

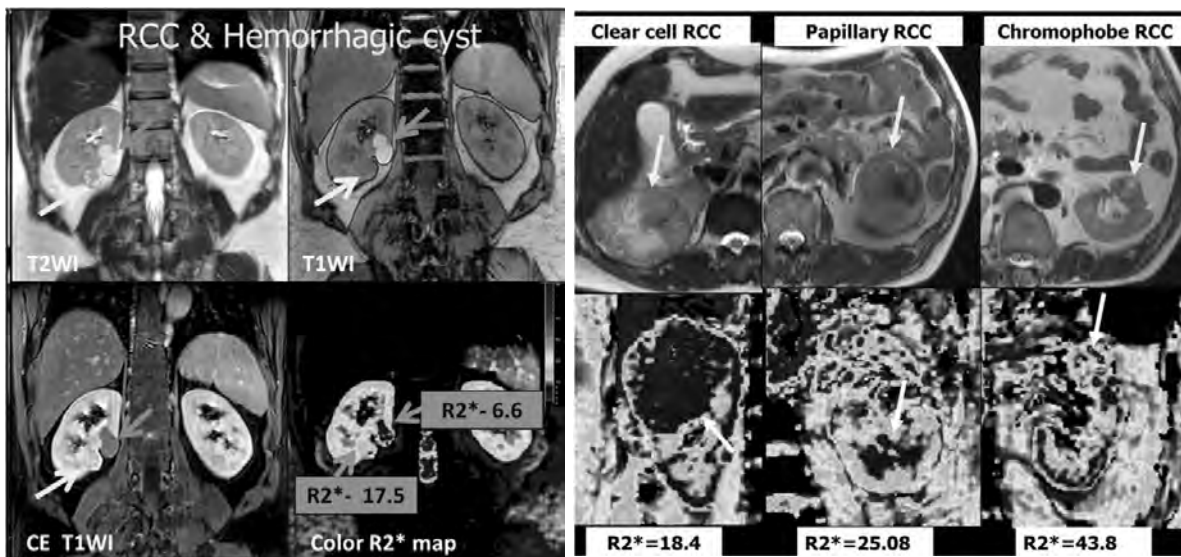
Kidney Int 2012;81:684-89
Radiology 2006;241:812-21
Am J Physiol Renal Physiol 2007;292:513-22
AJR 2012;198:1108-14
EJR 2014;83:2114-21



Renal Allograft



Renal Tumors

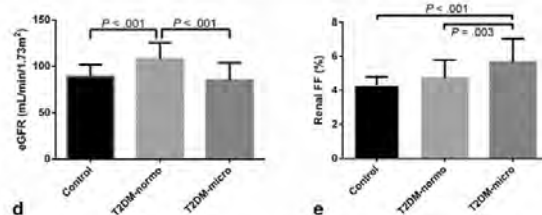
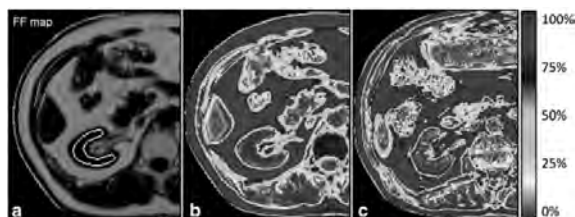


- Accurate characterization of renal lesions focusing on surgical lesions
- Different deoxyHb concentration in various renal lesions d/t different vascularity or perfusion
- Different $R2^*$ among RCC subtypes

AJR 2011;197:489-94
AJR 2014;203:78-84

Fat Fraction

- Renal fat quantification by Dixon technique
 - In-phase (water + fat) & out-of-phase (water-fat)
 - Water only or fat only images
 - Detecting early staged diabetic nephropathy



Eur Radiol 2018;28:3326-34



Future Directions & Limitations

- Need to be validated in future large-cohort, multi-center randomized trials
- Need for standardization of imaging techniques among centers & across different platforms
- Translational studies for emerging techniques
- Intrinsic low sensitivity & specificity
- Subject to injury-induced processes besides fibrosis including blood flow changes, hydronephrosis & edema
- Technical advancement to minimize imaging artifacts & optimize protocols
- Implementation of multiparametric imaging techniques to understand pathophysiologic changes in renal ds
- Future role for artificial neural network/artificial intelligence



Conclusion

- Recent advanced renal imaging that is noninvasive and can be translated to clinical protocols has become an inevitable research tool.
- Although several current limitations exist, it can offer valuable information and will remain essential for future research and potential clinical applications.



Urolithiasis basic and update

가천대 길병원
심영섭

- ▶ Nephrolithiasis, urolithiasis
 - : Nephros-(*for kidney*), uro-(*for urinary*) + lithos(*for stone*), Greek words
- ▶ Most common disorder of urinary tract.
- ▶ Disease with high recurrence rate and increased occurrence rate
- ▶ Risk factors
 - ▶ Age, sex, race, occupation, climate, diet & underlying disease
 - ▶ In developed country,
 - ▶ Increased salt and protein consumption, rising prevalence of metabolic syndrome
 - ▶ In developing country,
 - ▶ Malnutrition, water deprivation

Urolithiasis in Korea

- ▶ 2002-2013, South Korea.
- ▶ Increased annual incidence of urolithiasis, every year
- ▶ Disease recurrence within 5 years : 21.3%
- ▶ 11-year cumulative incidence was 5.71%
- ▶ Incidence : M > F (7.07% vs. 4.34%)
- ▶ 11-year cumulative incidence in the 60- to 69-year-old group (9.08%)

J Korean Med Sci. 2018 Jan 8;33(2):e13

Stone composition

- ▶ **Calcium containing stone**
 - ▶ Most common stones
 - ▶ Mixture of calcium oxalate and calcium phosphate

Table 1 Frequencies and mineral compositions of stones

Composition	Frequency (%) ^a
Calcium	70–80
Calcium phosphate	5–10
Calcium oxalate-phosphate	30–40
Calcium oxalate	20–30
Struvite	15–20
Cystine	1–3
Uric acid	5–10

^aIn order of decreasing radiographic opacity

Stone composition

► Calcium oxalate stone



Diagnostics 2023, 13, 951

Stone composition

► Struvite stone

- Magnesium Ammonium Phosphate
- 15-20%
- Associated with UTI (Proteus, Klebsiella, Pseudomonas)
 - : Infection-induced stone, M < F
- Associated with alkaline urine
- shape of staghorn or coral calculi

Stone composition

► Uric acid stone

- Hyperuricosuria and acidic concentrated urine
- A/W Distal small bowel disease, or resection, ileostomy, myeloproliferative disorders, treated with chemotherapy
- 5-10%
 - : Increased incidence d/t metabolic syndrome
 - : in USA, 7%(1980) → 14% (2015)
 - common in older, higher BMI, lower urinary pH

Microbiome on urolithiasis

- **microbiome** : the community of microorganisms that can usually be found living together in any given habitat
- Urease-producing bacteria
 - : Proteus mirabilis, Klebsiella pneumoniae, Staphylococcus aureus, Pseudomonas aeruginosa, Providencia stuartii, and Serratia marcescens and Morganella morganii
 - Break down urea and induce ammonia and carbon dioxide production,
 - Leading to renal tubular injury, urine alkalinization, and subsequent formation of phosphate salts
 - Form struvite stones

Microbiome on urolithiasis

- ▶ E. coli and P. mirabilis worsened calcium oxalate encrustation
- ▶ Bacteria bind to calcium oxalate crystals, causing pyelonephritis, which leads to changes in nephrons that form Randall's plaque.
- ▶ Chutipongtanate et al.
 - ▶ E. coli, K. pneumoniae, S. aureus, and S. pneumoniae had significant promoting effects on CaOx crystal growth and aggregation.

Microbiome on urolithiasis

Table 1. Urinary microbiome associated with urolithiasis.

Urinary Microbiome (Urinary Stone Disease Group)	Urinary Microbiome (Healthy Group)
<i>Escherichia coli</i>	<i>Lactobacilli</i>
<i>Staphylococcus aureus</i>	<i>Bifidobacterium</i>
<i>Streptococcus pneumoniae</i>	<i>Veillonellaceae</i>
<i>Pseudomonas aeruginosa</i>	
<i>Burkholderia</i>	
Urease-producing Organisms	
<i>Proteus mirabilis</i>	
<i>Klebsiella pneumoniae</i>	
<i>Staphylococcus aureus</i>	
<i>Pseudomonas aeruginosa</i>	
<i>Providencia stuartii</i>	
<i>Serratia marcescens</i>	
<i>Morganella morganii</i>	

Gut microbiome and urolithiasis

- ▶ Oxalotrophs : bacteria that use oxalate as an energy source
 - ▶ Lactobacilli, Bifidobacterium
 - ▶ **Oxalobacter formigenes**
 - : reduces mucosal absorption
 - promotion of endogenous oxalate secretion by the gut mucosa
- ▶ Absence of Oxalobacter formigenes
 - ▶ Induce hyperoxaluria
 - ▶ Leads to the formation of calcium oxalate stones
- ▶ Probiotics for prevention

Genomics for urolithiasis

- ▶ Monogenic causes & polygenic causes
 - ▶ Polygenic cause : almost patients
 - ▶ Monogenic cause : 10-20% of stone former
- ▶ **Oxlumo™ (Lumasiran)**
 - ▶ Treatment of primary hyperoxaluria type 1
 - ▶ Subcutaneously injected RNA interference(RNAi)
 - ▶ Targeting the mRNA for the hydroxyacid oxidase 1 gene (HAO1)
 - ▶ Inhibiting the synthesis of oxalate
 - ▶ FDA approved(2020)

Curr Opin Urol. 2023 Mar 1;33(2):73-76.

Table 1. Gene loci associated with monogenetic causes of urolithiasis [17,19]

Disease	Genes	Mode
Calcium metabolism		
Dents disease	CLCN5, OCLR	X chromosomal recessive
Lowe syndrome	OCLR	X chromosomal recessive
Batter syndrome	NKCC2 (SLC12A1), ROMK (KCNJ1), CLCNKB, BSND, CASR, CLCN5	Autosomal dominant, autosomal recessive, X chromosomal recessive
Familial hypercalciuria	VDR, ADCY10	Autosomal dominant
Autosomal dominant hypocalcaemia	CASR, GNA11	Autosomal dominant
Infantile hypercalcaemia	CYP24A1, SLC34A1	Autosomal recessive
Hypophosphataemic rickets	SLC34A1, SLC34A3, SLC9A3R1	Autosomal recessive
Oxalate metabolism		
Primary hyperoxaluria	AGXT, GRHPR, HOGA1, SLC2	Autosomal recessive
Cystinuria		
Cystinuria	SLC3A1, SLC7A	Autosomal dominant, autosomal recessive
Uric acid stones		
Renal hypouricemia	LSC22A12, SLC2A9	Autosomal dominant, autosomal recessive
Other		
Hyperoxaluria	AGXT, GRHPR, HOGA1, SLC26A1	Autosomal recessive
Xanthinuria	XDH	Autosomal recessive
Adenine Phosphoribosyltransferase deficiency	APRT	Autosomal recessive

Curr Opin Urol. 2023 Mar 1;33(2):73-76.

Stone composition prediction_DEI

- DEI (Dual Energy Index)
: $(HU80(100) - HU140)/(HU80(100) + HU140 + 2000)$

Somatom Definition

Type of calculi	Number of calculi	Mean HU	STD	Mean DE ratio	STD
Definition dual source (first generation)					
Mixed calcium	8	1287	973.4	0.088	0.04515
UA	0	492	130.97	0.018	0.02177
Mixed UA	1	564	23.3	0.001	0
COM	14	1188	480.42	0.118	0.02441
Calap	5	988	232.89	0.121	0.01598
Brushite	1	1995	19.4	0.151	0
Cystine	1	851	27.6	0.065	0
COD	3	1169	383.05	0.111	0.03818

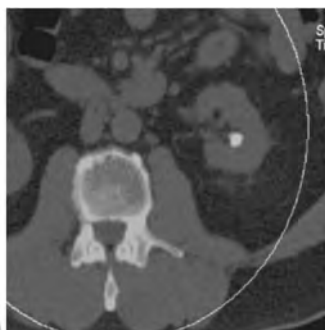
Somatom Definition Flash

Type of calculi	Number of calculi	Mean HU	STD	Mean DE ratio	STD
Definition flash					
Mixed calcium	6	976	238.8	0.077	0.01597
UA	3	453	25.81	0.001	5.25950E-5
Mixed UA	1	605	60.3	0.049	0
COM	12	883	385.42	0.073	0.02361
Calcium HA	2	955	131.1	0.075	0.00961
Brushite	1	784	81.5	0.073	0

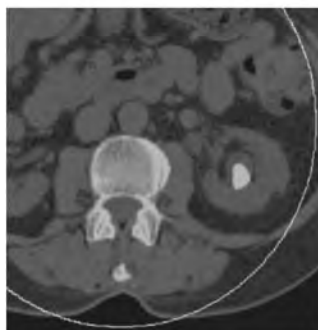
World Journal of Urology 34, 1297-1302 (2016)

Stone composition prediction_DEI

- DEI (Dual Energy Index)
: $(HU_{80}(100) - HU_{140}) / (HU_{80}(100) + HU_{140} + 2000)$
- Sensitivity 88.9 %, specificity 98.1 %, PPV 88.9 %, NPV 91.1 %



Uric acid stone



Calcium-containing stone

World Journal of Urology 34, 1297-1302 (2016)

Stone composition prediction_CT ratio

- Dual energy CT vs. Single energy CT
- Using software(Syngo.Via)

	Single-energy CT, attenuation at 120 kV (HU)	Dual-energy CT, 100/Sn140 kV attenuation ratio
Uric acid	<538	<1.13
Cysteine	538-1064	1.13-1.24
Calcium oxalates/phosphates	>1064	>1.24

	Mean diameter (mm)	Mean volume (mm ³)	Mean attenuation values at 100 kV (HU)	Mean attenuation values at Sn140 kV (HU)	Mean ratio 100/ Sn140 kV
Uric acid stones	7 (3.3-14)	138 (6-320)	430 ± 56 (217-669)	440 ± 70 (221-508)	0.97 (0.89-1.05)
Cysteine stones	7 (1-24)	353 (2-1390)	323 ± 52 (301-1063)	499 ± 57 (258-843)	1.24 (1.17-1.28)
Calcium oxalates/phosphates stones	5 (2-13)	97 (3-490)	936 ± 90 (121-1645)	703 ± 84 (91-1391)	1.35 (0.94-1.69)

Urolithiasis 45, 255-261 (2017)

Stone composition prediction_CT ratio

- Dual energy CT vs. Single energy CT
- Using software(Syngo.Via)

	Single-energy CT (%)	Dual-energy CT (%)
Sensitivity	94.12	100
Specificity	72.73	93.94
Positive predictive value (PPV)	64	89.47
Negative predictive value (NPV)	96	100
Accuracy	80	96

Urolithiasis 45, 255–261 (2017)

Stone composition prediction_Effective Z

- Effective Z & HU on keV
- Using software(Advantage Workstation)

Table 3 Table summarizing means of CT-derived parameters for different classes of urinary stones

	Struvite (n=2)	Cystine (n=4)	Calcium-based (n=25)	Total (n=31)	p values overall	p values calcium versus struvite	p values calcium versus cystine	p values struvite versus cystine
Size	10.15±1.90	8.75±0.77	10.06±2.65	9.90±2.45	0.618	1.000	0.113	0.643
Z _{eff}	11.10±0.68	10.23±0.75	12.01±0.54	11.72±0.83	<0.001*	0.042*	0.002*	0.355
HU 40 keV	1522.61±201.75	1357.05±450.09	1926.59±337.07	1829.36±392.66	0.012*	0.165	0.027*	0.643
HU 70 keV	715.40±110.24	650.67±191.14	942.19±95.57	889.94±197.60	0.006*	0.096	0.014*	0.355
HU 140 keV	432.73±62.84	420.00±88.89	576.39±99.38	546.94±112.09	0.007*	0.052	0.016*	0.643
HU 40/70 ratio	1.65±0.01	1.53±0.16	1.63±0.08	1.62±0.09	0.154	0.139	0.448	0.643
HU 40/140 ratio	3.52±0.04	3.23±0.61	3.34±0.26	3.34±0.31	0.594	0.165	0.569	1.000
HU 70/140 ratio	2.12±0.04	2.10±0.28	2.04±0.09	2.05±0.15	0.535	0.517	0.312	0.643

Abdominal Radiology (2020) 45:1092–1099

Stone composition prediction_texture analysis

- 45 patient (18 UA, 32 Non-UA)
- Ex vivo

UA stones

: lower mean, standard deviation and mean of positive pixels
higher kurtosis

No significant differences in entropy or skewness
between UA and non-UA stones.

Clinical Radiology 73 (2018) 792e799

Fragility for ESWL_Size of stone

In 427 patients,

Success rate stone size ≤ 10 mm : 90%, > 10 mm : 70 %

In 203 patients,

median stone diameter in the success group : 9.39 mm

in the failure group : 13.41 mm

Int. Urol. Nephrol. 38 (1) (2006) 63-67.

In 155 patients,

Success rate stone size

< 5 mm	: 73 %
5 – 10 mm	: 68.4%
> 10 mm	: 32 %

Investig Clin Urol 59 (1) (2018) 25-31

Annals of Medicine and Surgery 70 (2021) 102829

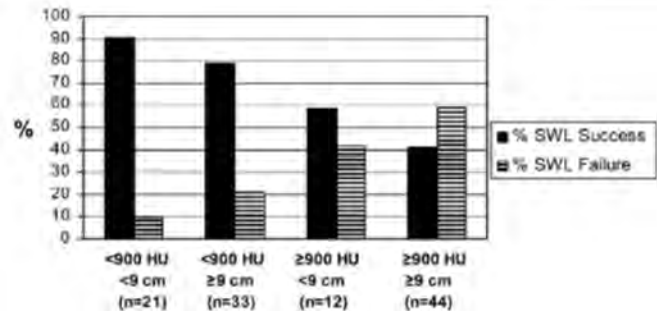
Fragility for ESWL_mean stone density(MSD)

Table 3 – Multivariate analysis for variables predicting failure of disintegration by extracorporeal shock wave lithotripsy

Variable	B	SE	RR	95% CI	p value
Stone attenuation (HU)					
≤1000 (reference)					
>1000	2.092	0.884	8.1	1.433–45.82	0.018
BMI (kg m ⁻²)	0.115	0.056	1.12	1.006–1.25	0.039

B, regression coefficient; SE, standard error; RR, relative risk; HU, Hounsfield units.
* Logistic regression analysis.

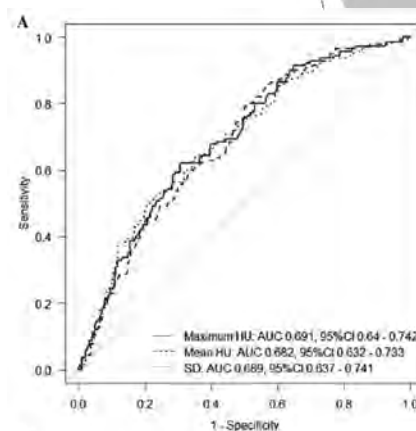
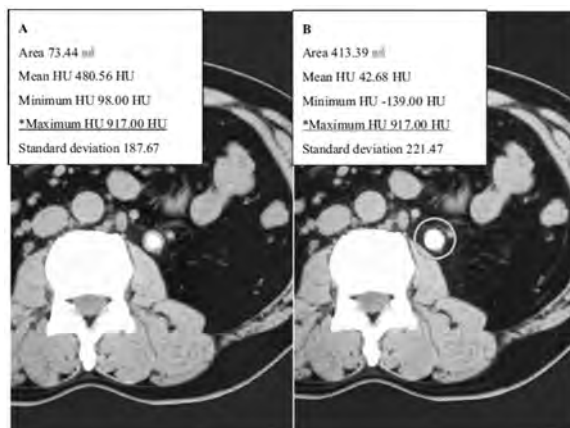
European Urology, vol. 51, no. 6. 1688-1694, 2007



Urology, vol. 72, no. 4, 765-769, 2008

Cutoff value of MSD : 593 – 1200 HU

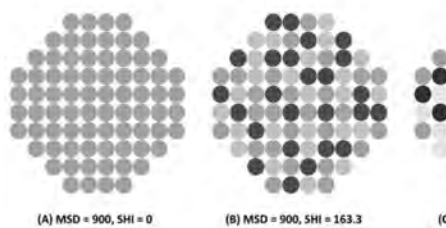
Fragility for ESWL_mean stone density(MSD)



Less bias using maximal HU than mean HU

Urolithiasis (2020) 48:85-91

Fragility for ESWL_stone heterogeneity index



Stone heterogeneity index (SHI),
: standard deviation of stone density (CT)

	Univariate			Multivariate		
	OR	95% CI	P-value	OR	95% CI	P-value
One-session success						
Age (year)	0.995	0.983–1.007	0.394			
Sex (Male)	0.831	0.574–1.195	0.323			
Stone size (mm)	0.832	0.789–0.874	<0.001	0.889	0.841–0.937	<0.001
SSD (mm)	0.999	0.990–1.008	0.769			
MSD (HU)	0.997	0.996–0.998	<0.001	0.995	0.994–0.996	<0.001
SHI (HU)	1.004	1.002–1.005	<0.001	1.011	1.008–1.014	<0.001
One-session stone-free						
Age (year)	0.991	0.979–1.003	0.128			
Sex (Male)	0.822	0.573–1.174	0.285			
Stone size (mm)	0.832	0.790–0.875	<0.001	0.886	0.839–0.933	<0.001
SSD (mm)	1.000	0.991–1.008	0.992			
MSD (HU)	0.997	0.996–0.998	<0.001	0.996	0.995–0.997	<0.001
SHI (HU)	1.002	1.000–1.004	0.017	1.008	1.005–1.010	<0.001

Scientific Reports, 2016;6:23988

Spontaneous passage

EAU Guidelines on Diagnosis and Conservative Management of Urolithiasis

Table 14 – Recommendation for the conservative management of ureteral calculi.

Recommendation	LE	GR
In patients with newly diagnosed ureteral stones <6 mm ^a , if active removal is not indicated, observation with periodic evaluation is an optional initial treatment. Such patients may be offered appropriate medical therapy to facilitate stone passage during observation.	1a	A
LE = level of evidence; GR = grade of recommendation, MET = medical expulsive therapy. ^a The exact cutoff size for ureteral stones cannot be determined from the literature, but the panel suggests <6 mm.		

Some 95% of stones ≤ 4 mm pass within 40 days.

Observation is feasible in informed patients who develop no complications.

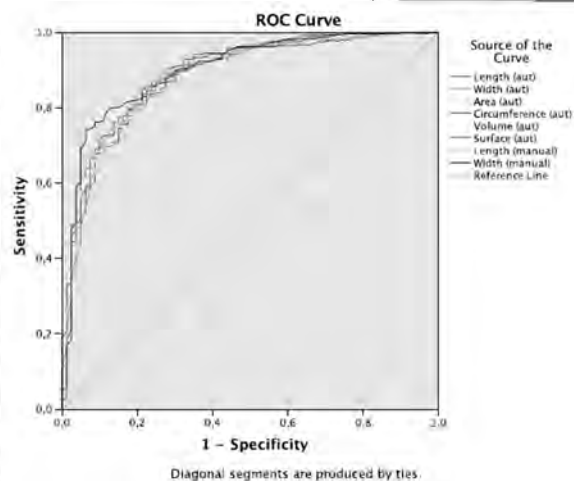
Stones >6mm are usually treated actively, although even such stones pass occasionally

Spontaneous passage

Automated 3D-measurement vs. manual measurement

Table 1 Area under the curve (AUC) for the prediction of spontaneous passage of a ureteral stone with different measurements - All stones

Measures	4 weeks			20 weeks		
	AUC	95% CI		AUC	95% CI	
		Lower	Upper		Lower	Upper
Length (aut)	0.85	0.79	0.90	0.88	0.84	0.93
Width (aut)	0.85	0.80	0.91	0.88	0.84	0.93
Area (aut)	0.82	0.75	0.88	0.89	0.85	0.93
Circumference (aut)	0.84	0.77	0.90	0.89	0.85	0.93
Volume (aut)	0.84	0.78	0.90	0.89	0.86	0.93
Surface (aut)	0.85	0.79	0.91	0.90	0.86	0.93
Length (manual)	0.84	0.78	0.90	0.89	0.85	0.93
Width (manual)	0.85	0.79	0.91	0.90	0.86	0.94



Eur Radiol (2018) 28:2474-2483

Current Urology Reports (2021) 22: 53
<https://doi.org/10.1007/s11934-021-01069-3>

ENDOUROLOGY (P. MUCKSAVAGE, SECTION EDITOR)



The Ascent of Artificial Intelligence in Endourology: a Systematic Review Over the Last 2 Decades

B. M. Zeeshan Hameed^{1,2} · Milap Shah^{1,2} · Nithesh Naik^{2,3} · Bhavan Prasad Rai^{2,4} · Hadis Karimi⁵ · Patrick Rice⁶ · Peter Kronenberg⁷ · Bhaskar Somani^{1,2,6}

For stone detection

Table 1 Applications of AI in diagnosis, imaging, and detection of composition of urolithiasis

Applications of AI in imaging and diagnosis of kidney stone disease (KSD)										
Author	Total (n)	Training set	Test Set	Technique/Model	Sensitivity	Specificity	Accuracy	PPV	ROC-AUC	Other Statistical Parameter
Langkvist et al. [5]	465: 437 (28 were removed)	348	88	CNN	100%				0.9971	2.68 false positive per scan
Parakh et al. [6]	535 patients	435	100	CNN			>90%			
De Perrot et al. [7]		369 kidney stones (n=211) phlebolith (n=201)	47 (kidney stones n=24; phlebolith n=23)	ML classifiers: AdaBoostSVMLR Stochastic gradient descent Gaussian Naïve Bayes kNNRF			AdaBoost: 86.3% SVM: 83.2% LR: 82.7% Stochastic gradient descent: 81.0% Gaussian Naïve Bayes: 76.6% kNN: 71.4% RF: 67.2%	81.50%	0.902	NPV: 90%
Jendeberg et al. [8]	Distal ureteric calculi: 267 Phlebolith: 217	Stones: 217 Phleboliths: 167	Stones: 80 Phleboliths: 50	CNN	94%	90%	92%			Semi-quantitative method accuracy: 49%

NCCT

Table 2

Confusion matrix for all CCs in the test set. F1-score 0.35, Recall 0.21, Precision 1.00.

		Predicted	
		Positive	Negative
Actual	Positive	88	0
	Negative	325	18829

For stone detection

USG	Krishna et al. [10]	250 normal, 138 stone, and 120 cyst kidney images	SVM: 75 cyst and 75 stone images	SVM: 45 cyst and 63 stone images	FPGA-based CAD, classifiers: SVM with MLP	100%	96.82%	98.14%	
USG X-ray	Li and Elliot [11]	248 (103 PCNL, under BUG, 105 X-ray guidance, remaining 40 BUG combined with X-ray)	208	47	Back-propagation n artificial neural network (ANN), MVR				ANN: R2 = 0.81 MVR: R2 = 0.63
USG	Selvarani and Rajendran [12]	250 US images (150 calculi, 100 healthy)		100 sample US images (50 normal and 50 stone images) using 10-fold approach	PSO-SVM/AMM-PSO-SVM			PSO-SVM: 97.4% AMM-PSO-SVM: 98.8%	EAR (%) PSO-SVM 2.6 AMM-PSO-SVM 1.8 FRR PSO-SVM 3.9 AMM-PSO-SVM 3.3
	Ishioaka et al. [13]	1017	827	190	CNN ResNet	0.72		0.49	F measure: 0.58
USG	Nithya et al. [14]	100 (40 normal, 30 tumor, 30 stone) for segmentation and classification	805	20%	ANN kNN Naïve bias (NB)	ANN: 100% kNN: 66.66% NB: 63.57%	ANN: 90% kNN: 90% NB: 89.7%	ANN: 93.45% kNN: 84.61% NB: 83.64% linear+quad ratio based segmentation: 99.61%	

For detecting stone composition

Ex vivo NCCT

Kriegshauser et al. [15]	32 stones dataset (24 stones data of size > 5 mm)	ANN SVM DT RF NBT	Distinguish UA and non-UA stones: ANN, SVM, and RF (highest): 97% and 100% Distinguish non-UA subtypes NBT and RT (highest): 72% and 75%	
Black et al. [18]	63 kidney stones: 17 UA, 21 COM, 7 struvite, 4 cystine, 14 brushite (total of 127 images)	DL-CNNResNet-101	UA: 94% COM: 90%, struvite: 86%, cystine: 75%, brushite: 71%	UA: 97.83% COM: 97.25% Struvite: 91.84% Cystine: 98.31% Brushite: 96.43%
Bejan et al. [19]	63 kidney stones: 17 UA, 21 COM, 7 struvite, 4 cystine, 14 brushite (total of 127 images)	DL-CNNResNet-101	>90% (COM, CODH, hydroxyapatite, brushite, struvite) uric acid :87.5%	

Overall recall:
85% Precision: 85% UA: 94.12% COM: 95% Struvite: 71.43% Cystine: 75% Brushite: 75%

Ex vivo DECT

Hokamp et al. [20]	200 kidney stone (monocrystal line 116; dicrystalline 84)	70% (test) 15% (validation)	DECTML	Overall (predicting main component): 91.1%
Sacchi et al. [21]	105 calculi (40 patients)	ML-ANN kNN	ANN: 97.1% kNN: 98%	ANN: 98.6% kNN: 98.6%

ANN Precision: 97.2% Recall: 98.6% F1 score: 96% kNN Precision: 97.5% Recall: 98.8% F1 score: 98.1%

Ex vivo NCCT

Cui et al. [22]	135 kidney stones (34 cystine, 34 purines, 32 phosphates, 35 oxalates kidney stones)	ML (kNN and SVM) with Raman spectroscopy	PCA-kNN: 0.963 PCA-SVM: 0.963	PCA-kNN: 0.995 PCA-SVM: 0.985	PCA-kNN and PCA-SVM: 96.3%
-----------------	--	--	-------------------------------	-------------------------------	----------------------------



**11:20 – 12:20 Gynecologic and Obstetric
Imaging**

좌장: 이은주 (아주대병원)

강병철 (세브란스병원)

The 30 th Anniversary of KSUR) April 21 (Friday) 2023 ~ 23 (Sunday), Jeju island

Category	Gynecologic Imaging (April 22 2023)
Duration	Lecture Title
30 min	Next Generation MRI in Gynecology Oncology

Title

Next Generation MRI in Gynecology Oncology

Abstract

Molecular imaging armamentarium has redefined our understanding of cancer biology, and has improved management of uterine malignancy, for tumor detection, primary staging, treatment planning, prediction of prognosis. It is critical that radiologists understand the technological aspects, so we can see beyond the hype, and acknowledge the limitations and opportunities. This presentation aims to serve as a short and digestible repository of information, and details every radiologist might need to know. We will describe the basics and update the applications of diffusion-weighted imaging (DWI), chemical exchange saturation transfer (CEST) imaging, dynamic contrast enhancement (DCE)-MRI, and magnetic resonance spectroscopy (MRS). We will introduce the next generation MRI, dynamic nuclear polarization (DNP), increasing signal over 10,000-folds of magnitude for stable isotope carbon-13 (^{13}C) enriched compounds on MRI, has entered the clinical investigation recently. Meanwhile, ^{18}F -fluorodeoxyglucose (FDG) PET provides quantitative and functional readouts, such as standardized uptake value maximum (SUVmax), total lesion glycolysis (TLG), metabolic tumor volume (MTV). Radiomics approach converts high-throughput extraction of quantitative imaging features into mineable data by artificial intelligence will evolve rapidly for decision support in the near future. We believe the emerging MRI-based technologies will continuously improve our practice. In combination with artificial intelligence, we are entering a new era of personalized medicine, enabling a more delicated decision-making and precisely guided radiation treatment plan, which could directly improve patient survival in the near future. We hope this talk will inspire the audience to think about the potential benefits and challenges of molecular imaging, as well as attempt to provide a futuristic vision to use it in everyday medical practice.

MRI approach for Adnexal Lesions

박계진

서울아산병원 영상의학과

MRI 는 초음파에서 진단이 불분명한 난소 및 자궁부속기의 종괴가 발견된 경우 문제해결기법으로 많이 이용된다. 난소 및 자궁부속기 종괴에 대해서 기존 영상의학과 교과서에서는 주로 난소종양(표면상피-기질종양, 생식세포종양 및 성끈기질종양) 혹은 자궁내막증과 같은 주로 조직학적 분류에 따라 병변의 특징에 대해 기술하고 있다. 그러나 2020 년 미국영상의학협회(American College of Radiology) O-RADS MRI 위원회에서 발표한 O-RADS 기반의 자궁부속기 병변의 분류에서는 자궁부속기 병변을 양성 및 고형성 병변, 조영증강 특성 등의 정의된 lexicon 에 따라서 구분하며, 이를 토대로 악성의 위험도를 총 5 단계(1-5)로 구분하고 있다. 이러한 병변 형태에 따른 접근 및 감별진단은 실제 진단 현장에서는 조직학적 분류에 따른 접근법보다 좀 더 실용적일 수 있다. 따라서 이 강의에서는 자궁부속기 종괴에 대해 병변의 형태에 따른 접근법과 감별 진단에 대해 다룰 것이다.

1. 병변 형태에 의한 감별

자궁부속기의 종괴는 크게 형태에 따라 양성, 양성 및 고형성과 고형 병변으로 분류할 수 있다. 고형종괴는 병변의 80% 이상이 고형조직일 때로 정의하며, 여기서 고형 조직은 조영증강을 보이는 유두모양돌기, 벽 결절, 3 mm 이상의 불규칙한 격막 및 큰 고형성분을 보일 때를 의미한다.

(1) 양성 종괴

단순 액체를 포함한 경우와 비단순 액체(지질 성분, 자궁내막종 성분, 단백질성 액체)를 포함한 경우로 나눌 수 있다. 단순 액체를 포함한 경우로는 대표적으로 serous cystadenoma 가 있으며, 드물게 점액의 농도가 낮은 mucinous cystadenoma 도 단순 액체를 동반한 양성 종괴로 보일 수 있다.

비단순 액체를 포함한 낭성 종괴로는 성숙기형종(mature teratoma), 자궁내막종 및 점액을 분비하는 점액낭선종이 있으며, 점액낭선종은 흔히 얇은 격막으로 구분되는 다양한 신호강도의 다방성 종괴로 보인다.

(2) 낭성 및 고형성 종괴

종괴 내에 고형조직을 포함한 경우, 먼저 T2 강조영상과 확산강조영상에서 신호강도를 평가하여 주변 근육과 비슷하거나 낮은 강도의 균질한 저신호강도를 보이는지 확인한다. 이런 경우는 섬유화에 기인하며 대표적으로 fibroma 및 Brenner tumor 가 특징적인 T2 강조영상에서 낮은 신호강도를 보인다. 특징적인 저신호강도를 보이지 않는 경우에는 역동적 조영증강 영상에서 time-signal intensity curve 를 통한 조영증강 패턴으로 악성 여부 감별에 도움을 받을 수 있다.

1) 일측성 낭성 및 고형성 종괴

대개 표면상피에서 기원한 종양 중 경계성 종양 및 악성 종양이 이러한 형태로 보인다. 대표적으로 mucinous, endometrioid, clear cell 및 seromucinous tumor 들이 일측성으로 보인다. Adult granulosa cell tumor 도 일측성 낭성 및 고형성 종괴로 보일 수 있다.

2) 양측성 낭성 및 고형성 종괴

표면상피에서 기원한 종양 중 장액종양은 악성에서 약 50%가 양측성으로 나타난다. 또한 난소의 전이암도 80%가 양측성으로 나타난다.

(3) 고형성 종괴

T2 강조영상에서 특징적인 저신호강도를 보이는 고형성 종괴로는 fibroma, fibrothecoma 및 Brenner tumor 가 있다. 이러한 특징적인 저신호강도를 보이지 않는 경우는 표면상피-기질에서 기원한 악성종양, 생식세포종양, 성관기질종양이 모두 고형성 종괴로 보일 수 있고, 이 경우 환자의 연령이 감별진단에 중요한 역할을 한다.

30 세 이하 여성에서는 생식세포종양이 흔하며, juvenile granulosa cell tumor 도 감별진단에 포함시킬 수 있다. 30 세 이상 여성에서는 악성 표면상피-기질종양, 성관기질종양, 전이성 암 혹은 림프종을 감별해 볼 수 있다.

Pregnancy-related Genitourinary Emergency

박성빈

중앙대학교병원 영상학과

Introduction

- Diagnostic imaging during pregnancy – US & MRI
- US – most widely accepted primary and valuable imaging modality of choice
- Unique or closed to the pregnancy and postpartum
- It is important and critical to keep in mind these disorders or condition → proper diagnosis and patients, fetal care as well

Unique to Pregnant Women

- Ectopic Pregnancy
- Spontaneous Abortion
- Subchorionic Hemorrhage
- Gestational Trophoblastic Disease
- Placental Abnormalities
 - Placenta Previa
 - Vasa Previa
 - Adhesive Placental Disease
 - Retained Products of Conception (RPOC)

자궁외임신 (Ectopic pregnancy: EP)

자궁외임신은 수정된 난자가 자궁강외에 착상하는 것으로 전체 임신의 1%를 차지한다. 질부터 복부까지 어디에서나 생길 수 있지만 97%가 난관에서 생긴다.

β -HCG 측정 예민도가 높아져 작은 크기의 자궁외임신을 조기에 진단하여 보존적인 치료를 할 수 있게 되었다. 임신 양성 반응을 보이는 환자에서 자궁강내 태낭(gestational sac, G-sac)이 없으면 자궁 부속기를 잘 관찰하여야 한다. β -HCG 가 discriminatory level (1000 IU/L (SIS), 1800 IU/L (IRP))이상이면 경질초음파 검사로 자궁강내 태낭이 보여야 한다. 일단 자궁내 태낭이 확인되면 실질적으로 자궁외임신을 배제할 수 있다 (1/30000). 그러나 IVF 환자에선 자궁내외임신 heterotopic pregnancy)이 1%이므로 이를 염두에 두어야 한다.

자궁외임신의 초음파 검사상 cystic or solid adnexal mass ("tubal ring"), free echogenic or sonolucent intraperitoneal fluid, hematosalpinx, 혹은 extrauterine gestational sac containing a yolk sac with or without an embryo 소견이 흔하다. Color Doppler로 trophoblastic flow를 확인하면 진단에 도움이 될 수 있다. "tubal ring"은 외장성 황체낭과 구별이 어려운 경우가 있는데 난소와의 위치를 확인하여 감별하여야 한다.

난황낭이 생기기 전의 정상 태낭은 자궁외임신 때 자궁강내 액체 저류에 의한 pseudogestational sac과 구별해야 되는데, 자궁내 태낭은 자궁강내에 비대칭적으로 비후된 탈락막에 낭성 구조물이 치우쳐서 생긴 double-decidual sac sign을 보여 구별된다.

초음파 소견상 명확한 "tubal ring"소견을 보이면 파열되지 않은 자궁외임신이며, 그렇지 않은 부속기 종괴이거나 복강내 출혈이 있으면 파열된 것일 가능성이 있다. 그러나 복강내 출혈의 양이 난관 파열과 상관관계가 있는 것은 아니며, 난관채를 통한 출혈이나 난관 유산, 임신중 황체낭의 파열로 대량의 복강내 출혈이 발생할 수 있다.

임신 양성 반응을 보이면서 자궁내 태낭이 보이지 않는 경우, 초기 정상 임신, 자연 유산, 너무 작거나 유산된 자궁외임신의 가능성이 모두 있으므로 β -HCG와 함께 추적 초음파 검사를 해야 한다.

난관임신의 자연흡수(spontaneous resolution)되는 경우도 있는데, β -HCG가 감소하거나-1000(mIU/mL, SIS)이하-, 확실한 태낭 형성이 없이 난관혈종소견을 보이고, 태낭 주위의 혈류가 없는 경우 그 가능성이 높아 약물치료를 하기도 한다.

자궁각임신(interstitial or cornual pregnancy)은 자궁외임신의 2-4%를 차지하나, 자연 파열로 출혈이 심해 이환율과 사망률이 높다. 초음파 검사상 자궁각 부위가

돌출되고 얇아진 자궁근층이 태낭을 둘러싸고 있으면 자궁각임신으로 진단할 수 있다.

자궁경부임신(cervical pregnancy)은 자궁외임신 중 1%가 안되지만 출혈 조절이 안될 가능성이 커 난관임신보다 예후가 나쁘다. 초음파로 trophoblastic flow나 embryo가 있는 태낭이 자궁 경부에 있으면 초음파로 진단을 할 수 있다. 심박동이 없는 배아가 있는 태낭이 자궁 경부에서 발견되면 절박유산과 감별해야 한다. 이때, 좀더 원형이나 난형 모양의 태낭, 심박동의 존재, 자궁 내구의 폐쇄, 추적 검사상 태낭이 일정한 모양과 위치를 보이면 자궁 경부 임신으로 진단 할 수 있다. 자궁외임신에 있어 MRI는 문제해결 방법(problem-solving tool)이 될 수 있으며,

착상위치를 정확하게 알 수 있고 난관을 비롯한 골반의 구조를 이해하는데 도움을 준다. MRI는 또한 Pregnancy of unknown location, heterotopic pregnancy, chronic ectopic pregnancy, unusual located ectopic pregnancy의 진단에 유용하다.

MRI소견은 자궁 밖의 태낭이나 혹은 혈종(extrauterine G-sac or hematoma)이다.

T2강조영상에서 세개의 층("three rings")을 보일 수 있으며, 확산강조영상과 ADC map에서 낭종의 벽을 따라 확산제한을 보인다("ring of restriction").

Closed to Pregnant Women

- Hemorrhagic Corpus Luteum
- Theca Lutein Cyst
 - Ovarian Hyperstimulation Syndrome (OHSS)
 - Hyperreactio Luteinalis
- Adnexal Torsion
- Red Degeneration of Uterine Leiomyoma
- Ovarian Vein Syndrome

출혈성 난소 낭종 (Hemorrhagic ovarian cyst/Ruptured ovarian cyst)

출혈성 난소 낭종은 갑작스러운 통증을 호소하며 대부분 40대 이하에서 발생한다. 기능성 낭종 특히 황체낭(corpus luteum cyst)의 출혈이 가장 흔한데 황체 내강으로의 과도한 출혈이나 흡수실패로 생기며 그 크기가 6 cm를 넘지 않는 것이 보통이다. 황체낭이 커지면 그 자체로도 pelvic pain을 일으킬 수 있지만 어떤 이유로 파열이 되면 비록 소량의 blood라도 peritoneum을 자극하게 되므로 acute abdominal pain을 호소한다. 거의 20, 30대의 젊은 여성에서 생긴다.

초음파 소견상, 시간에 따라 낭종의 내부에코가 변한다. 첫 6시간이내에는 저 에코, 혹은 불균일하게 보이며, 수 일 까지 에코도가 증가하다가 1-2주가 지나면서 점차 저에코로 변한다. echogenic complex mass면서도 후방 음영 증강을 보이며, 낭종은 다양한 내부에코를 보일 수 있다. 미세한 거미줄("web-like") 같은 소견이나, strands, homogenous low level echo, fluid-debris level, echogenic retracting clot, irregular nodular wall 등의 소견을 보여 종양과의 구별을 요하는 경우도 있다. Color Doppler 검사상 낭종 주변부의 "hypervascular ring"이 보이는 특징으로 감별이 가능하다.

단방성의 자궁내막증과 감별이 힘들지만 단기간의 추적검사에서 내부 에코가 변하는 소견으로 유추할 수 있으며, 다음 월경 주기에 재검사하면 줄어든 것을 확인할 수 있다.

출혈성 낭종이 파열되면(ruptured ovarian cyst), 초음파 소견상 낭종이 더 이상 보이지 않거나 낭벽이 쭉그러들어 불규칙해지고 두꺼워 보일 수 있으며, 복강내 출혈이 생겨 복강내 유 에코성 액체의 hemoperitoneum이 동반된다. 임상양상과 영상소견이 ruptured ectopic pregnancy와 유사하므로 pregnancy test나 serum β -HCG level이 매우 중요하다.

자궁 부속기 염전 (Adnexal torsion)

난소염전은 ovarian pedicle이 그 축을 중심으로 꼬여서 ovary나 ipsilateral fallopian tube (대개는 ovary와 tube 모두)가 partial or complete rotation되는 것이다. 먼저 venous and lymphatic drainage가 차단되어 ovary에 congestion and edema가 생기고, 시간이 흐르면서 arterial perfusion마저 차단되어 infarction이 생긴다. 주로 소아나 10대, 20대의 젊은 연령층에서 흔한데 성인 환자는 많은 수에서 underlying ovarian mass (mature cystic teratoma가 가장 흔하다) 가 있는 반면 소아는 adnexa가 mobile하기 때문에 ovarian mass가 없어도 torsion이 생길

수 있다. 간헐적인 심한 복통이 특징적이며 groin이나 thigh, back, flank으로 퍼지는 경우가 자주 있다. 난소 염전은 우측에서 더 흔하며(60%) 태아부터 폐경 후까지 모든 연령에서 생길 수 있다.

영상소견은 혈류 손상의 정도와 기간, 자궁부속기의 동반여부에 따라 다르다. 염전이 생긴 난소 종괴는 자궁 저부의 상부, 정중선상에 위치하는 경우가 자주 있다. 염전된 종괴나 낭종의 2차적 변화는 낭종벽의 비후와 종괴내 출혈을 보일 수 있고, 가끔은 부종으로 인해 비후된 정상 난소조직이 종괴 주변부에 보이기도 한다. 정상 난소가 염전되면 난소가 커지고 다수의 피막하 난포가 보이는데 이 소견은 임상적으로 적합할 경우 비교적 특이한 소견이다. 난관 염전이 동반되면 종괴나 커진 난소 주변부 근접한 비후된 난관이 관상 구조로 보이기도 한다. 막힌 림프와 정맥혈의 삼출로 소량의 저류액이 난소 종괴주위로 동반될 수 있다.

Twisted vascular pedicle은 adnexal torsion의 direct and specific finding이지만 보고자의 경험과 숙련도에 따라 sensitivity가 다양하다. Pedicle은 broad ligament, fallopian tube, adnexal and ovarian branches of uterine artery and vein으로 구성된다. Pedicle은 난소 종괴에서 돌출되는 solid mass처럼 보이며 자궁각쪽으로 연결된다. 평균크기는 약 4 cm이며 round echogenic mass with multiple concentric hypoechoic stripes (target appearance)로 보이는 경우가 많다. Color Doppler를 이용하면 염전경의 관찰이 더 용이하며, 내부 혈관의 혈류를 검사하여 난소의 생존성이 있을 경우 조기 진단 치료로 난소를 보존할 수 있다. 염전경내에 동, 정맥혈류가 존재하면 난소의 생존성이 94%로 보고된 바 있다. Doppler 스펙트럼상 초기에는 난소 내부의 정맥혈이 감소되고 동맥혈은 “spiky” 혈류를 보이다가, 나중에는 동맥과 정맥혈류가 모두 소실된다.

전통적으로 난소 염전의 치료는 색전증의 위험으로 염전정복(detorsion)을 하지 않고 자궁부속기 절제술을 시행하였다. 그러나, 실제로 보고된 색전증이 드물고 수술장이나 현미경 검사로 난소의 생존성을 예측하기 어려워 요즈음은 난소조직의 기능을 보존하기 위해 염전정복술이 우선되는 경향이다.

Postpartum

- Endometritis
- Placental Abnormalities
 - Retained Products of Conception (RPOC)
- Ovarian Vein Thrombosis
- Bladder Flap Hematoma
- Uterine Dehiscence and Rupture
- HELLP Syndrome
 - Hemolysis
 - Elevated Liver enzyme
 - Low Platelet count

Conclusion

The major teaching points of this lecture are

- It is important to know this pregnancy-related genitourinary emergency because it may influence the fetus as well as the pregnant woman.
- Familiarity with the clinical setting and imaging feature of pregnancy-related genitourinary emergency as depicted with US, CT and MRI will facilitate prompt and accurate diagnosis and treatment.

참고 문헌

- Andreotti RF, Harvey SM. Sonographic evaluation of acute pelvic pain. J Ultrasound Med. 2012; 31:1713-8.
- Kaakaji Y, Nghiem HV, Nodell C, Winter TC. Sonography of obstetric and gynecologic emergencies. Part I, Obstetric emergencies. AJR 2000; 174:641-9.
- Kaakaji Y, Nghiem HV, Nodell C, Winter TC. Sonography of obstetric and gynecologic emergencies. Part II, Gynecologic emergencies. AJR 2000; 174:651-6.
- Moore L, Wilson SR. Ultrasonography in obstetrics and gynecologic emergencies. RCNA 1994; 32:1005-22.
- Gopireddy DR, Le R, Virarkar MK, et al. Magnetic Resonance Imaging Evaluation of Ectopic Pregnancy: A Value-Added Review. J Comput Assist Tomogr. 2021; 45:374-82.
- Si MJ, Gui S, Fan Q, et al. Role of MRI in the early diagnosis of tubal ectopic pregnancy. Eur Radiol. 2016; 26:1971-80.
- Durur-Karakaya A, Seker M, Durur-Subasi i. Diffusion-weighted imaging in ectopic pregnancy: ring of restriction sign. Br J Radiol. 2018; 91:20170528.

13:30–14:00 Plenary lecture

좌장: 조정연 (서울대병원)



KSUR-30 years, The International Path

Seung Hyup KIM

Professor-emeritus of Radiology, SNUH

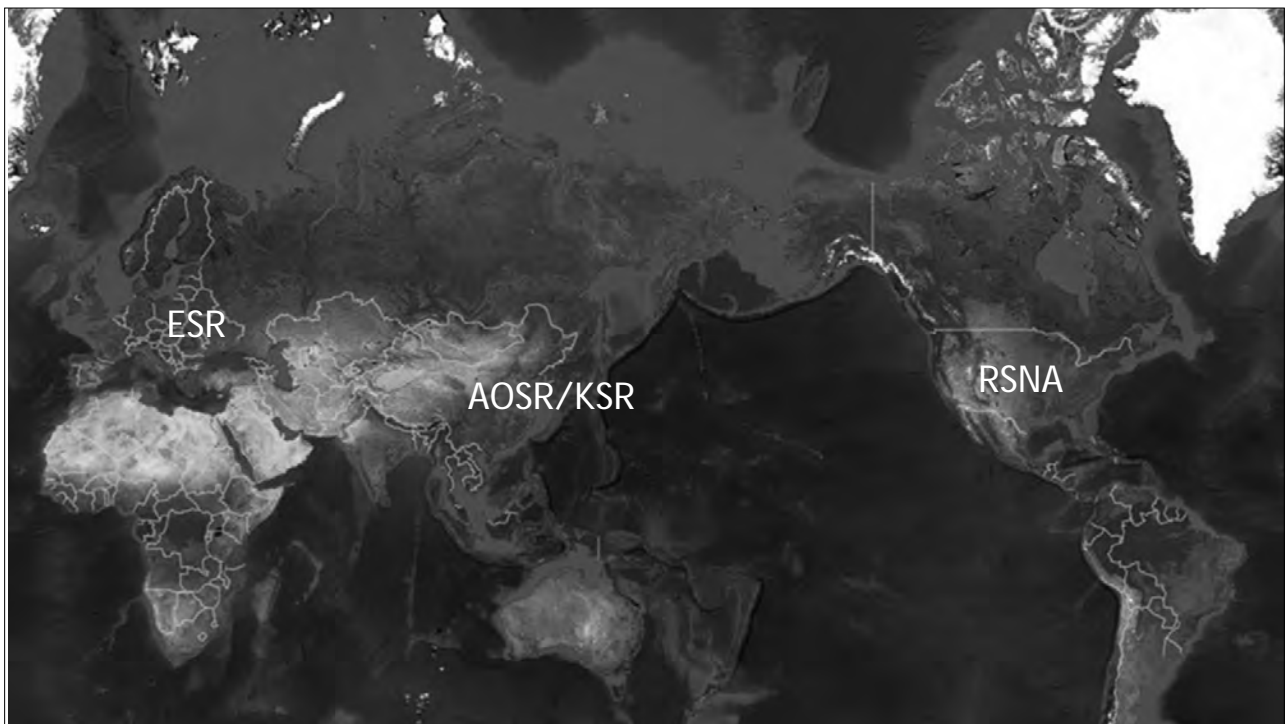
Consultant professor, EUMC

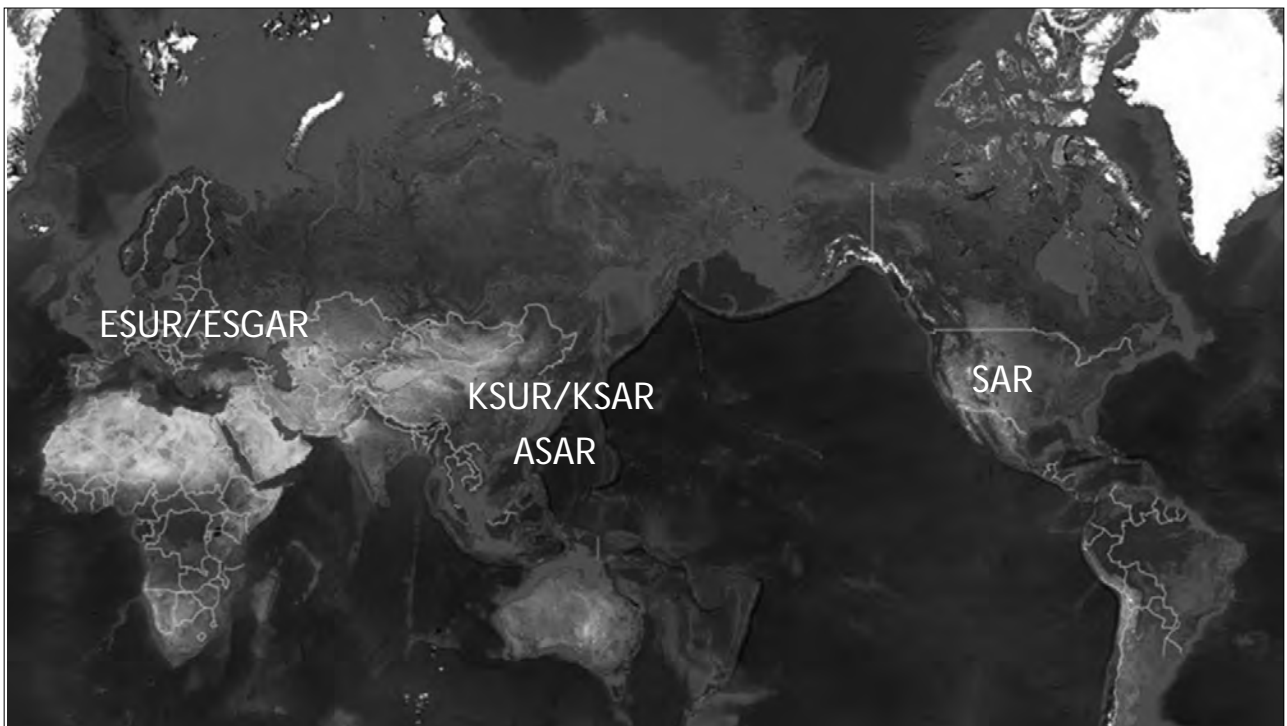
Director, K-Radiology Clinic and Research Institute of NCS

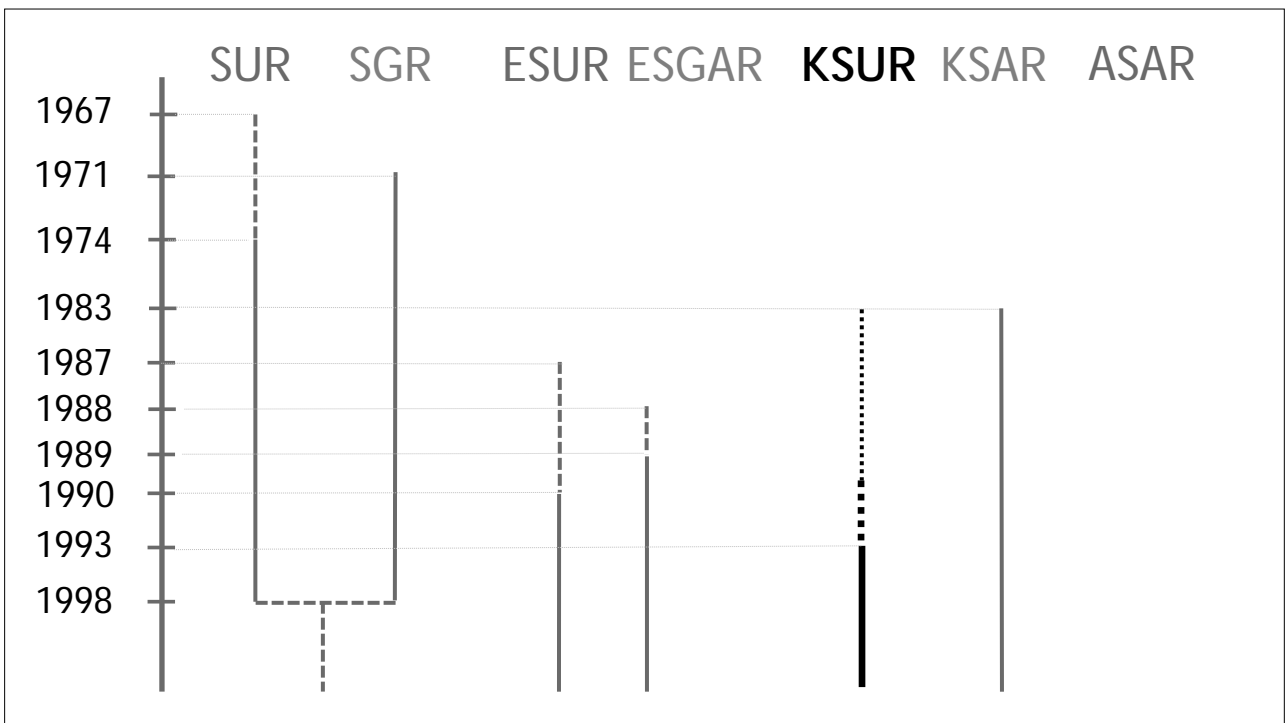


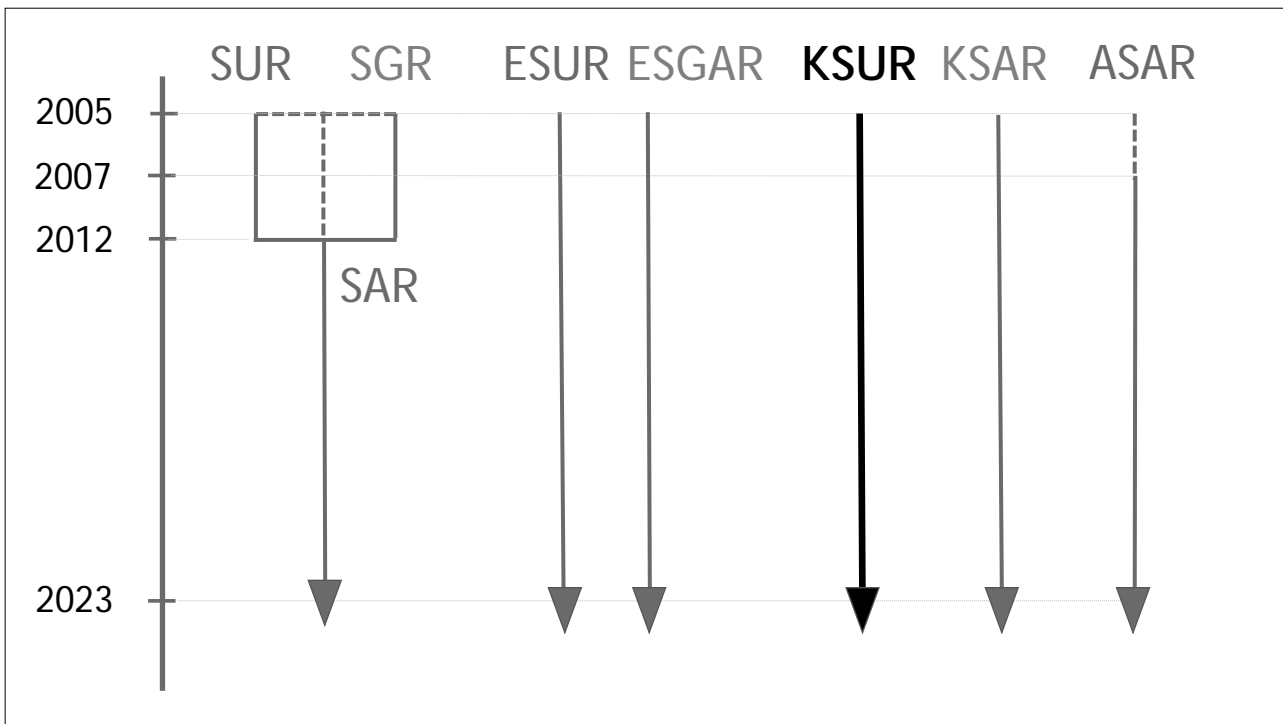
KSUR Founded in 1993

- Early 1980s, CT Study Group
- 1983, CT Study Group divided into
 - Neuroradiology Study Group
 - Abdominal Radiology Study Group
- 1993.2.22: Inaugural Meeting of KSUR (8 members)
- Bimonthly meeting → Monthly meeting











SUR Society of Uroradiology

- 1967 Correspondence Group
- 1974 SUR founded
- 1992 Cohabitation with SGR
- 2000 Partnership with SGR
- 2004 Abdominal Radiology Consortium
- 2012 SAR founded and SUR merged to SAR



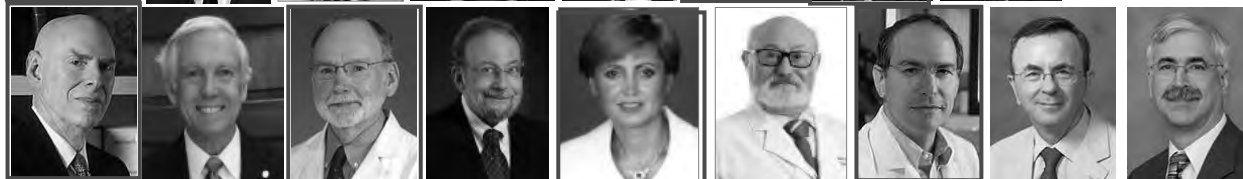
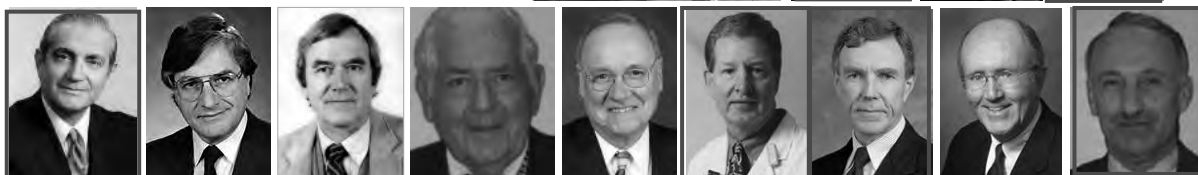
Howard Pollack



Joshua Becker



SUR Presidents (1974~2012)





ESUR European Society of Urogenital Radiology

1987 1st Copenhagen Symposium on Uroradiology

1990 ESUR founded

On August 26th, 1990, twelve uroradiologists met in the garden of Sven Dorph in Copenhagen



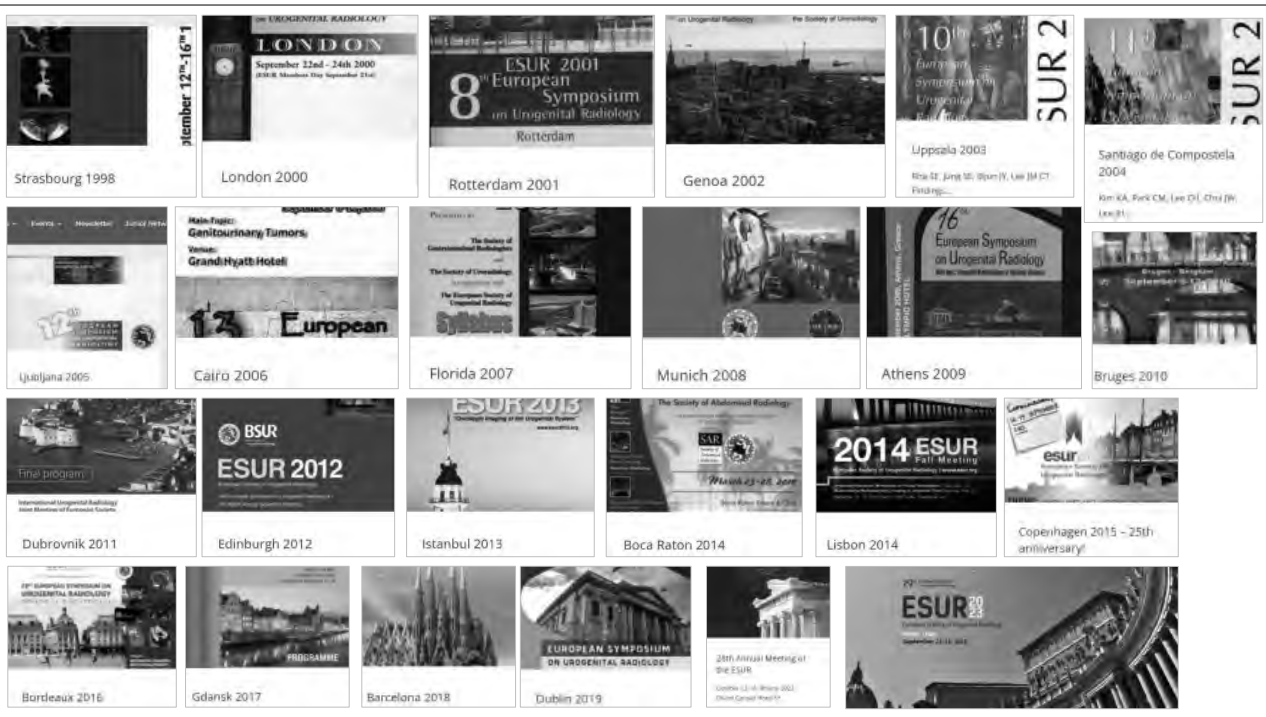
Ludovico Dalla Palma (IT)
Raymond Oyen (BE)
Henrik S. Thomsen (DK)



ESUR is an institutional member of ESR



ESUR Presidents (1990~)



Jean Francois Moreau



Bernd Hamm





ASAR Asian Society of Abdominal Radiology



- 2003 — Yuji Itai passed away
- 2005 — Agreed on forming ASAR at JSAR congress
- 2005 — 1st ACAR, Miyajaki, Japan



Choi BI. History of ASAR. KJR 2020;21:5-14



ASAR Presidents

Year	President	Country
2007 (Founding)	Osamu MATSUI	Japan
2007-2009	Jae Hoon LIM	Korea
2009-2011	Qiyong GUO	China
2011-2013	Byung Ihn CHOI	Korea
2013-2015	Yi-Hong CHOU	Chinese Taipei
2015-2017	Hiromu MORI	Japan
2017-2019	Seung Hyup KIM	Korea
2019-2021	Chang-Hong LIANG	China
2021-2022	Manabu MINAMI	Japan
2022-2023	Myeong-Jin KIM	Korea



2005, BSUR (British Society of Uroradiology)
 2013, DURS (Danish Society of Uroradiology)
 2022, ESGUR (Egyptian Society of Genitourinary Radiology)



Andrea Rockall



Evis Sala



Henrick Thomsen



Tarek El Diasty

2013, JSURT (Japanese Society of Uroradiologic and Therapeutic Technology)

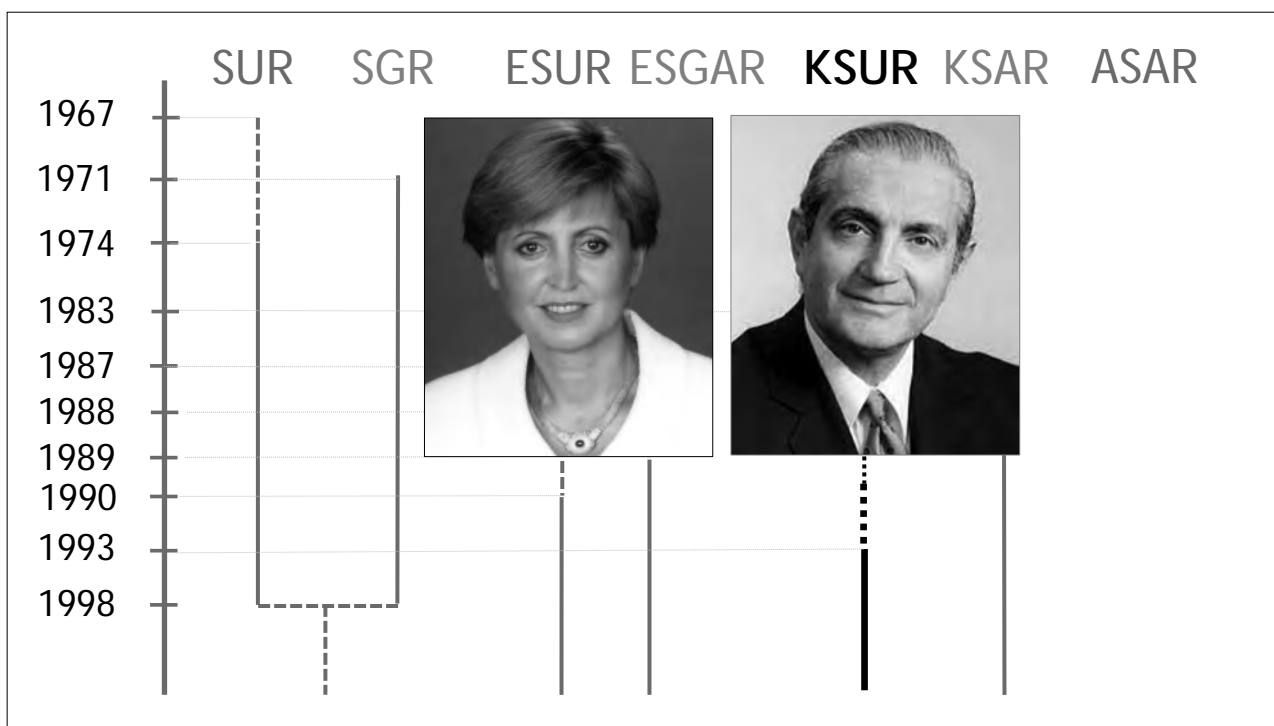


Kazuro Sugimura

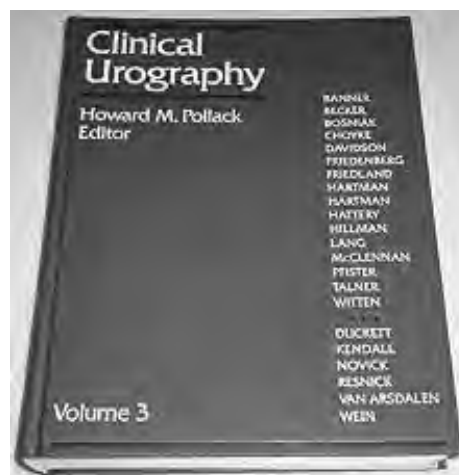


Masato Fujisawa





Howard M. Pollack, Great mentor

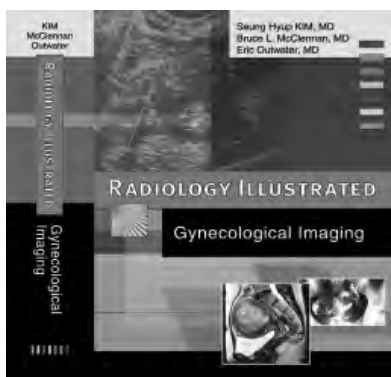
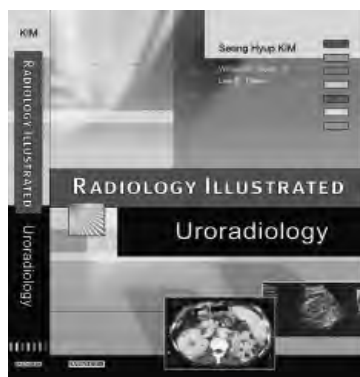


RADIOLOGY ILLUSTRATED

First edition

2003 Saunders / Elsevier

2005 Elsevier

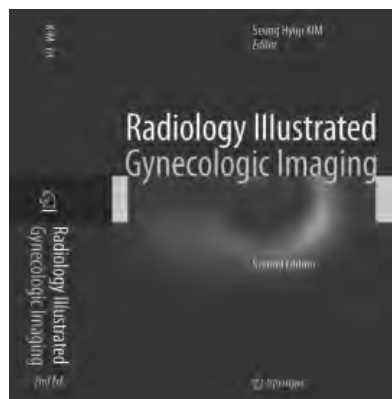
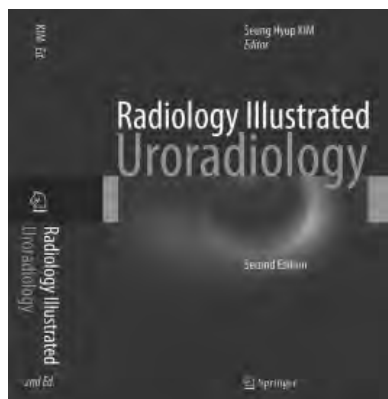


RADIOLOGY ILLUSTRATED

Second edition

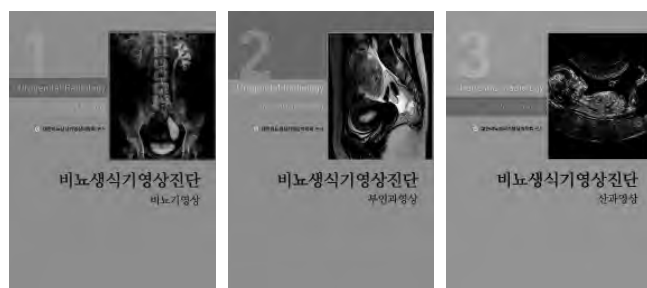
2011 Springer

2013 Springer



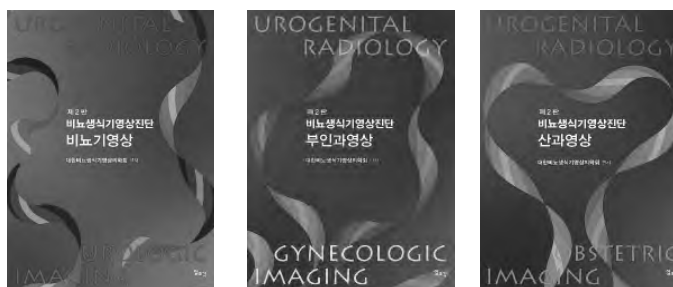


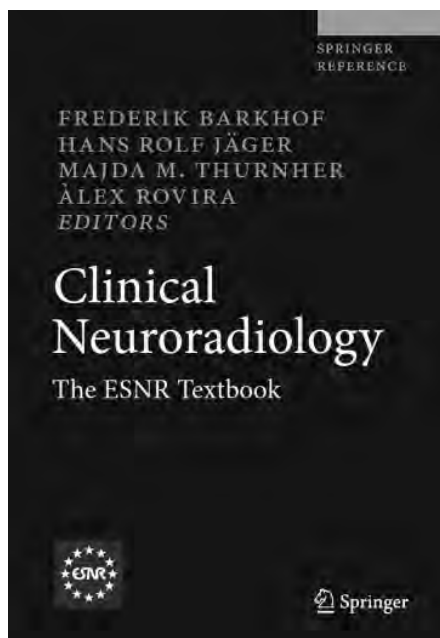
KSUR Publications



Second edition, 2019, 일조각

First edition, 2009, 일조각





Springer Major Reference Work
URORADIOLOGY
The KSUR Textbook

Springer Major Reference Work
GYNECOLOGIC IMAGING
The KSUR Textbook



Korean Academy of Medical Science has 158 member societies



대한영상의학회
The Korean Society of Radiology



KSR has 13 subspecialty societies



- KSNHNR Korean Society of Neuroradiology and Head and Neck Radiology
- KSTR Korean Society of Thoracic Radiology
- KSAR Korean Society of Abdominal Radiology
- KSPR Korean Society of Pediatric Radiology
- KSUR Korean Society of Urogenital Radiology**
- KSIR Korean Society of Interventional Radiology
- KSBI Korean Society of Breast Imaging
- KOSCI Korean Society of Cardiovascular Imaging
- KSMR Korean Society of Musculoskeletal Radiology
- KSTR Korean Society of Thyroid Radiology
- KSPSR Korean Society of Pain and Spine Radiology
- KSITA Korean Society of Image-guided Tumor Ablation
- KSER Korean Society of Emergency Radiology



14:20–15:50 Scientific Session (I)

좌장: 이영준 (은평성모병원)

정대철 (세브란스병원)

1

Fully automatic volume measurement of the adrenal gland on CT using deep learning to classify adrenal hyperplasia

김택민, 최승재, 조정연, 김영곤, 김상윤

서울대학교병원

Objectives: To develop a fully automated deep learning model for adrenal segmentation and to evaluate its performance in classifying adrenal hyperplasia.

Methods: This retrospective study evaluated automated adrenal segmentation in 308 abdominal CT scans from 48 patients with adrenal hyperplasia and 260 patients with normal glands from 2010 to 2021 (mean age, 42 years; 156 women). The dataset was split into training, validation, and test sets at a ratio of 6:2:2. Contrast-enhanced CT images and manually drawn adrenal gland masks were used to develop a U-Net-based segmentation model. Predicted adrenal volumes were obtained by fivefold splitting of the dataset without overlapping the test set. Adrenal volumes and anthropometric parameters (height, weight, and sex) were utilized to develop an algorithm to classify adrenal hyperplasia, using multilayer perceptron, support vector classification, a random forest classifier, and a decision tree classifier. To measure the performance of the developed model, the dice coefficient and intraclass correlation coefficient (ICC) were used for segmentation, and area under the receiver operating characteristic curve (AUC), accuracy, sensitivity, and specificity were used for classification.

Results: The model for segmenting adrenal glands achieved a Dice coefficient of 0.7009 for 308 cases and an ICC of 0.91 (95% CI, 0.90-0.93) for adrenal volume. The models for classifying hyperplasia had the following results: AUC, 0.98-0.99; accuracy, 0.948-0.961; sensitivity, 0.750-0.813; and specificity, 0.973-1.000.

Conclusion: The proposed segmentation algorithm can accurately segment the adrenal glands on CT scans and may help clinicians identify possible cases of adrenal hyperplasia.

2	<p>Optimal threshold values for the reduction of false-positive results of adrenal CT washout criteria</p> <p>강경아, 곽환민, 김찬교 삼성서울병원</p>
---	---

Objectives: To re-evaluate of the performance of modified criteria for the diagnosis of non-adenoma and investigate the change of false-positive rate of adrenal CT washout criteria after the addition of modified criteria.

Methods: We retrospectively included 266 patients with surgically proven lipid-poor adenoma (155/266, 58.3%) and non-adenoma (111/266, 41.7%) from two different cohorts. Non-adenoma group consisted of pheochromocytoma (n=66), metastasis (n=15), adrenocortical carcinoma (n=9) and neurogenic tumor (n=21). We subdivided previously reported modified criteria into three criteria to classify whether adrenal tumor is non-adenoma or not. Criteria I: absolute percentage washout (APW) <60% and relative percentage washout (RPW) <40%, Criteria II: intralesional cystic degeneration, and Criteria III: lesion attenuation on unenhanced CT ≥ 40 Hounsfield unit (HU), 1-min enhanced CT ≥ 160 HU or 15-min enhanced CT ≥ 70 HU. We analyzed are under the curve (AUC) and false positive rate before and after the addition of criteria II and III.

Results: Total 174 adenomas were diagnosed using adrenal CT washout criteria (APW $\geq 60\%$ or RPW $\geq 40\%$), however, 33 cases were actually non-adenomas (pheochromocytoma (n=28), metastasis (n=3) and adrenocortical carcinoma (n=2). This means that the false positive rate of adrenal CT washout criteria was 29.7%. The false positive rate was decreased from 29.7% to 7.2% after adding criteria II and III. At optimal threshold values for 40 HU for unenhanced CT, 160 HU for 1-min enhanced CT and 70 HU for 15-min enhanced CT for the diagnosis of non-adenoma, specificity were 92.9%, 94.8%, and 94.8%, respectively. The AUC was higher when criteria II and III were added (0.858) for the diagnosis of non-adenoma than when only criteria I was applied (0.806) ($P=0.047$).

Conclusion: The addition of modified criteria to the adrenal CT washout criteria has the potential to reduce false-positive results in the assessment of adrenal masses.

3

Differentiating Papillary Renal Neoplasm with Reverse Polarity from Papillary Renal Cell Carcinoma: Using a Radiomics Model Combined with CT Imaging Characteristics

이효정¹, 김택민², 조정연², 김상윤²

이화여대 서울병원¹, 서울대학교병원²

Objectives: This study aims to assess the computed tomography (CT) findings of papillary renal neoplasm with reverse polarity (PRNRP) and develop a radiomics-based model for differentiating PRNRPs and papillary renal cell carcinomas (PRCCs).

Methods: This retrospective study included 31 histologically confirmed PRNRPs and 68 PRCCs with preoperative three-phase kidney CTs. We conducted subjective image analysis to determine the CT parameters that can distinguish PRNRPs from PRCCs. A radiomics score was constructed with features selected using a least absolute shrinkage and selection operator algorithm. A radiomics-based model was built based on a radiomics score consisting of three reliable features and the subjective CT parameters using multivariate logistic regression. The diagnostic performance of the subjective CT parameters, radiomics model, and combination of them was compared using the area under the receiver-operating characteristic curve (AUC).

Results: The mean size of PRNRP was 16.7 ± 8.7 mm. On multivariate analysis, smaller mass size (OR 0.9; 95% CI 0.9–1.0, $P=0.013$), tumor heterogeneity (OR 8.8; 95% CI 1.9–41.4, $P=0.006$), and higher attenuation in pre-contrast CT (OR 1.1; 95% CI 1.0–1.2, $P=0.011$) were significant independent factors for identifying PRNRPs. The diagnostic performance of the combination model (AUC 0.923) was superior to that of subjective CT parameters (AUC 0.917) and the radiomics model (AUC 0.829).

Conclusion: A smaller size, heterogeneity and higher attenuation in pre-contrast CT were more closely associated with PRNRPs than with PRCCs. A combination of subjective CT features with radiomics model was useful for differentiating PRNRPs from PRCCs.

4

Preoperative Evaluation of Perirenal Fat Invasion of Renal Cell Carcinoma: Quantitative CT Imaging Characteristics

이효정¹, 김택민², 조정연², 김상윤²

이화여대 서울병원¹, 서울대학교병원²

Objectives: This study aims to evaluate the accuracy of CT in the diagnosis of perirenal fat invasion (PFI) of RCC and identify objective imaging characteristics based on CT.

Methods: This retrospective case-control study included 88 patients with PFI and 170 patients without PFI with appropriate preoperative CTs. We analyzed subjective and objective CT imaging parameters that can predict PFI. Multivariate logistic regression analyses were performed and diagnostic performance was calculated.

Results: The PFI group tended to have lobulated shape (71.6% vs. 40.0%), irregular margin (45.5% vs. 10.6%), and frequent perinephric changes including increased perirenal vascularity (62.5% vs. 40.6%), thickened fascia (47.7% vs. 11.8%), perinephric septation (56.8% vs. 25.3), perinephric stranding (59.1% vs. 25.3%) and perirenal nodule (9.1% vs. 0.6%) than the no-PFI group. The contact length (CL) and protruding distance (PD) were significantly longer in the PFI group (125.6 vs. 100.5mm, 31.2 vs. 25.5mm, respectively). The lobulated shape (OR=2.03), irregular margin (OR=3.59), thickened perirenal fascia (OR=4.38), and longer CL (OR=3.89) were significant predictors of PFI ($P<0.05$ for all).

Conclusion: The lobulated shape, irregular margin, thickened perirenal fascia, and longer CL might be useful for predicting the risk of PFI and selecting treatment options.

5	Evaluation of Renal Tumors with Ultrasound Shear-Wave Elastography 김민제, 김범준, 김찬교 삼성서울병원
---	--

Purpose: Ultrasound (US) shear-wave elastography (SWE) assesses quantitatively the tissue stiffness. The aim of our study was to investigate the utility of SWE in evaluating patients with various renal tumors.

Materials and Methods: 92 patients (mean age, 61.9 years; range, 23–90 years) with pathologically confirmed 69 malignant renal tumors [45 renal cell carcinomas (RCCs), 14 urothelial carcinomas, 6 metastasis, and 4 lymphomas] and 23 benign renal tumors [20 angiomyolipomas (AMLs) and 3 oncocytomas] performed SWE before biopsy or surgery. All US and SWE examinations of renal tumors were performed using the Philips EPIQ ultrasound system. Tissue stiffness in the renal tumors was measured using a region of interest, and maximum (E_{max}), mean (E_{mean}), and median (E_{med}) values were generated. Clinical and US variables were compared between malignant and benign renal tumors, between RCCs and AMLs, and among RCCs, AMLs, and urothelial cancers. The diagnostic performance of quantitative SWE and clinical variables to distinguish between malignant and benign tumors, and between RCCs and AMLs was performed using a receiver operating characteristics (ROC) curve analysis.

Results: The values of all SWE variables of malignant tumors were significantly lower than those of benign tumors (all $P < 0.05$). The E_{mean} (8.3 kPa), E_{med} (7.9 kPa) and E_{max} (15.8 kPa) values of RCCs were significantly lower than those of AMLs (13.8 kPa, 13.4 kPa, and 12.3 kPa, respectively: all $P < 0.01$). All SWE variables of AMLs had significantly higher values than those of urothelial cancers (all $P < 0.01$), but no significant differences between RCCs and urothelial cancers were found ($P > 0.05$). For distinguishing between malignant and benign tumors, the areas under the ROC curve (AUCs) of the E_{mean}, E_{med}, and sex were 0.775, 0.773, and 0.723, followed by E_{max} (AUC = 0.699). For distinguish between RCCs and AMLs, the AUCs of the sex, E_{mean}, and E_{med} were 0.850, 0.782, and 0.781, followed by E_{max} (AUC = 0.756); AUC of combined the sex and E_{mean} reached 0.921.

Conclusion: SWE, as a noninvasive tool, may be useful in distinguishing between malignant and benign renal tumor, between RCC and AML, and between AML and urothelial cancer. A larger study is warranted for further validation.

6

A machine learning model for predicting the genetic subtypes of prostate cancer using radiomics data extracted from T2-weighted prostate MRI images

윤종진, 한현호, 정대철, 강병철, 이종수, 오영택
세브란스병원

Objectives: Prostate cancer is a heterogeneous disease with a diverse transcriptome landscape, and its various genetic subtypes can result in variations in serum markers, drug sensitivities, androgen receptor activity, and prognosis. Previous research has identified four major genetic subtypes of prostate cancer (luminal A(Adipogenic/AR-active/PSA-high), luminal S(Secretory/PAP-high), AVPC-I(Aggressive Variant Prostate Cancer-Immune-infiltrative), and ACPV-M(Myc-active)) using public single cell-RNA sequencing database. Notably, the AVPC subtype has been found to be more resistant to AR inhibitor than the luminal subtype, while both the luminal-A and AVPC-M subtypes are resistant to docetaxel. The purpose of this study is to develop a machine learning model for predicting the genetic subtypes of prostate cancer using radiomics features extracted from T2-weighted prostate MRI images.

Methods: A total of 86 patients(median age : 74 years old) with pathologically proven prostate cancer were prospectively enrolled in this study between July 2020 and April 2022. For each patient, RNA sequencing was performed using the NovaSeq 6000 platform to calculate the probabilities of belonging to the four genetic subtypes: luminal-A, luminal-S, AVPC-I, and ACPV-M. Radiomics features were extracted from T2-weighted MRI images of the index lesion using PyRadiomics, resulting in 1,446 features. Feature selection was performed using the forward feature selection, and classification and regression were performed using support vector machine. To address imbalanced data, sample amplification was performed using SMOTE (Synthetic Minority Over-sampling Technique). Classification performance was evaluated using AUROC(Area Under the Receiver Operating Characteristic Curve), TPR(True Positive Rate), TNR(True Negative Rate), PPV(Positive Predictive Value), NPV(Negative Predictive Value), FPR(False Positive Rate), FNR(False Negative Rate), FDR(False Discovery Rate), and ACC(Accuracy), while regression performance was evaluated using MAE(Mean Absolute Error), MSE(Mean Squared Error), RMS (Root Mean Squared Error), and R-squared score. Statistical analysis was performed using scikit-learn and Python.

Results: Two binary classification SVM models were evaluated for predicting cancer types: one distinguishing between luminal (A or S) and AVPC (I or M) types, and the other distinguishing between luminal-A or ACPV-M types and luminal-B or ACPV-I types. Both models performed well, with AUROCs of 0.98 and 1.00, and TPRs, TNRs, PPVs, NPVs, FPRs, FNRs, FDRs, and ACCs close to or at 1.00. The regression SVM model showed moderate performance in predicting the probability of a tumor being luminal or luminal-A/AVPC-M type, with MAEs of 0.13 and 0.10, MSEs of 0.03 and 0.02, RMSEs of 0.16 and

0.13, and R-squares of 0.45 and 0.40, respectively. In the luminal vs. AVPC binary classification model, the following four features were selected using forward feature selection: 'diagnostics_Image-original_Minimum', 'original_glcM_MCC', 'wavelet-HLL_firstorder_Kurtosis', and 'wavelet-HLL_glszm_SizeZoneNonUniformity'. In the luminal-A/ACPV-M vs. luminal-B/ACPV-I binary classification model, 'wavelet-LLH_glszm_High Gray Level Zone Emphasis', 'wavelet-HLL_glszm_Size Zone Non Uniformity Normalized', 'square root_firstorder_Kurtosis', and 'square root_firstorder_Root Mean Squared' were selected.

Conclusion: In this study, we successfully developed radiomics models with high performance in binary classification and moderate performance in regression, demonstrating its potential as a non-invasive and cost-effective alternative to expensive RNA sequencing for predicting genetic subtypes of prostate cancer. This result suggests that the radiomics approach has the potential to be utilized not only for predicting genetic subtypes of prostate cancer, but also for assisting in the selection of treatment drug and prognosis prediction.

16:00–17:00 Scientific Session (II)

좌장: 김시형 (경북대병원,

조범상 (충북대병원)

7	<p>Utility of accelerated T2-weighted turbo spin-echo imaging with deep learning reconstruction in female pelvic MRI: A multi-reader study</p> <p>이은지 순천향대학교병원</p>
---	---

Objectives: To determine the clinical feasibility of T2-weighted turbo spin-echo (T2-TSE) imaging with deep learning reconstruction (DLR) in female pelvic MRI compared with conventional T2 TSE in terms of image quality and scan time.

Methods: Between May 2021 and September 2021, 52 women (mean age, 44 years±12) who underwent 3-T pelvic MRI with additional T2-TSE using a DLR algorithm were included in this single-center prospective study with patient's informed consents. Conventional, DLR, and DLR T2-TSE images with reduced scan times were independently assessed and compared by four radiologists. The overall image quality, differentiation of anatomic details, lesion conspicuity, and artifacts were evaluated using a five-point scale. Inter-observer agreement of the qualitative scores was compared and reader protocol preferences were then evaluated.

Results: In the qualitative analysis of all readers, fast DLR T2-TSE showed significantly better overall image quality, differentiation of anatomic regions, lesion conspicuity and lesser artifacts than conventional T2-TSE and DLR T2-TSE, despite approximately 50% reduction in scan time (all $p < 0.05$). The inter-reader agreement for the qualitative analysis was moderate to good. All readers preferred DLR over conventional T2-TSE regardless of scan time and preferred fast DLR T2-TSE (57.7–78.8%), except for one who preferred DLR over fast DLR T2-TSE (53.8% vs. 46.1%).

Conclusion: In female pelvic MRI, image quality and accelerated image acquisition for T2-TSE can be significantly improved by using DLR compared to conventional T2-TSE. Fast DLR T2-TSE was non-inferior to DLR T2-TSE in terms of reader preference and image quality. DLR of T2-TSE in female pelvic MRI enables fast imaging along with maintaining optimal image quality compared with parallel imaging-based conventional T2-TSE.

8	<p>Pretreatment CT differential diagnosis of tuberculous peritonitis from peritoneal carcinomatosis of advanced epithelial ovarian cancer</p> <p>이철민 한양대학교병원</p>
---	---

Objectives: Delayed diagnosis of female genital tuberculosis (FGTB) can lead to inappropriate treatment and unnecessary surgical procedures rather than standard anti-TB medication. We tried to evaluate the use of computed tomography (CT) imaging to differentiate TB peritonitis from peritoneal carcinomatosis of advanced epithelial ovarian cancer (AEOC).

Methods: We investigated women who underwent CT to distinguish between TB peritonitis and peritoneal carcinomatosis of AEOC. We evaluated various CT imaging features to identify differences between the two diseases. In addition, we performed univariate and multivariate logistic regression analyses to identify the independent imaging parameters associated with TB peritonitis and evaluated the diagnostic performance of the combined imaging parameters. We also performed the histopathological analysis of the available salpinx specimens of TB peritonitis.

Results: We included 25 women with TB peritonitis and 34 women with peritoneal carcinomatosis of AEOC. A multivariate analysis of the discriminant CT imaging features between the two diseases revealed that changes in fallopian tubes and peritoneal micronodules were independent parameters associated with TB peritonitis ($p \leq 0.012$). Combining the two imaging parameters showed an area under the receiver operating characteristic curve of 0.855, a sensitivity of 88.0%, and a specificity of 67.7% for differentiating TB peritonitis from peritoneal carcinomatosis. Furthermore, changes in fallopian tubes were correlated with histopathological abnormalities in salpinx specimens.

Conclusion: Pretreatment CT evaluation with useful imaging features could help differentiate TB peritonitis from peritoneal carcinomatosis of AEOC.

9

Pelvis MRI finding of Zinner syndrome: a case report

문성경

경희대학교병원

Zinner syndrome is a male counterpart of RMKH syndrome. It is resulted from the maldevelopment of distal part of mesonephric duct. Its typical triad of Mullerian duct abnormality is compromised of unilateral renal agenesis, ipsilateral seminal vesicle cyst, and ejaculatory duct obstruction. We experienced a 26-year-old male patient with Zinner syndrome. He had the fever and lower urinary symptoms of urethral pain and dysuria. The findings of TRUS, pelvic MRI, and cystoscopy was consistent with Zinner syndrome. Review of the image findings and literature will be discussed in this case presentation.

10

Granulomatous prostatitis and epididymitis after BCG instillation: a case report

문성경

경희대학교병원

A 66-year-old male has an elevated serum PSA level up to 51.26 ng/mL. He had a past history of bladder cancer and underwent the TUR-BT and BCG instillation 3 years ago. Serum PSA level has decreased, but been consistently high up to 11.732 ng/mL. Transrectal ultrasound (TRUS) and prostate MRI showed the several multifocal lesions. Pathologic diagnosis after TRUS-guided biopsy was prostate cancer with the granulomatous prostatitis. He underwent radical prostatectomy. Six months later, he had the right scrotal discomfort and underwent the scrotal US. US showed the right epididymis swelling and hyperemic change of right epididymitis. The inflammation was aggravated despite of the antibiotics therapy and hydrocelectomy. Scrotal US and MRI showed the massive swelling of right epididymitis and abscess ruptured toward the scrotal wall. The final diagnosis was the necrotizing granulomatous epididymo-orchitis with BCG granuloma with the specimen of right orchiectomy.

As the number of multiparametric prostate MRI has increased recently after PI-RADS version 2.1, the detection of granulomatous prostatitis also has been increased in the patients with BCG instillation histories accordingly. MR and US findings of granulomatous prostatitis and epididymo-orchitis will be reviewed in this case presentation.

11

Endocervical polyp presenting as a cystic cervical mass with concerning MRI features: a case report.

박수민

일산백병원 영상의학과

A 45-year-old woman with abnormal uterine bleeding with a cervical mass found on physical examination. Pelvic MRI revealed a multilocular cystic lesion in the cervix with a T2-weighted heterogeneous high/T1-weighted intermediate signal intensity, and an enhanced solid portion or septa-like structure on T1-weighted contrast-enhanced images, measuring 4.4x3.4x4.0cm. These MRI features are concerning for malignancy, particularly adenocarcinoma. Hysteroscopy was performed for the final diagnosis, and excisional biopsy confirmed that the lesion was an endocervical polyp.

This case highlights the importance of careful interpretation of MRI findings in patients with cervical cystic masses because benign lesions such as endocervical polyps can have concerning MRI features that mimic malignancy.

12

Cardiac metastasis from clear cell type renal cell carcinoma

박소형

일산백병원 영상의학과

A 62-year-old female patient who underwent Rt. nephrectomy due to clear cell type renal cell carcinoma didn't show evidence of metastasis in five annual follow-up chest and abdominopelvic CT. Enhanced chest CT in 2009 showed multiple lung metastasis and hypervascular nodular soft tissue mass with internal necrotic portion in left ventricular septum. There was no pericardial effusion. Although cardiac MR is not implemented in our patient, it could be suspected for cardiac metastasis from RCC, because the mass has increased in size in follow-up CT and the metastatic RCC was confirmed in tongue base and scalp additionally.

10:00 – 11:00 Prostate Imaging

좌장: 성득제 (고대안암병원)

윤성국 (동아대병원)

APIWG SURVEY: WHAT'S NOW AND NEXT

LI-JEN WANG, M.D., M.P.H.

CHAIR, DEPARTMENT OF MEDICAL IMAGING AND INTERVENTION, NEW TAIPEI MUNICIPAL
TUCHENG HOSPITAL, CHANG GUNG MEDICAL FOUNDATION, NEW TAIPEI CITY, TAIWAN

OUTLINES

- Asian Prostate Imaging Working Group (APIWG)
- APIWG survey: domains and results
- What are the lessons learned and perspectives

ASIA PROSTATE IMAGING WORKING GROUP (APIWG)



Professor, Chan Kyo Kim, South Korea, Past top-chair: 2019-2022



Professor Masahiro Jinzaki, Japan, co-chair



Professor Cher Heng Tan, Singapore, co-chair

Professor, Li-Jen Wang, Taiwan, current top-chair since 2023, Research subcommittee



Professor, Young Taik Oh, South Korea, International Liaison subcommittee (left)



Professor, Hiroshi Shinmoto, Japan, Clinical practice subcommittee (middle)



Professor, Chau Hung Lee, Singapore, Education subcommittee (right)

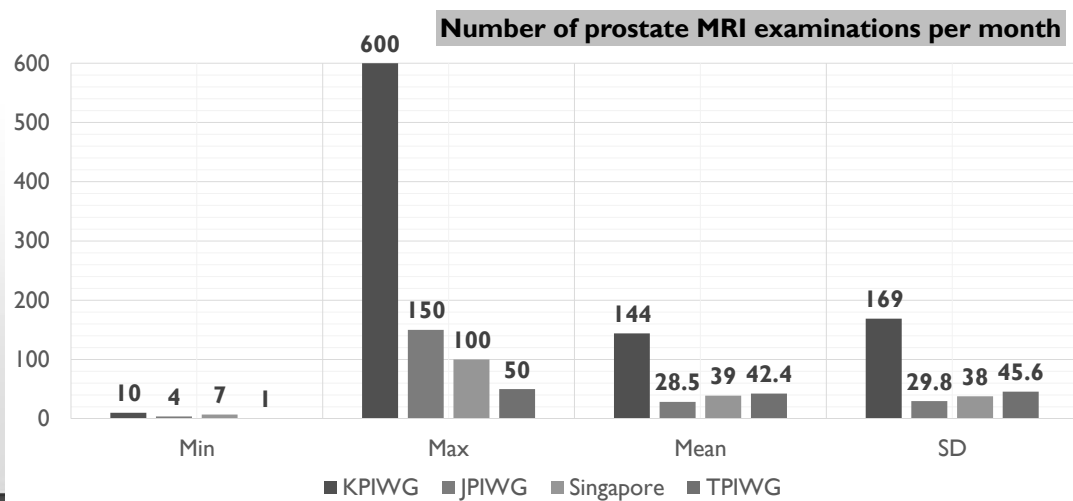
DOMAINS OF APIWG SURVEY

- Prostate MRI
 - Number, indications, scanners, coils, and preparations
 - Protocols, pulse sequences and imaging parameters, PIRADS
- Other prostate imaging: TRUS, prostate PET and PET/MRI
- Prostate biopsy: prostate target biopsy and MRI timing in relation to biopsy
- Prostate cancer status: PSA screening, stages and treatment

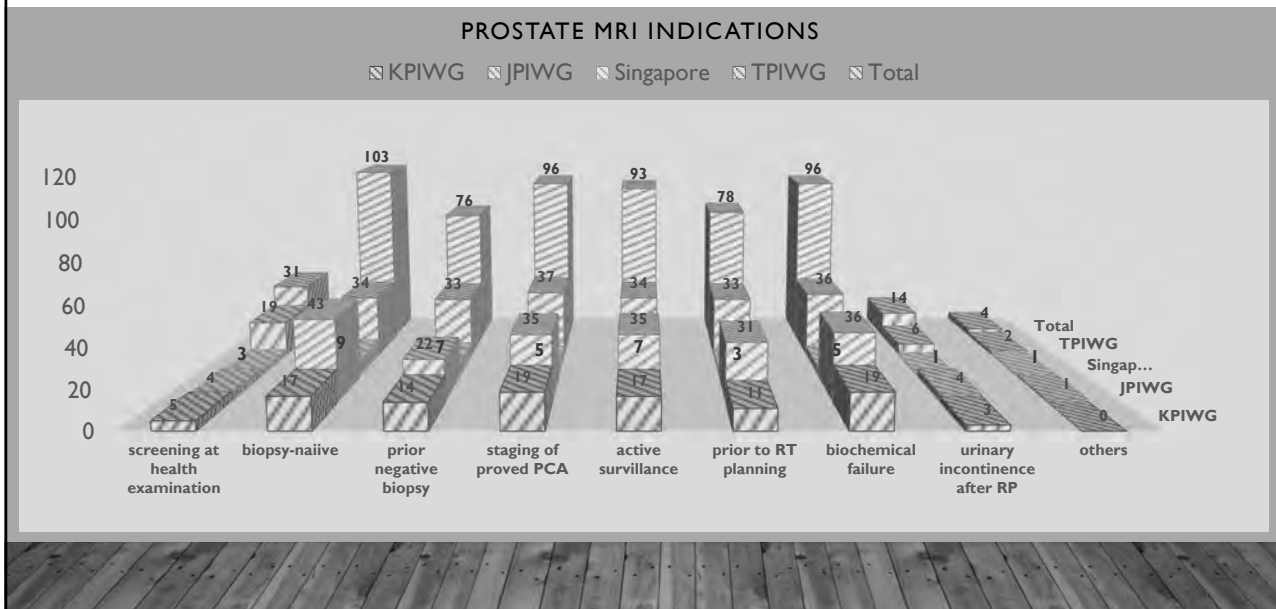
PROSTATE MRI_PART I

Number, scanners, coils, and preparations

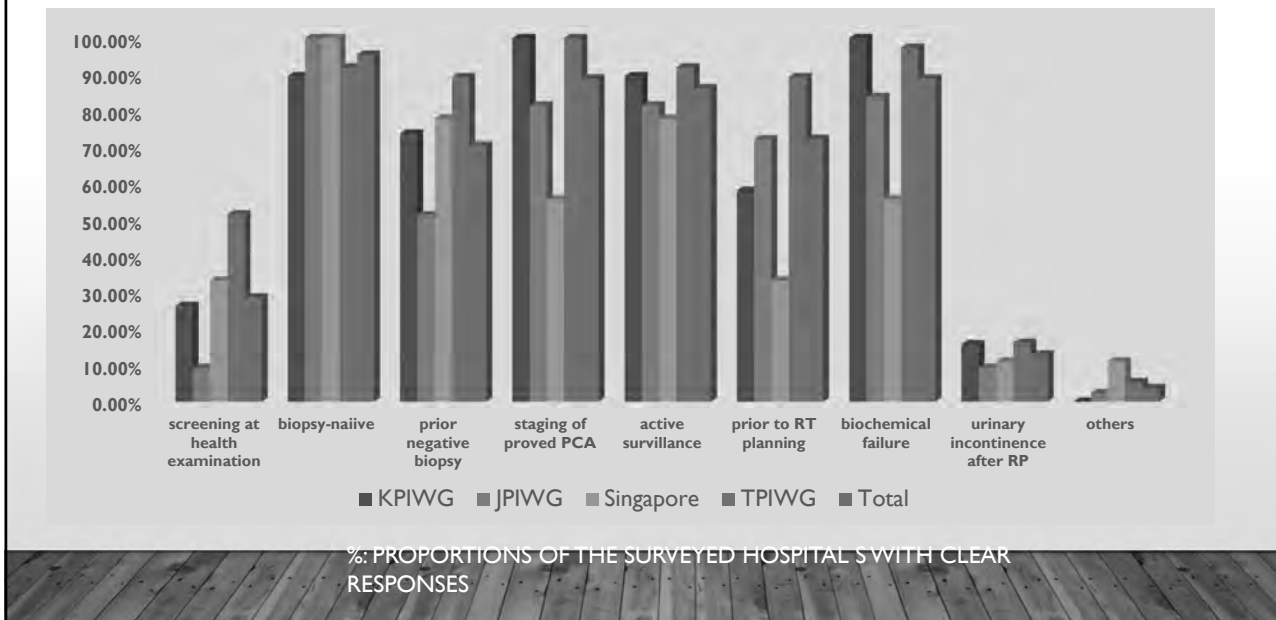
How many prostate MRI examinations are performed per month in your hospital?



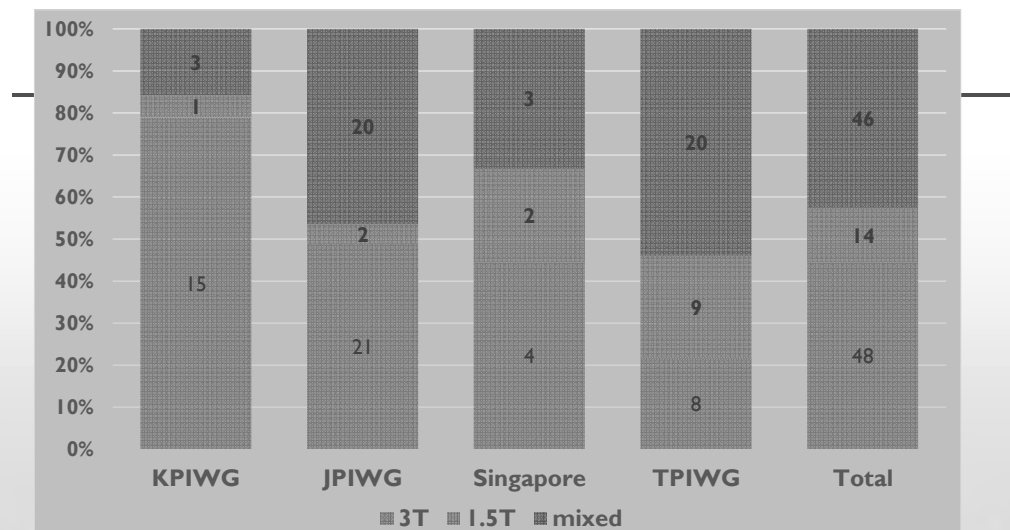
What are the indications for prostate MRI in your hospital (multiple



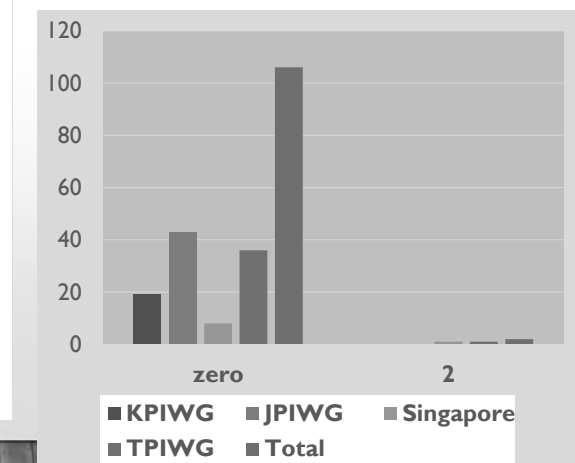
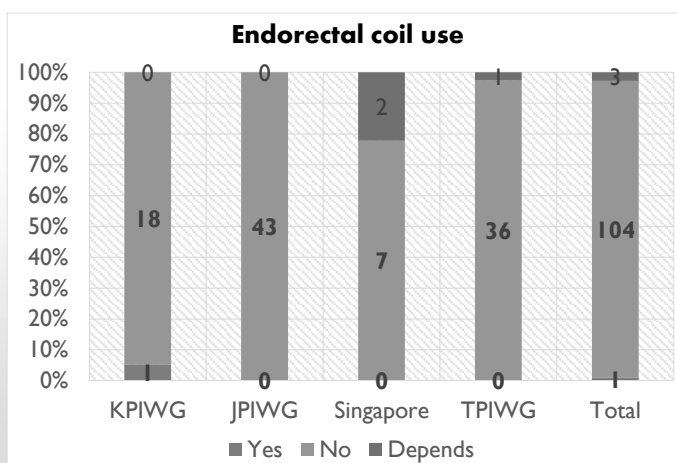
What are the indications for prostate MRI in your hospital (multiple choices)?



What kinds of MR scanners do you use for prostate MRI?

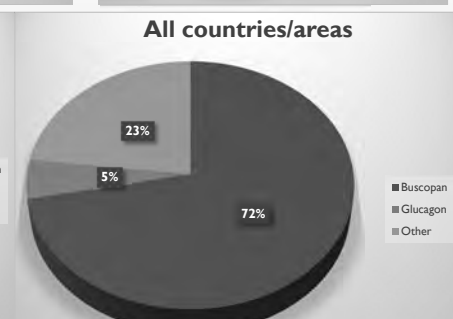
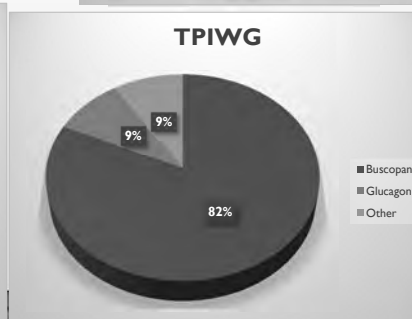
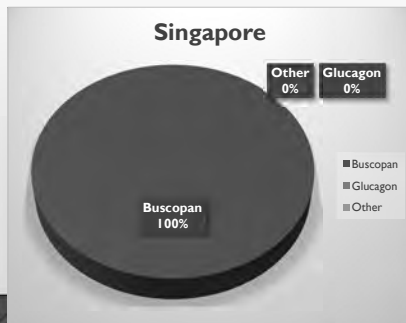
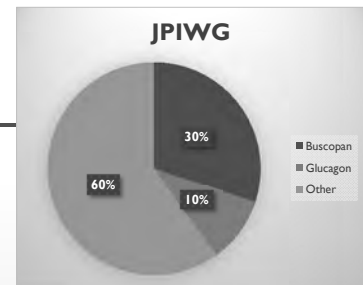
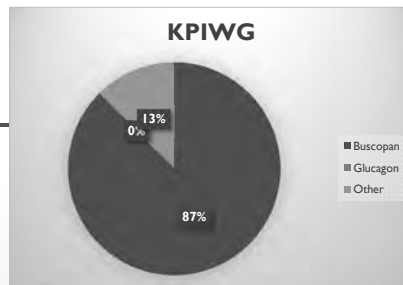


Do you use endorectal coils routinely for prostate cancer MRI? If used, how many per month?

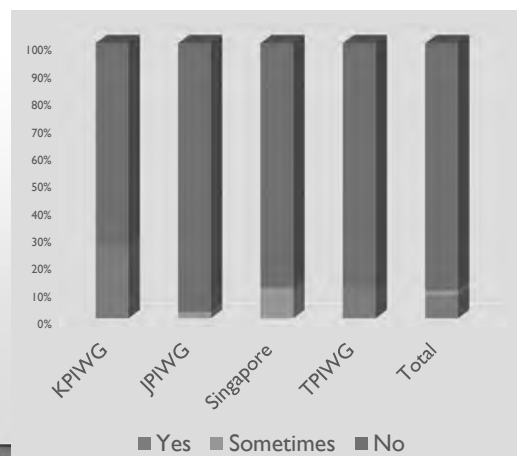
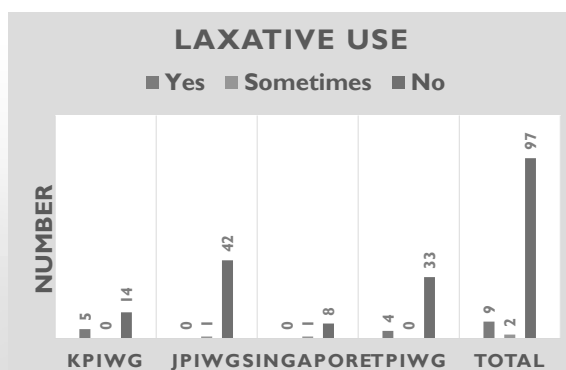


Do you use anti-spasmodic agent for prostate MRI routinely?

Society	Yes	No Use
KPIWG	16 (84 %)	3 (16 %)
JPIWG	10 (23%)	33 (77 %)
Singapore	2 (22 %)	7 (78 %)
TPIWG	11 (30%)	26 (70%)
Total	39 (36%)	69 (64 %)



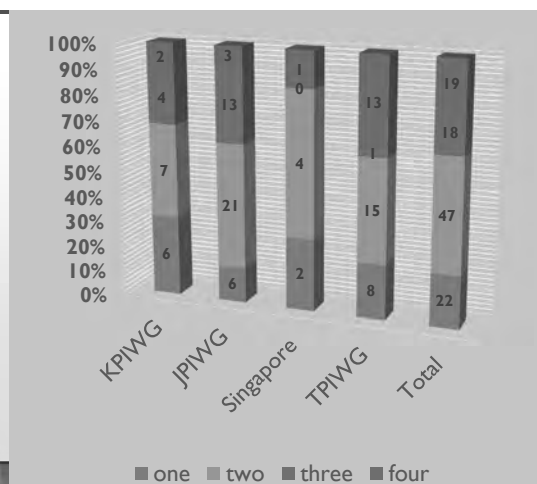
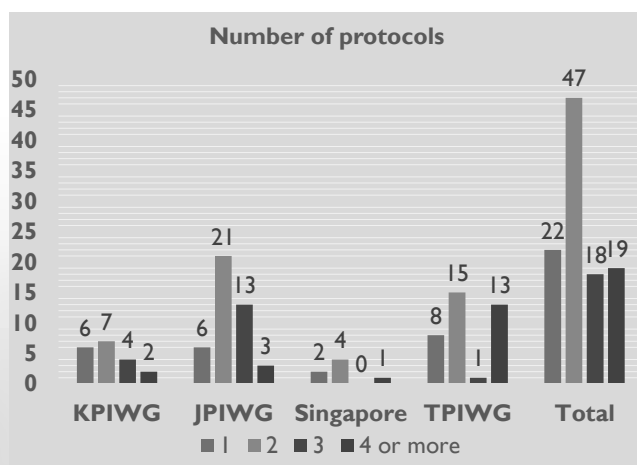
Do you prescribe laxatives to patients for prostate MRI routinely?



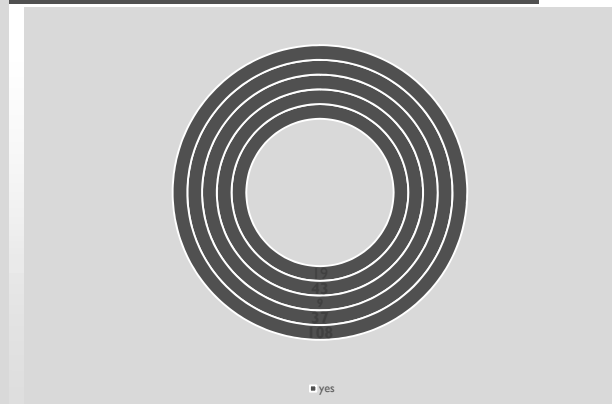
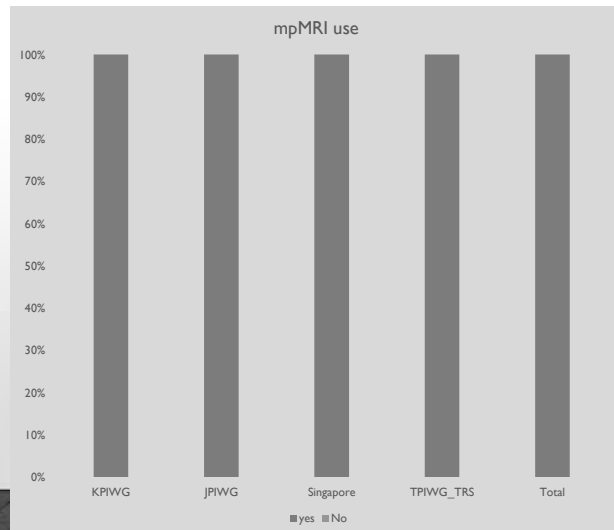
PROSTATE MRI_PART 2

Protocols, pulse sequences and imaging parameters
as well as PIRADS

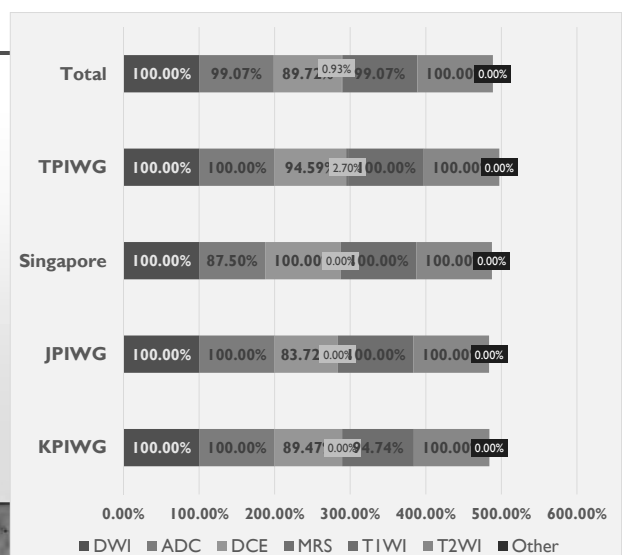
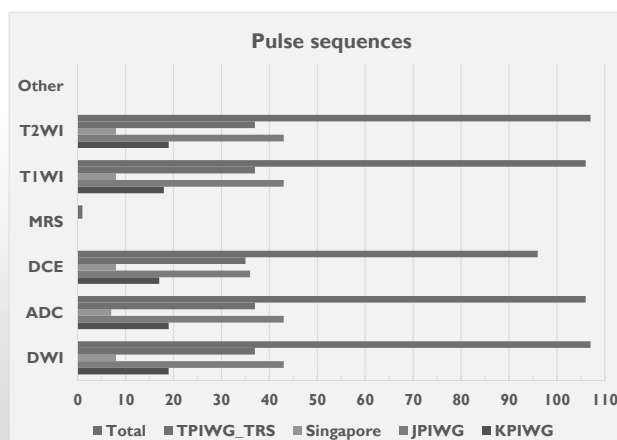
How many routine protocols for prostate MRI in your hospital?



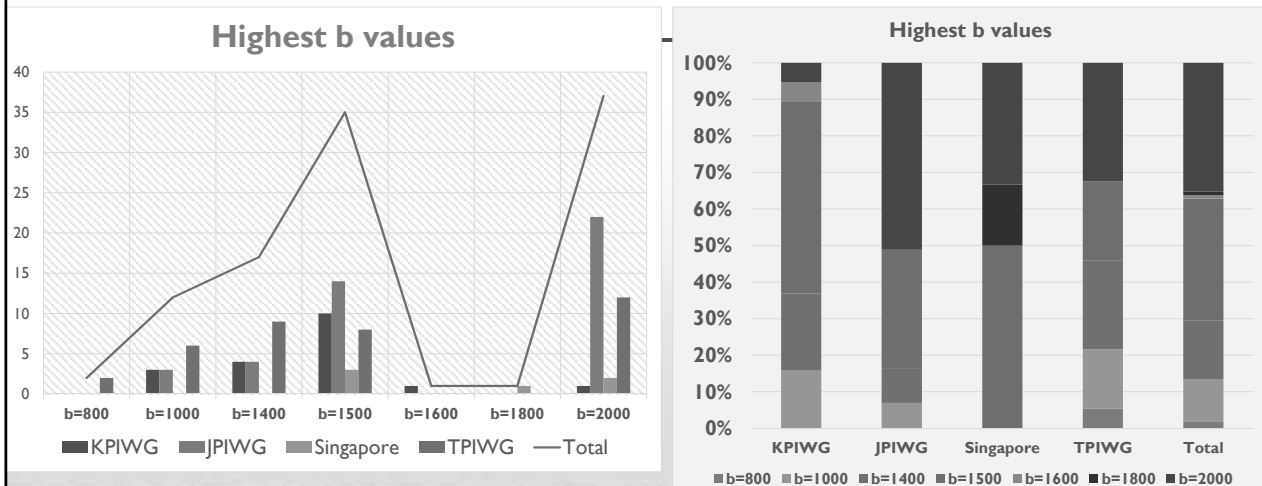
Do you use multiparametric prostate MRI for prostate imaging?



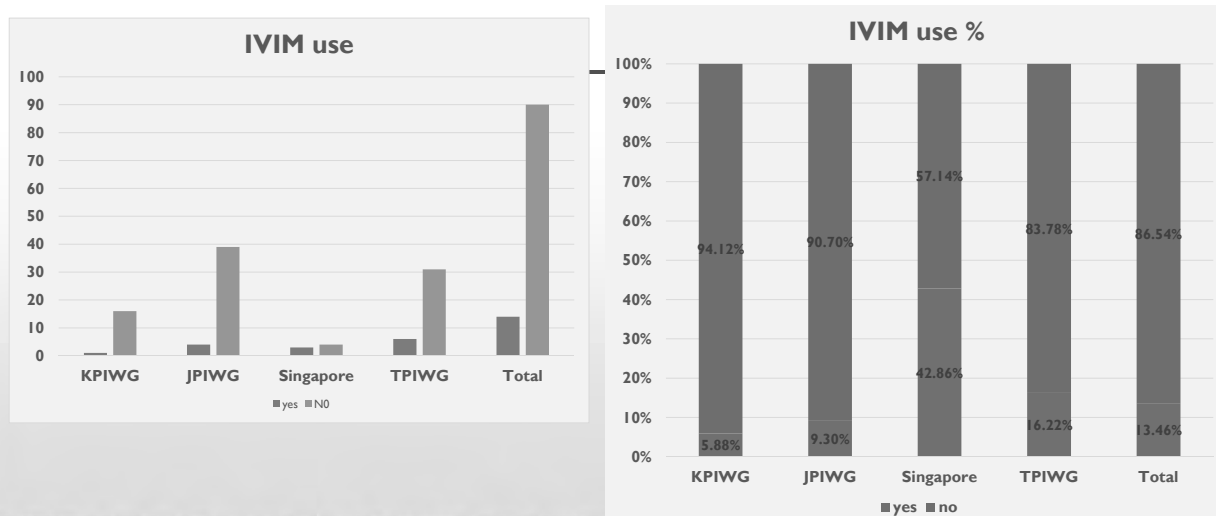
Q10. What are the pulse sequences included of your mpProstate MRI (Multiple choices if yes)?



What are your highest b values used in mp prostate MRI?

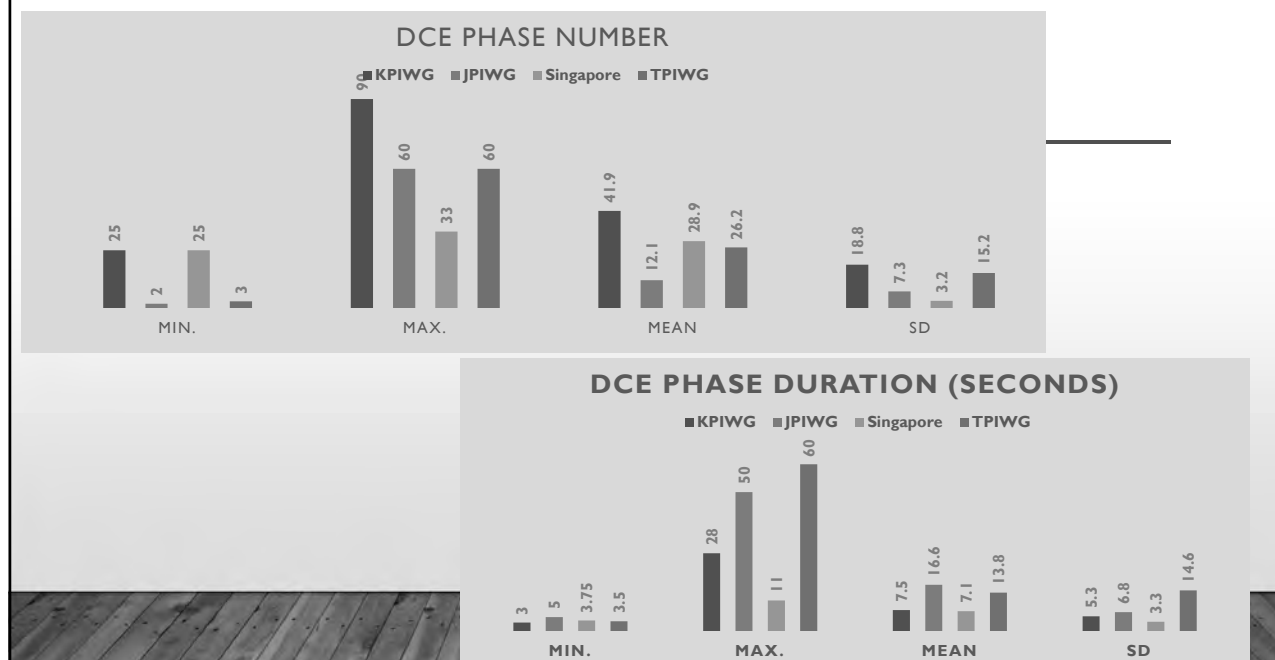


Do you use IVIM for prostate MRI?

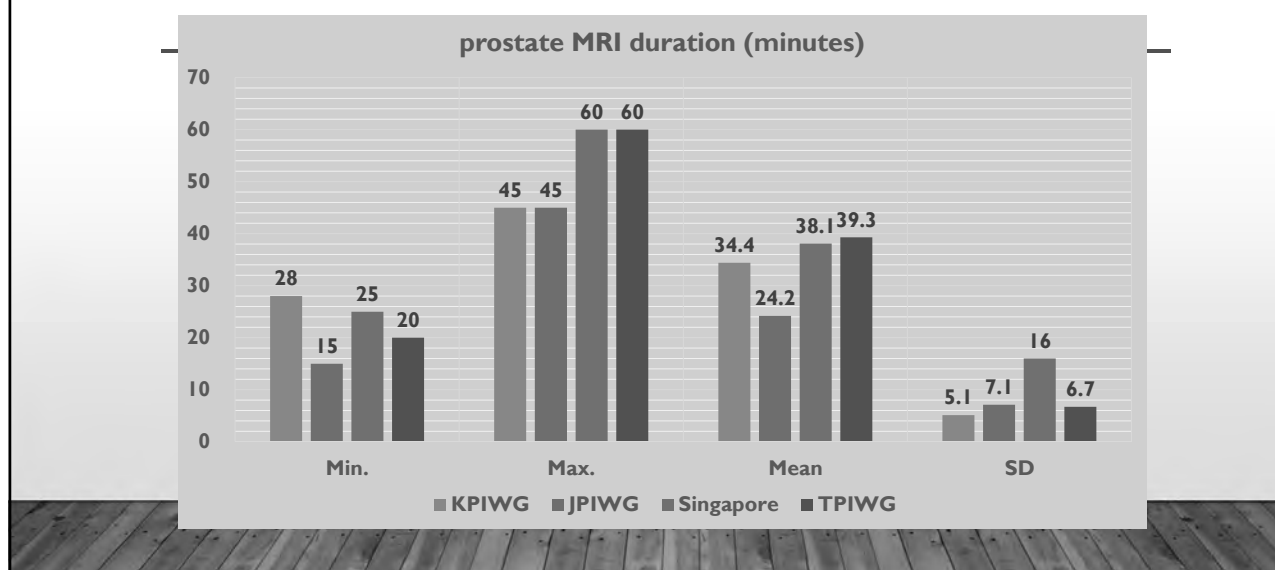


%: PROPORTIONS OF THE SURVEYED HOSPITAL S WITH CLEAR RESPONSES

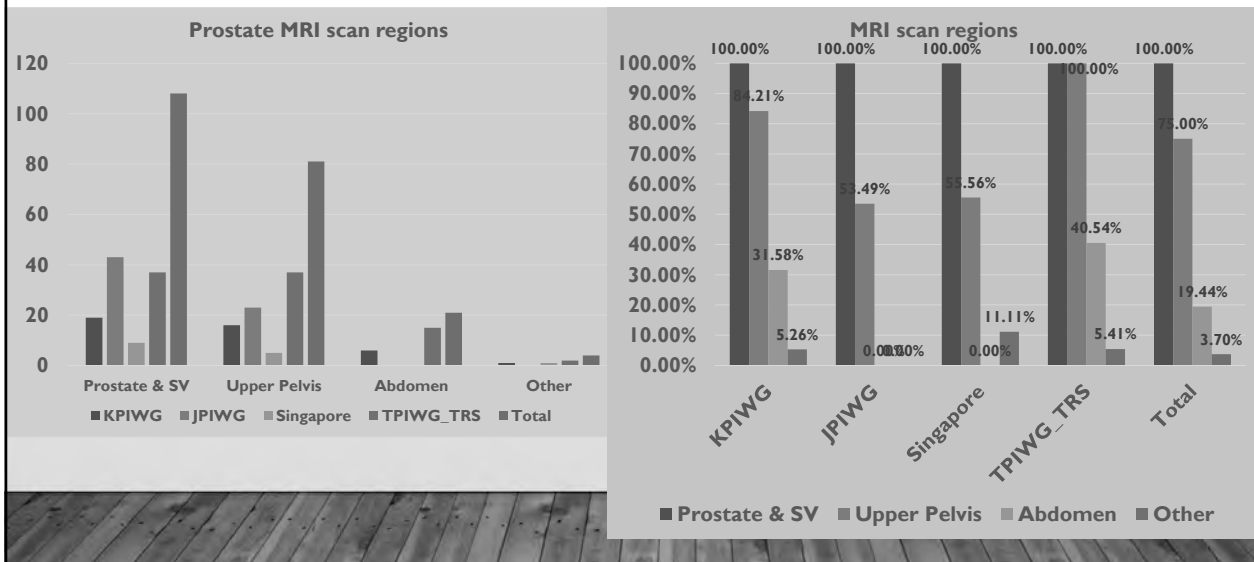
How many phases and the duration of each phase of your DCE protocol



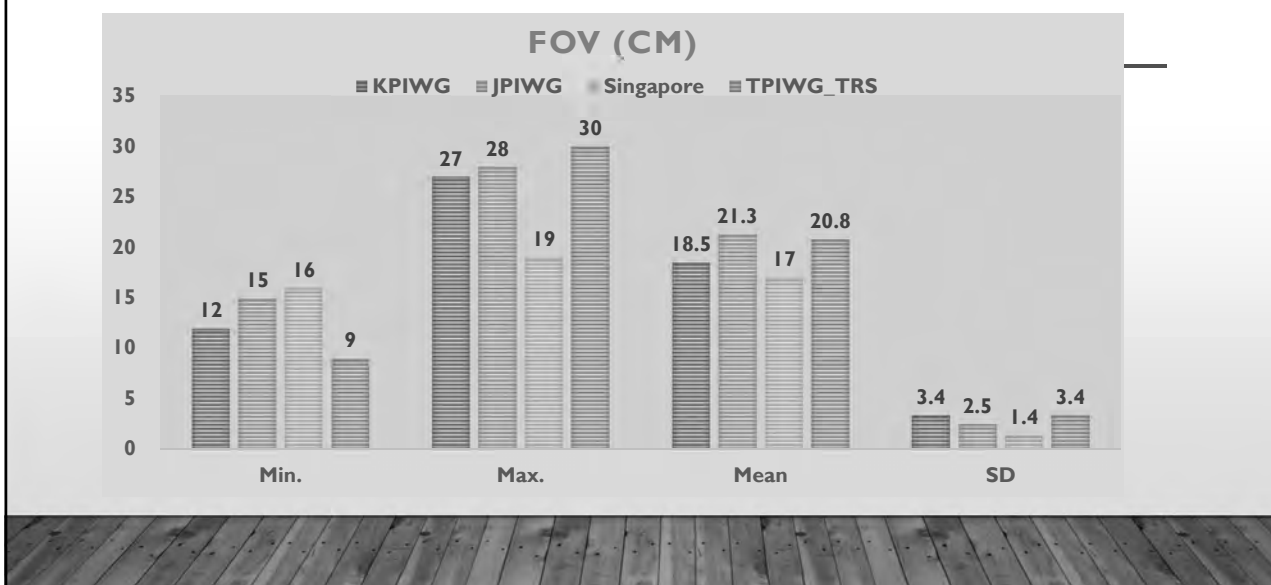
How long does it take for each prostate MRI examination in your hospital (in average)?



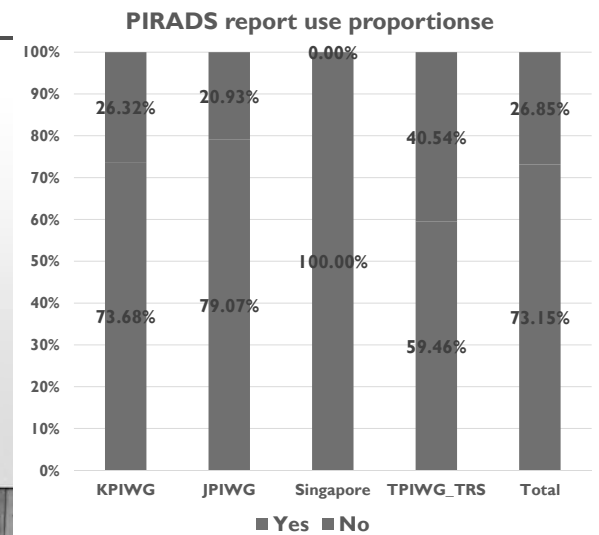
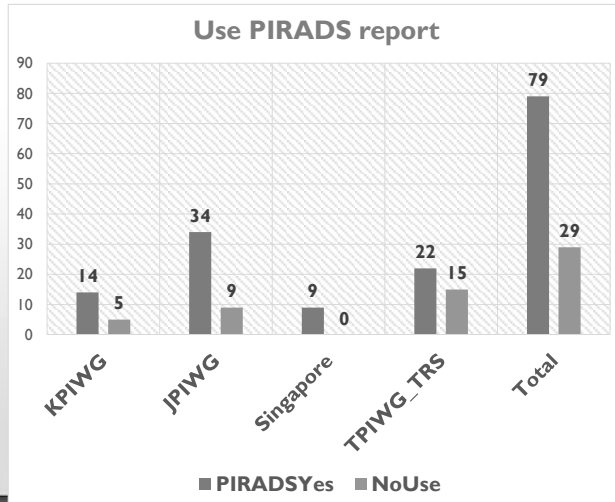
**Which of the followings are the scan regions of your routine prostate MRI
(multiple choices)?**



What is your FOV of scanning prostate and seminal vesicle regions on prostate MRI?



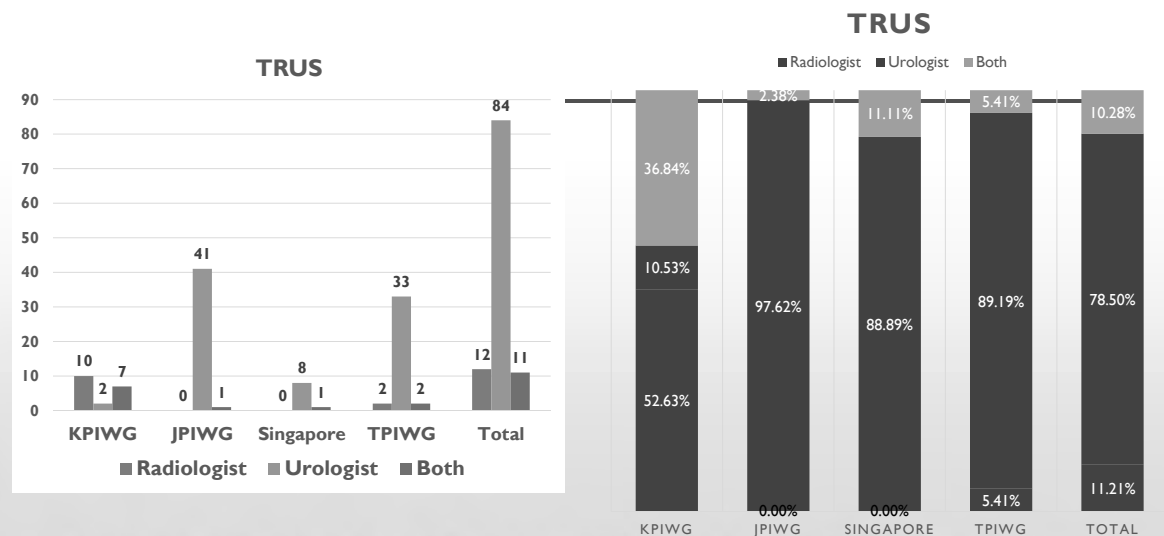
Do you use structured report for prostate MRI reporting?



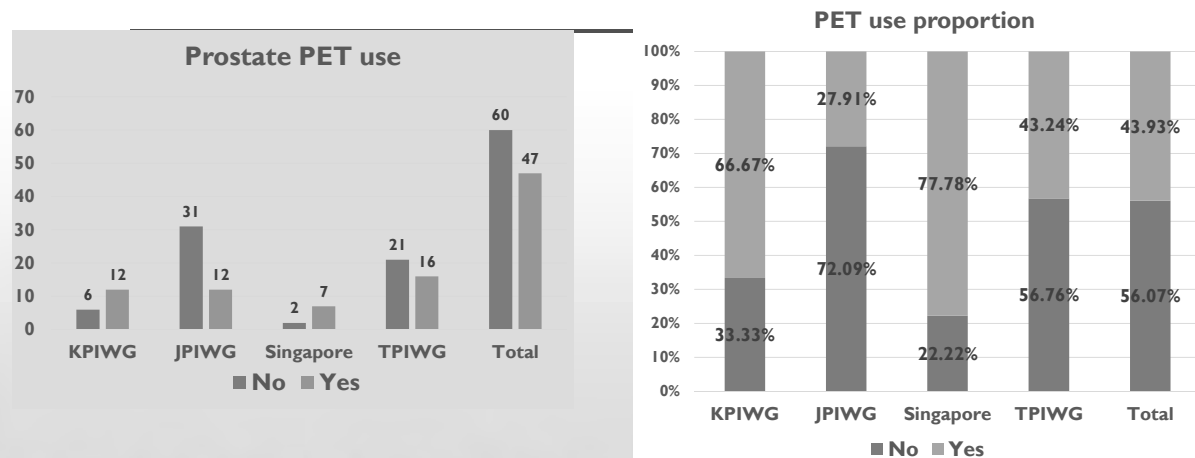
OTHER PROSTATE IMAGING

TRUS, Prostate PET and PET/MRI

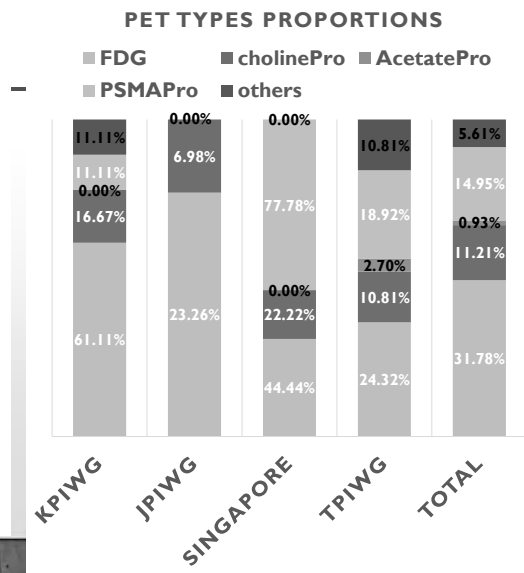
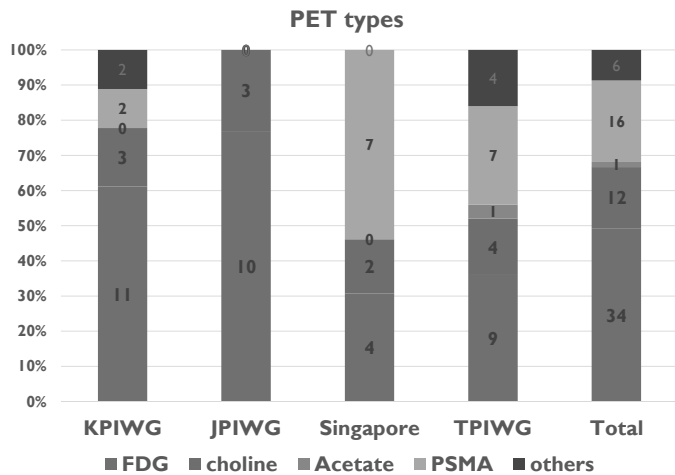
Who performs the TRUS procedure in your hospital?



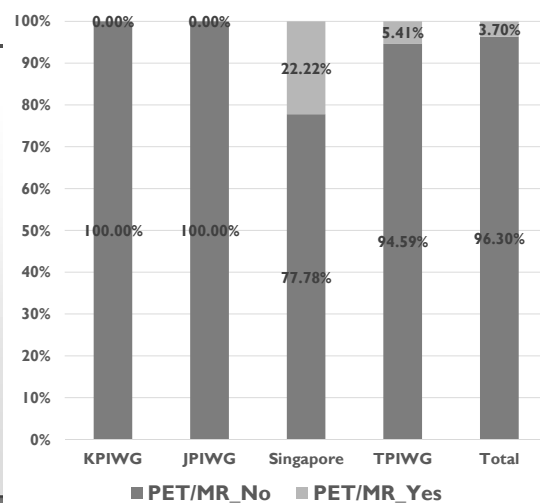
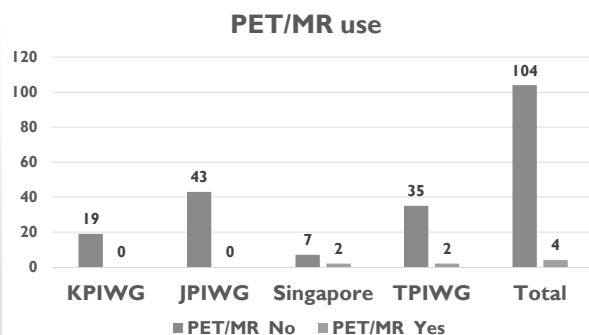
Does your hospital perform prostate PET (multiple choices)?



Prostate PET types (multiple choices)



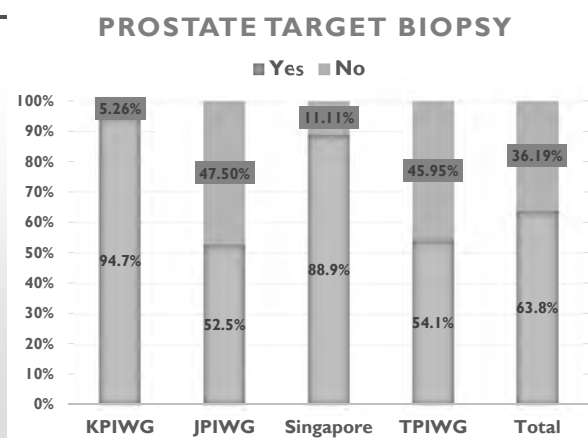
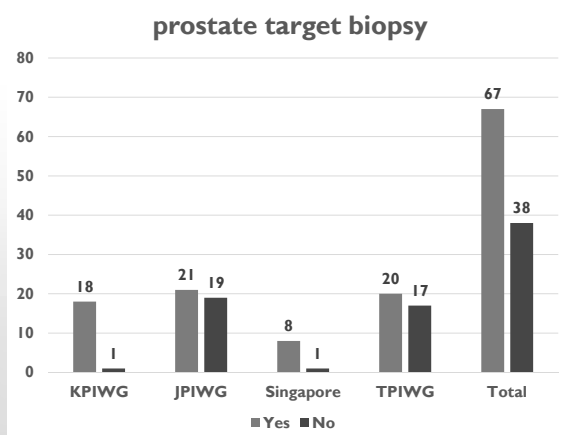
Does your hospital perform prostate PET/MR?



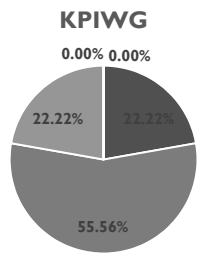
PROSTATE BIOPSY

prostate target biopsy, MRI timing

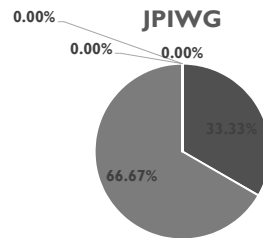
Does your hospital offer targeted prostate biopsy?



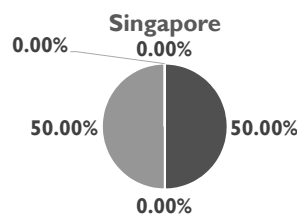
Distribution of types of targeted prostate biopsies



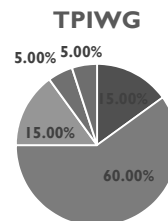
■ cognitive ■ fusion ■ both ■ in bore ■ all three



■ cognitive ■ fusion ■ both ■ in bore ■ all three

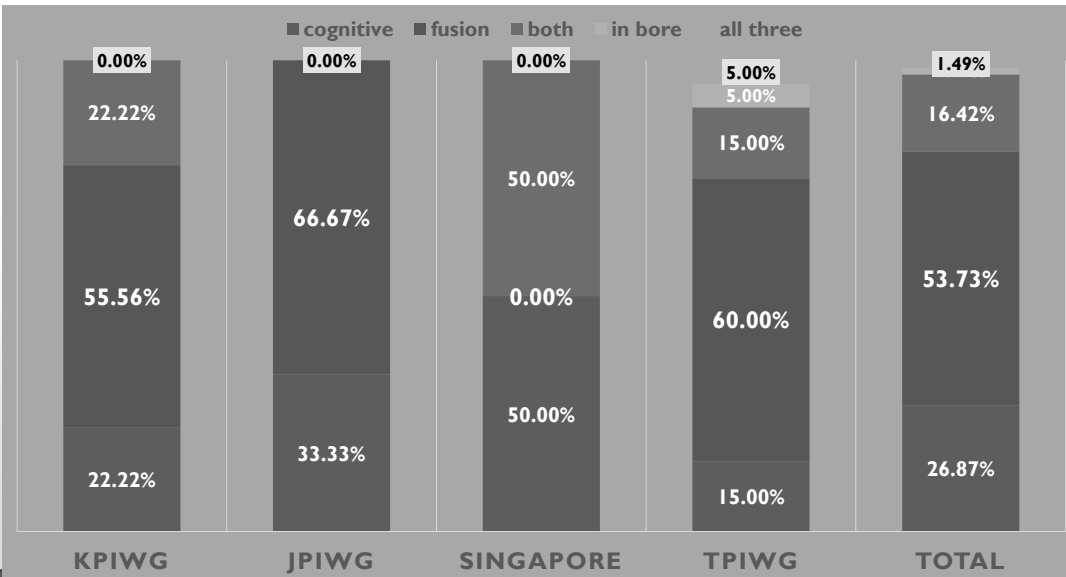


■ cognitive ■ fusion

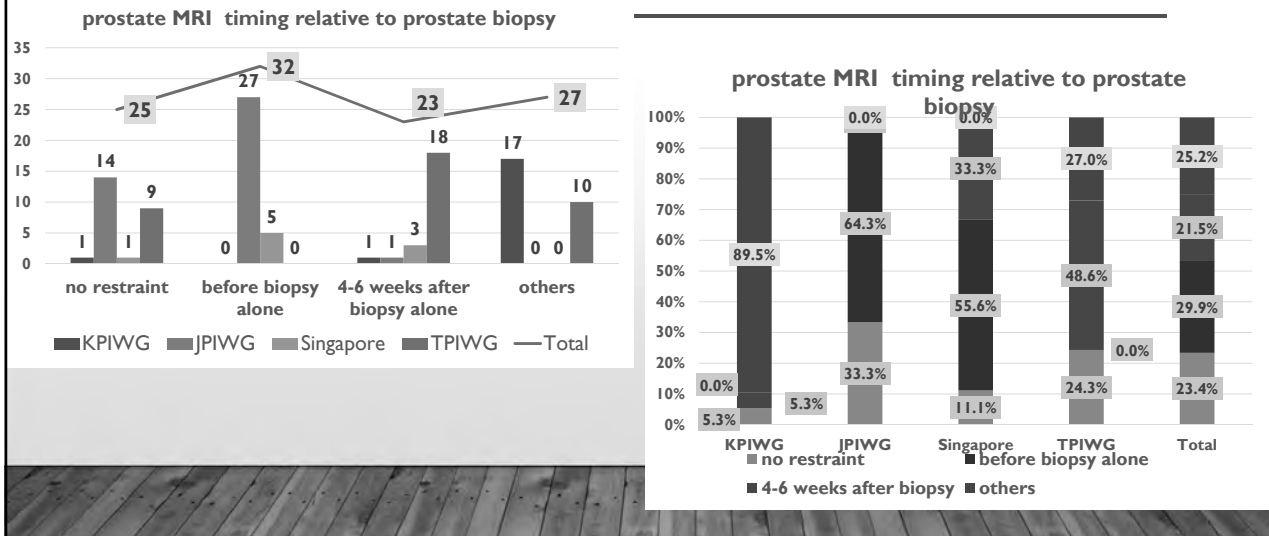


■ cognitive ■ fusion ■ both ■ in bore ■ all three

Distribution of types of targeted prostate biopsies



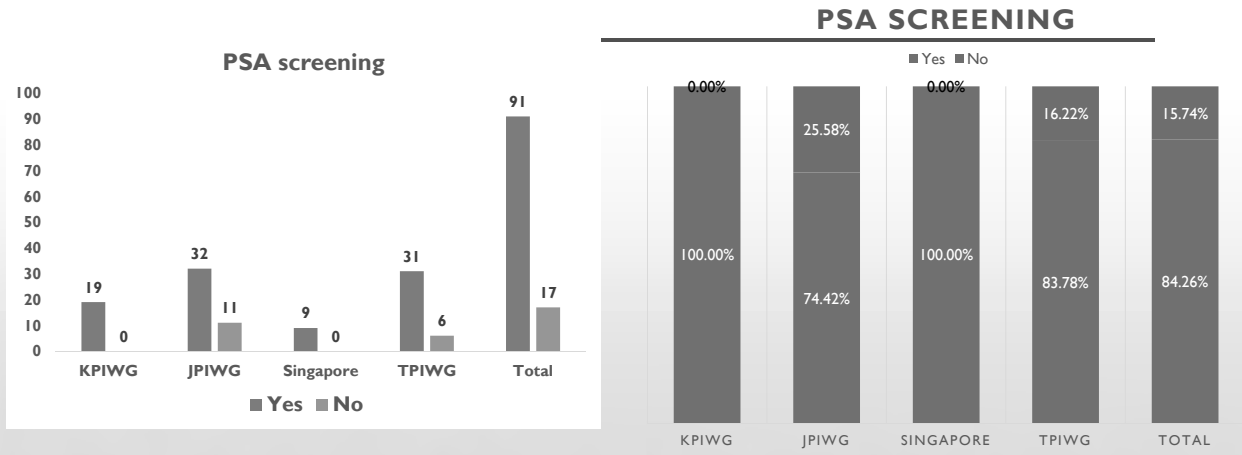
What is the timing of patients undergoing prostate MRI if he has planned to undergo or has undergone prostate biopsies?



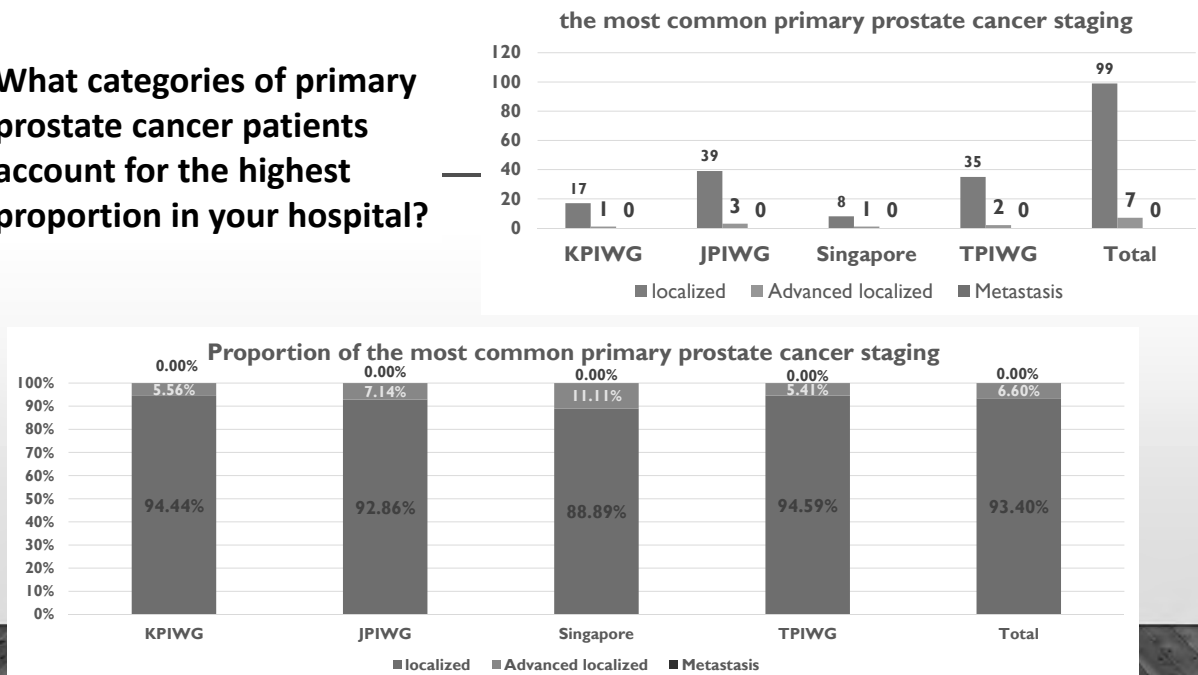
PROSTATE CANCER STATUS

PSA screening, disease extension, treatment

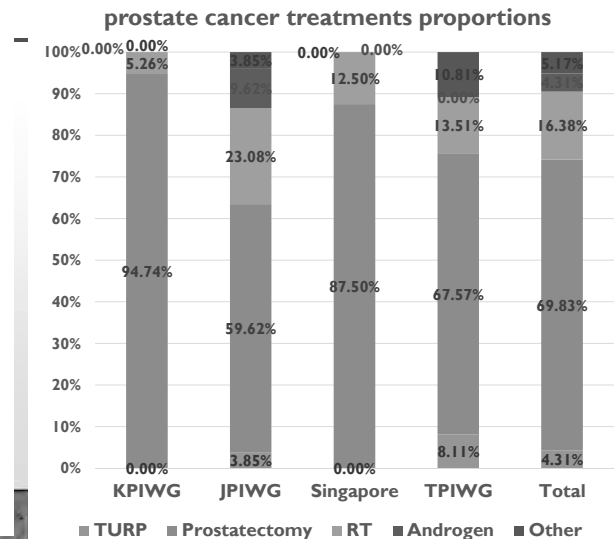
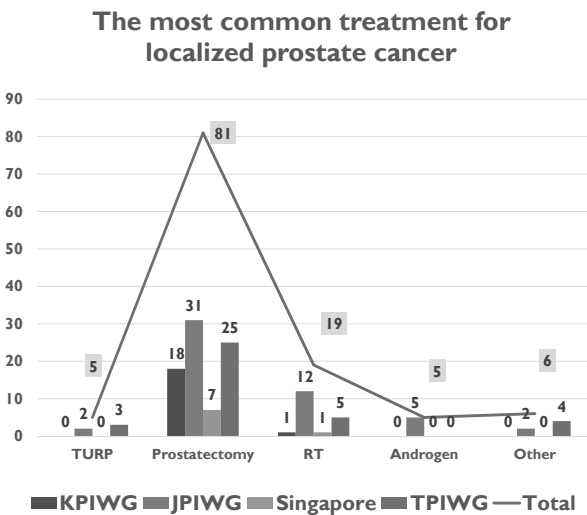
Does your country perform PSA screening test for prostate cancer?



What categories of primary prostate cancer patients account for the highest proportion in your hospital?



What treatment is the most commonly used for localized disease of prostate cancer in your hospital?



WHAT ARE THE LESSONS LEARNED FROM APIVG SURVEY?

- Diversities of prostate MRI usage---not PIRADS compliant techniques for all
- Diversity of prostate MRI report for treatment-naive patients—not all of radiologists in charge of prostate MRI familiar with PIRADS
- On the way of participating or performing prostate targeted biopsy---prostate cancer detection on MRI is the fundamental for this
- TRUS for prostate cancer---a tool familiar by few radiologists
- PSMA PET and PET/MR---experienced by few radiologists (especially in regard of its theranostics use).
- Basic knowledge of prostate cancers—PSA screening, treatments, distributions, etc.--- common language and core knowledge need to be built up for radiologists.

EDUCATION PROGRAMS DEDICATED FOR ASIAN RADIOLOGISTS WORKING ON PROSTATE IMAGING

- Basic knowledge of prostate cancer
 - PSA testing, PSA density, free PSA
 - Clinically significant and insignificant prostate cancers---Gleason scores, ISUP grades
 - Epidemiology of prostate cancer--overdiagnosis and overtreatment
- Treatment-naïve patients proved or suspected of having prostate cancer
 - PIRADS compliant techniques.
 - PIRADS report
 - Prostate MR diagnostic pathway
- Prostate cancer patients on active surveillance
 - PRECISE
- Prostate targeted biopsy
 - TRUS
 - Prostate cancer detection and contouring/labelling on MRI

ENROLL, EMPOWER AND MOTIVATE MORE ASIAN RADIOLOGISTS TOGETHER

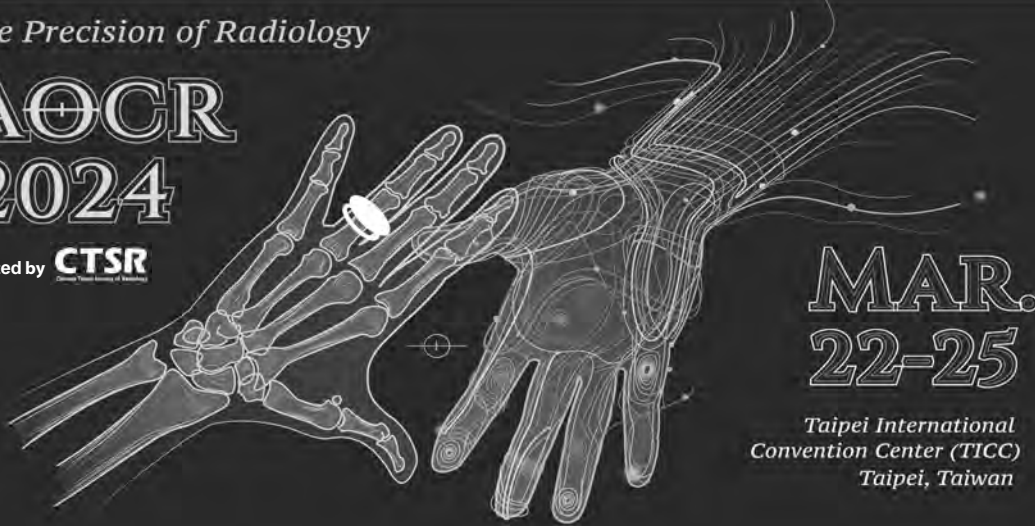
- Organize and held prostate imaging symposium
- Built up and provide prostate education programs as a service
- Collaborate with other societies—ACAR,AOCR,AOSOR, etc.
- Invite more Asian key radiologists to join APIWG
- Meet and share experiences with ESUR and ARRS experts
- Empower more Asian radiologists serving as mentors, educators and speakers
- Certificates of APIWG educational programs for radiologists, urologists, oncologists and other physicians.

Looking forward to meeting you in *Taiwan*

The Precision of Radiology

AOCR
2024

Hosted by **CTSR**
Chinese Taipei Society of Radiology



MAR.
22-25

*Taipei International
Convention Center (TICC)
Taipei, Taiwan*

THANK YOU FOR YOUR ATTENTION

PI-RADS v2.1: An institution experience

Dr Chau Hung LEE

Objective:

To highlight experience with PI-RADS v2.1 at a single institution, Tan Tock Seng Hospital, Singapore.

Results:

We have been performing mpMRI of the prostate and targeted prostate biopsies since 2016. MRI-US fusion is our preferred technique. Currently we utilize both TRUS and TP approaches, increasingly favouring the TP approach. Diagnostic performance is comparable to published literature. However the positive rates for PI-RADS 3 lesion particularly in the TZ, remains low. We are exploring various methods to increase detection rates in PI-RADS 3 TZ lesions while avoiding unnecessary biopsies for this group of lesions – such as combining with clinical parameters and use of AI. We have also integrated MRI as part of AS surveillance for patients with low-risk prostate cancer.

RADSs in urological imaging beyond PI-RADS: PI-RR, MET-RADS-P and NODE-RADS

Satoru Takahashi MD, PhD

Imaging research centre, Aijinkai Takatsuki General Hospital, Takatsuki, Japan

Reporting and data systems (RADSs) have been introduced to help radiologists classify and report imaging findings using a standardized terminology. PI-RADS, Prostate Imaging Reporting and Data System, is one of the most successfully accepted RADSs by referring physicians, namely urologists. There are, however, another less familiar or newly introduced RADSs in urological imaging. In this talk, we would like to review another RADSs in urological imaging, including PI-RR, MET-RADS-P and Node-RADS.

Prostate Magnetic Resonance Imaging for Local Recurrence Reporting (PI-RR)

PI-RR was published in 2021 to propose a standardized method for image acquisition and assessment of prostate cancer local recurrence using MRI after radiation therapy and radical prostatectomy (Panebianco V, et al. Eur Urol Oncol, 4: 868-876, 2021).

Similar to PI-RADS, PI-RR was simplified and standardized five categories to summarize the suspicion of local recurrence; scores 1 and 2 assigned to lesions with a very low and low likelihood of recurrence, respectively, score 3 for uncertain recurrence, and scores 4 and 5 for a high and very high likelihood of recurrence, respectively. PI-RR combines criteria for DCE and DWI to assess the likelihood of relapse, but overall assessment is different between post radical prostatectomy (PI-RR RP) and post radiotherapy (PI-RR RT). Basic idea for scoring is similar to those of PI-RADS, although DCE is also categorized to 5 scores. In addition, score 5 is applied in cases with focal suspicious lesion is located on the same side as the primary tumor, while score 4 in case with the contralateral side of the primary tumor or unknown primary side. In PI-RR RP, DCE is the primary score of the assessment, and DWI score of 4 or more upgrades DCE score 2 and 3 to 3 and 4, respectively. In PI-RR RT, on the other hand, overall category is determined by the sequence with the highest score for any of the DWI and DCE. When both DWI and DCE show score 4, overall category will be upgraded to 5.

Pecoraro M, et al (Radiology, 304: 342-350, 2022) reported that PI-RR 3 or greater yielded diagnostic performances of 71-81% sensitivity, 74-93% specificity, 71-89% PPV, 79-86% NPV, and 77-88% accuracy across the four readers in 48 patients after radiotherapy, while those of 59-83% sensitivity, 87-100% specificity, 88-100% PPV, 66-80% NPV, and 75-85% accuracy in 52 patients after radical prostatectomy.

METastasis Reporting and Data System for Prostate Cancer (MET-RADS-P)

MET-RADS-P was published in 2017 to propose a recommendation that promote standardization and diminish variations in the acquisition, interpretation, and reporting of whole-body MRI scans for use in advanced prostate cancer clinical trials (Padhani AR, et al. Eur Urol, 71: 81-92, 2017).

The aims of MET-RADS-P are to establish minimum acceptable technical parameters for whole-body MRI data acquisition and to develop standardized data collection methods that enables detailed descriptions of the disease phenotype based on imaging patterns of metastatic spread. Thus, comprehensive response criteria for assessing bone, soft tissue, and local disease will be developed to record the presence, location, and extent of mixed imaging responses.

The core whole-body MRI protocol, including whole spine sagittal T1w and STIR, whole body axial or coronal T1w-DIXON, and whole-body DWI with 2 b-values, designed for bone and lymph node metastasis detection should be completed within 30 min for the detection of metastatic disease in the setting of biochemical recurrence after primary therapy, or in the setting of M0-CRPC to detect the onset of metastatic disease. In contrast, more comprehensive assessments designed for patients with established metastatic including visceral disease could be completed within 45–50 min for known metastatic disease and for those patients in whom serial tumor response assessments are planned.

Although the number of validation studies for MET-RADS-P is limited, Pricolo P et al (Cancer Imaging, 20: 77, 2020) stated that MET-RADS-P could provide excellent inter-observer agreement of whole-body MRI in bone metastasis assessment but mixed in other body regions. Furthermore, Yoshida S et al (Clin Genitourin Cancer, 18: e391-e396, 2020) reported that MET-RADS-P score could be a prognostic imaging biomarker for CRPC, as cancer-specific survival was significantly stratified according to the MET-RADS-P scores of osseous metastatic burdens and the presence of visceral metastasis.

Node Reporting and Data System (Node-RADS)

Node-RADS was published in 2021 to systematically classify the degree of suspicion of lymph node involvement based on the synthesis of established imaging findings (Elsholtz FHJ, et al. Eur Radiol, 31: 6116-6124, 2021). Node-RADS can be applied at any anatomical site, and to regional and non-regional lymph nodes in relation to a primary tumor location.

Scoring categories for "size" and "configuration" are combined into assessment categories between 1 ("very low likelihood") and 5 ("very high likelihood"). First, nodes are classified into one of three categories based on the size (Normal, <10mm in short axis in general or <5mm in obturator or mesorectal nodes; Enlarged, larger than normal, but no Bulk, or 2mm or more increase to prior imaging; Bulk, 30mm or more in any axis). Then, configuration scores are assessed for texture (0-3), border (0,1), and shape (0,1) and the sum of three configuration scores consecutively translated into the respective final Node-RADS score for each size category as follow: In Normal, configuration sum score of 0, 1, 2, >2 will be the final Node-RADS score of 1, 2, 3, 4 respectively; in Enlarged, configuration sum score of 0, 1, 2, >2 will be 2, 3, 4, 5 respectively. Final Node-RADS score of 5 is also applied for Bulk.

Lucciola S et al (Prostate Cancer Prostatic Dis, 2022. DOI: 10.1038/s41391-022-00564-z) evaluated the predictive value of preoperative Node-RADS for patients undergoing radical prostatectomy with extended lymph node dissection. They reported that Node-RADS yielded 100% PPV and specificity, but showed a low sensitivity of 16.7%

11:00 – 12:00 Clinical Issues

좌장: 성창규 (보라매병원)

김경아 (고대구로병원)

주사용 요오드화 조영제 및 MRI용 가돌리늄 조영제 유해 반응에 대한 한국 임상진료지침: 개정된 임상적 합의 및 권 고안 (3판, 2022)

- 요약 및 2023 ACR MANUAL, 2018 ESUR GUIDELINE 비교

서울특별시 보라매병원 영상의학과

이 명 석

진료지침 개정의 배경 및 과정

- 2016 년 “주사용 요오드화 조영제 및 MRI용 가돌리늄 조영제 유해 반응에 대한 한국 임상진료지침”에 대한 개정
- 주요 추가 내용
 - 조영제 사용 시 감염관리를 위한 자동주입기 및 연결선에 대한 기술
 - 급성 유해반응
 - 고위험군 확인을 위한 피부 검사
 - 조영제의 교체 사용
 - 신장 유해반응의 정의, 발생기전, 진단, 위험인자, 검사 전 신 기능 측정
 - 신독성 예방: 조영제 회피 및 선택과 수액 등의 기타 요법

조영제를 이용하는 검사의 준비

카테터 구경 및 조영제의 가온

- 성인기준 **20G** 혹은 더 큰것. **Antecubital vein** 또는 **forearm** 의 큰 정맥
- 조영제의 가온 (**Warming**): **37°C**
 - 가온 → 점도 감소 → 조영제 주입 압력 감소 및 유속 증가 → 작은 직경의 **catheter** 를 써도 적절한 주입속도 얻을 수 있음
 - 임상적인 장점 (**20°C vs. 37°C**)
 - 급성 유해반응의 감소
 - 혈관외 누출 감소 (고삼투성 제제 사용 시)
 - Bolus injection 시 혈관내 **peak enhancement** 높고 **peak enhancement** 까지 걸리는 시간이 감소
 - ACR Manual 2023: External warning is beneficial in the cases
 - For high-rate (> 5 mL/second) IV LOCM power injections
 - For injections of viscous iodinated contrast (e.g., iopamidol 370, a similar or higher viscosity)
 - For direct arterial injections through small-caliber catheters (5 French or smaller)
 - For intravenously injected arterial studies in which timing and peak enhancement are critical features

금식

- **CT 또는 MRI 조영제를 사용하는 검사 전, 흡인성 폐렴의 예방을 위한 금식이 필요하다는 확실한 근거는 없다**
 - 물 등의 맑은 액체류는 검사 직전까지 섭취해도 안전한 검사가 가능
 - 고형식의 경우 위 배출 시간 및 환자에게 큰 불편을 주지 않는 범위 내에서 위험과 이득을 고려하여 금식 시간을 정해야 함
 - 금식을 시행한 군에서 합병증 발생의 차이는 없고 오히려 오심 관련 증상의 발생이 많았다(0.4% vs. 0%) 는 연구 결과가 있음 (Rofo 1997;166:370-5)
- **ACR Manual 2023**
 - Fasting is not required prior to routine IV CM administration (both iodine and Gd-based CM)
- **ESUR Guideline v10.0 2018**
 - Fasting is not recommended before administration of low- or iso-osmolar non-ionic iodine-based contrast media or of gadolinium-based agents.
 - HOCM: fasting 필요하나 거의 쓰이지 않음

감염 관리

- 개정 의료법 4조 6항: 의료인은 일회용 의료기기(한 번 사용할 목적으로 제작되거나 한 번의 의료행위에서 한 환자에게 사용하여야 하는 의료기기로서 보건복지부령으로 정하는 의료기기를 말한다. 이하 같다)를 한 번 사용한 후 다시 사용하여서는 아니 된다. <신설 2016. 5. 29., 2020. 3. 4.>
- **CT 및 MRI 촬영에 사용하는 Auto injector**에 연결되는 주사기와 연결줄도 일회용으로 사용하여 매 환자마다 교체하는 것을 원칙
 - 물자낭비, 환경오염, 검사시간 증가에 따른 효율성 감소
- 환자 쪽 연결선에 두 개의 체크밸브를 갖는 역류방지 필터를 설치하고 이러한 필터는 매 환자마다 교환하되 나머지 주사기와 연결줄은 허가된 시간(12시간 혹은 24시간) 동안 교체 없이 사용.

조영제의 혈관 외 누출

- 혈관외 누출 (Extravasation)

- 요오드화 조영제의 경우 0.13~0.94% 빈도로 발생
- 통증 (m/c), 부종 및 국소발적. 대개 하루~4일 내 회복
- 피부궤양, 연조직 괴사, 구획증후군: 대량 유출시 발생 가능성 있어 주의를 요함 (<1% of extravasations)
- GDCM: 조직 독성 낮고 적은 용량 사용으로 심각한 손상 발생 확률이 매우 드물다

- 위험 인자

- 기술적 요인: **autoinjector** 의 사용, **catheter** 부위가 좋지 않을 때 (하지나 말단정맥), 고장성 조영제, 대량의 조영제
- 환자 요인: 항암치료, 혈관이 손상되어 있는 경우, 의사소통 불가 (영유아), 동맥허혈 등
- 감소 대책: 적절한 크기의 **catheter** 를 적절한 정맥에, 비이온성 조영제 사용, 생리식염수 **test injection**, 주입 초기에 주사부위 관찰하고 의심되면 즉시 주입 중단

- 치료

- 보존적인 치료로 충분, 표준 치료에 대한 합의는 없음
- 냉찜질 및 온찜질: 무엇이 더 좋은지에 대한 분명한 근거는 없고 실제 혼용되어 사용
- 히알루론산 분해효소 주입: 효과가 확실히 입증되어 있지 않음.
- 중증 손상 의심 시는 수술적 치료 등 관련 전문의의 조언을 구해야 함.

- ACR manual 2023
 - No known effective treatment for contrast medium extravasation,
 - Initial steps should include elevation of the affected extremity above the level of the heart
 - Use of cold or warm compresses
 - Surgical consultation should be obtained for a severe extravasation injury
 - severe pain, progressive swelling or pain, decreased capillary refill, change in sensation, worsening active or passive range of motion, skin ulceration or blistering
 - reliance on an extravasation volume threshold to trigger surgical consultation is not recommended
- ESUR Guideline v10.0 2018
 - To reduce
 - appropriate sized plastic cannula placed in a suitable vein
 - Consider use of cannulas with sideholes.
 - Test injection with normal saline.
 - Use non-ionic iodine-based contrast medium.
 - Management
 - CT scan or MR scan of the affected region may be helpful.
 - Conservative managements: Elevation, Ice Pack, Careful monitoring
 - If a serious injury is suspected, seek the advice of a surgeon.

요오드화 조영제의 유해반응

급성 유해 반응 (ACUTE ADVERSE REACTION): 1시간 이내
 지연성 유해 반응 (LATENT ADVERSE REACTION): 1시간 이후

급성 유해 반응

- 발생 기전
 - 생리적 반응: 조영제의 직접적인 화학 독성과 삼투압 차이에 의해 발생. 고용량에서 빈도 높음
 - 과민 반응
 - 알러지 반응 / 비알레르기성 과민 반응 (Basophil, Mast cell 직접자극)
 - Iodine CM 에 의해 과민반응이 발생하는 기전은 잘 알려져 있지 않음
- 중증도 분류
 - 저절로 호전되는 경증
 - 경증보다 심하여 치료를 필요로 할 정도인 중등증
 - 생명을 위협하거나 영구적인 장애, 사망을 초래하는 중증
- 위험 인자
 - 조영제 과민반응의 과거력: 과거력이 있는 환자에서 향후 과민반응이 발생할 가능성은 약 10%~35%로 알려졌다며 과거력이 있는 환자에서 전 처치를 하더라도 약 10 %에서 발생.
 - 동반 질환: 천식 등 알레르기 질환. 심각한 심혈관계 질환
 - 약물 (베타차단제): 중등증 또는 중증 유해반응 발생위험이 높다고 알려짐
 - 조영제 종류: 이온성 고삼투성 조영제

급성 유해 반응

Table 2. 요오드화 조영제 급성 유해반응의 분류

	과민반응	생리적 반응(기타 유해반응)
경증	국소적인 두드러기·가려움증 국소적인 피부 부종 목(인후두) 가려움 코 충혈, 재채기, 콧물, 결막염	경미한 메스꺼움·구토 일시적인 화끈거림·열감·오한 두통, 어지러움, 불안, 맛의 변화 장중 고혈압 저절로 호전되는 혈관미주신경항진 반응
중등증	광범위한 두드러기·가려움증 광범위한 홍반 안면부종 목이 붓거나 씹 저산소증이 없는 천명, 기도수축	지속되는 메스꺼움·구토 흉통 고혈압성 긴급증(hypertensive urgency) 치료가 필요한 혈관미주신경항진 반응
중증	호흡곤란을 동반한 심한 부종과 안면부종 저혈압을 동반한 심한 홍반 그림거림/저산소증을 동반한 후두부종 심한 저산소증이 있는 천명, 기도수축 아나필락시스 쇼크	부정맥 경련 고혈압성 응급증(hypertensive emergency) 치료를 반응하지 않는 혈관미주신경항진 반응

고혈압성 긴급증: 수축기 혈압 180 mm Hg 이상 또는 이완기 혈압 110 mm Hg 이상이며 장기 손상 소견은 없을 경우

고혈압성 응급증: 혈압 상승(> 180/120 mm Hg)과 표적장기손상이 진행되는 경우(고혈압으로 인한 뇌졸중, 의식저하, 기역력 저하, 협심증 또는 심장발작, 눈 및 신장 손상, 대동맥 파열, 폐부종, 경련 등)

급성 유해 반응

- 과민반응과 생리적 반응 모두에서 발생을 예측하기 위한 검사는 권고되지 않는다
- 과민반응의 병력이 있는 환자에서 과민반응의 원인 약물을 확인하거나 요오드화 조영제에 대한 재노출이 필요할 때 안전한 조영제를 선택하기 위해서 피부시험을 시행할 수 있다.
- 피부 시험
 - 피부단자시험 (조영제 원액) → 음성인 경우 피내 시험 (1:10 희석 조영제)
 - Overall PPV: 즉시형반응 16.8%, 지연성반응 25.7%
중증 즉시형 반응이 있었던 환자 → PPV 51.9% → 중증 과민반응이 있던 환자에게 유용!
 - Overall NPV: 93% → 피부시험 음성으로 확인된 조영제로 교체하는 것이 안전!
 - 피부반응시험 음성인 조영제를 재노출시 재발율: 즉시형 반응 7.1%, 지연성 반응 34.5%
→ 완벽히 유용하다고 할 만한 근거는 부족
 - 결론적으로, 중증 이상의 요오드 조영제에 대한 과민반응을 경험한 환자에서 피부시험 고려 가능

급성 유해 반응

구역/구토	경과관찰, 필요시 항구토제 고려
두드러기/발적	경증: 경과관찰, 필요시 항히스타민제 중증: 중증: 활력징후 감소, 경맥주사 경로 확보, 항히스타민제, 필요시 전신 스테로이드제 사용
안면 또는 후두부종	기도 확보 산소포화도 유지(성인 90% 이상, 소아 95% 이상) 활력징후 감소 항히스타민제, 필요시 전신 스테로이드제 사용 심한 안면부종 혹은 급성 후두부종: 에피네프린 0.01 mg/kg 군주, 5-15분마다 반복 (최대 용량: 성인 0.5 mg, 6-12세 0.3 mg, 6세 미만 0.15 mg)
기관지수축	기도를 확보하고, 활력징후와 산소포화도를 감시하며(성인 90% 이상, 소아 95% 이상), 저산소증일 경우 산소를 공급 속효성 기관지 확장제(salbutamol) 흡입: 정량식 흡입기 혹은 연무기 항히스타민제, 필요시 전신 스테로이드제 사용 계속 진행 시: 에피네프린 0.01 mg/kg 군주, 5-15분마다 반복 (최대 용량: 성인 0.5 mg, 6-12세 0.3 mg, 6세 미만 0.15 mg)
아나필락시스 쇼크	기도 확보 산소포화도 유지(성인 90% 이상, 소아 95% 이상) 활력징후 감소 쇼크체위 정맥주사 경로 확보 빠른 속도의 수액 정주 계속 진행 시: 1:1000 에피네프린 0.01 mg/kg 군주, 5-15분마다 반복(최대 용량: 성인 0.5 mg, 6-12세 0.3 mg, 6세 미만 0.15 mg) 군주 투여에도 반응이 없을 경우 1:10000 에피네프린을 서서히 정맥으로 투여해 볼 수 있음. ² 2차 치료: 항히스타민제, 전신 스테로이드제, 속효성 기관지 확장제(salbutamol) 등



<https://www.osmosis.org/answers/shock-position>



보통 1mg / amp
근육주사시
반응률 투여
정맥주사시
10배로 희석하여
투여

급성 유해 반응

발작 또는 경련	<p>주변 정리</p> <p>기도를 확보하고, 활력징후와 산소포화도를 감시하며(성인 90% 이상, 소아 95% 이상), 저산소증일 경우 산소를 공급</p> <p>정맥주사 경로 확보</p> <p>디아제팜 5 mg, 미다졸람 0.5~1 mg, 로라제팜 2~4 mg 서서히 정주</p> <p>가능하면 신경 전문의 자문 요청</p>
폐부종	<p>기도를 확보하고, 활력징후와 산소포화도를 감시하며(성인 90% 이상, 소아 95% 이상), 저산소증일 경우 산소를 공급</p> <p>이뇨제(푸로세마이드 20~40 mg)를 2분에 걸쳐 정주</p>
혈관미주신경반사	<p>기도를 확보하고, 활력징후와 산소포화도를 감시하며(성인 90% 이상, 소아 9% 이상), 저산소증일 경우 산소를 공급</p> <p>쇼크체위</p> <p>정맥주사 경로 확보</p> <p>빠른 속도의 수액 정주</p> <p>필요시 아트로핀(0.5 mg/mL) 0.5~1 mg를 천천히 정주(3~5분 간격으로 반복 투여, 최대 누적 투여량 3 mg)</p>
고혈압성 위기	<p>관련 장기 이상 소견(의식저하, 흉통, 빈호흡, 오심/구토, 어지러움, 시야 혼미 등) 확인</p> <p>기도를 확보하고, 활력징후와 산소포화도를 감시하며(성인 90% 이상, 소아 95% 이상), 저산소증일 경우 산소를 공급</p> <p>정맥주사 경로 확보</p> <p>라베탈롤 20 mg 정주(2분에 걸쳐 천천히) → 10분마다 반응 확인, 목표 혈압이 될 때까지 2배씩 증량(최대 80 mg) → 초기 부하 용량 투여 후 지속 정주 (1~2 mg/min으로 시작하여 증감량)</p> <p>(정맥로가 없거나 정맥용 항고혈압제가 없으면 니트로글리세린 0.4 mg 설하 투여 → 5~10분 후 반응 확인, 필요시 재투여)</p> <p>고혈압성 폐부종 의심될 때: 이뇨제(푸로세마이드 20~40 mg) 정주 (2분에 걸쳐 천천히)</p>

급성 유해 반응

• ACR 2023 Manual

Epinephrine (IV)*

IV 1 mL of 0.1 mg/mL (1:10,000) dilution (0.1 mg); administer slowly into a running IV infusion of fluids; can repeat every few minutes as needed up to 10 mL (1 mg) total

Epinephrine (IM)*

IM 0.3 mL of 1.0 mg/mL (1:1,000) dilution (0.3 mg); can repeat every 5-15 minutes up to 1 mL (1 mg) total

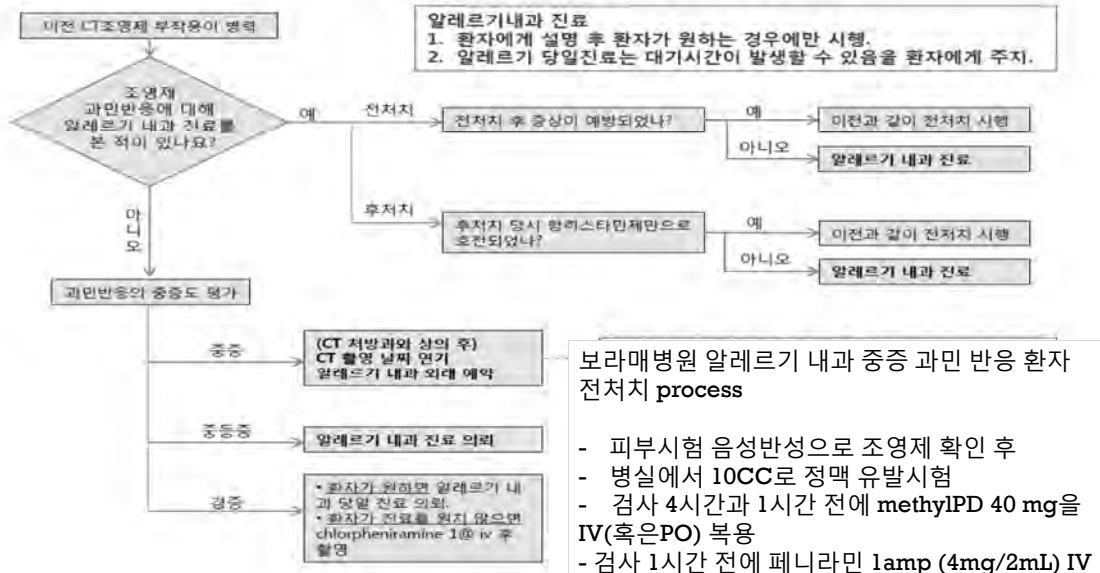


Hypotension, Bronchospasm, Laryngeal edema

급성 유해 반응

- 요오드화 조영제 쓰지 않는 다른 검사 안내, 조영제 교체
- 전처치
 - 구역, 구토 등 생리적 반응에 대한 전처치는 불필요
 - 중등도 이상의 급성 과민반응이 있던 경우에만 전처치 권고
 - 과민반응 고위험군 (중증도 상관없이 과민반응 병력, 알러지, 약물과민반응, 천식): 임상사의 판단에 따라 전처치 시행 가능.
- ACR 2023 Manual
 - 예정된 검사에 대한 전 처치
 - ① 조영제 주입 13시간, 7시간, 1시간 전 프레드니솔론 50 mg을 경구투여하고, 조영제 주입 1시간 전 클로르페니라민 4 mg 주사(근주 혹은 정주) 하거나 경구용 항히스타민제를 복용한다.
 - ② 조영제 주입 12시간, 2시간 전 프레드니솔론 30 mg 혹은 메칠프레드니솔론 32 mg을 경구 투여하고, 항히스타민제를 추가 해 볼 수 있다.
 - *환자에게 경구투여가 불가능한 경우, 대신 히드로코르티손 200 mg을 정주한다.
 - 응급 상황에서의 전 처치
 - 조영제 주입 전까지 매 4시간마다 메칠프레드니솔론 40 mg 혹은 히드로코르티손 200 mg을 정맥주사를 하고, 조영제 주입 1시간 전에 클로르페니라민 4 mg 정주한다.
- ESUR Guideline v10.0 2018
 - 전처치를 권고하지 않음

조영제 과민반응 전처치



지연성 과민 반응

- 대부분 3시간~48시간 이내 발생
- 생리적 반응 / 과민반응
- 임상 양상
 - 대부분 과민반응으로 나타남. 피부발진(70%) 이 가장 흔한 증상
 - Maculopapular rash (m/c), Acute Generalized Exanthematous Pustulosis, Stevens-Johnson syndrome, Toxic Epidermal Necrosis
- 예방과 예측
 - 피부반응은 T 세포에 의한 과민반응 가능성이 높을 것으로 예측
 - 치명적 지연성 반응이 있었던 환자는 조영검사 하지 않을 것을 권고
 - 전처치 효과가 입증되어 있지 않고 지연성 유해반응은 중증 반응이 드물어 전처치는 권고하지 않음
 - 이전에 심각한 지연성 유해반응을 겪은 경우 경구 스테로이드제 예방요법을 시도해 볼 수 있다

Dose modulation in CT

김상윤

서울대병원

CT scan 의 증가에 따른 Radiation exposure를 줄이기 위한 여러 방법들이 제시되고 있고, Dose reduction 에 따른 Noise증가와 영상 질 감소를 보정하기 위한 여러 Post processing 기법들이 개발되고 있다.

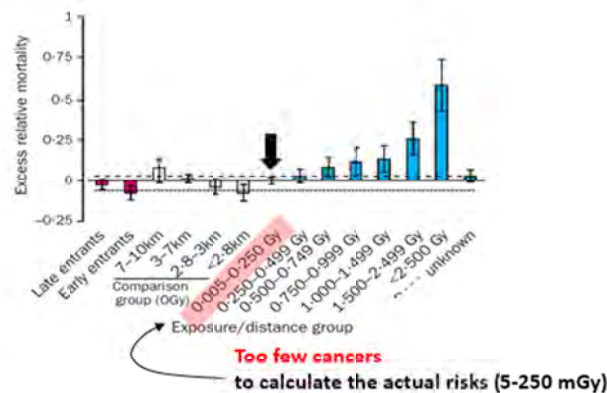
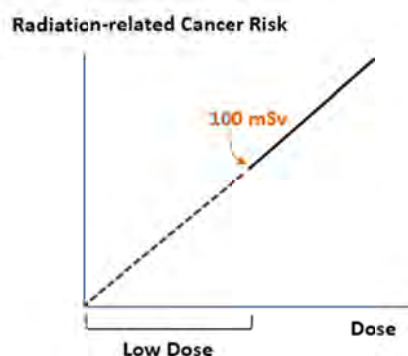
Dose reduction techniques

- Reduce tube voltage (kVp)
- Automated tube current (mAs) modulation (ATCM) & Automated Exposure Control (AEC)
- Dual energy CT
- Others
 - Decrease in exposure time & Increase in pitch
 - Reduce the number of phases
 - Minimize scan coverage

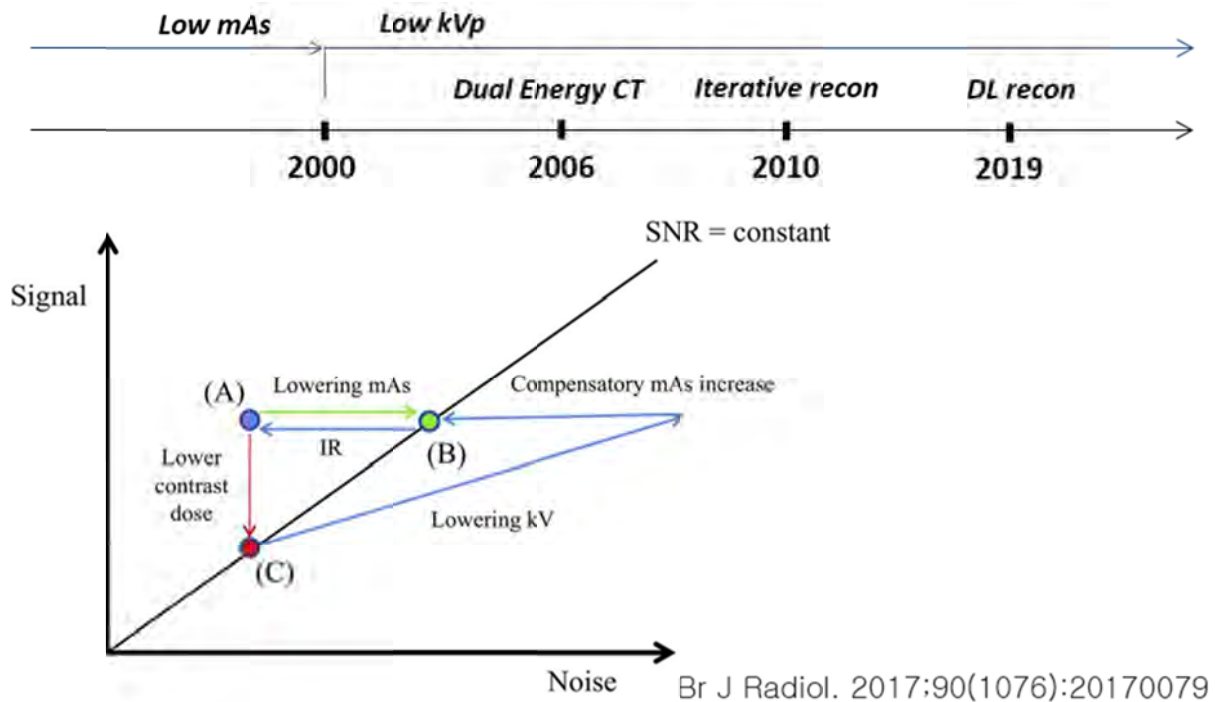
Post reconstruction techniques using Iterative / deep learning reconstruction algorithms for noise reduction

BEIR VII: < 100 mSv

- Statistical limitations make it difficult to evaluate cancer risk in humans
- The committee conclusion: Linear No Threshold model (아무리 작은 선량의 방사선이라도 암 발생의 확률이 있으며 이는 방사선의 양과 비례하며 역치는 없다)



National Research Council (US); Committee to Assess Health Risks from Exposure to Low Levels of Ionizing Radiation. Health risks from exposure to low levels of ionizing radiation: BEIR VII phase 2. Washington DC: National Academies Press; 2006
J Korean Med Assoc 2011 December; 54(12): 1253-1261



Vendor Tradename	Type
Standard vendor offering on all systems	FBP
Canon AiDR™, GE ASiR™, iDose ⁴ , Siemens SAFIRE, Siemens IRIS	Iterative
GE ASiR-V, Canon FIRST, Siemens ADMIRE, Philips IMR	Advanced Iterative (some elements of model based present)
Canon FIRST, GE Veo™	Model based
Canon AiCE, GE, TrueFidelity Clari.Pi, AlgoMedica Pixelshine	Deep learning based

Special thanks to 박성빈, 조은석, 최문형, 심영섭, 김택민

AI APPLICATIONS IN THE PROSTATE GLAND

Sung Il Hwang

Department of Radiology, Seoul National University Bundang Hospital

Disclosure

- I was the principal investigator of this prospective studies using PROMISE-I funded by a grant of the Korea Health Technology R&D Project through the Korea Health Industry Development Institute (KHIDI), funded by the Ministry of Health & Welfare, Republic of Korea (grant number: HI20C2092).
- The authors declare no conflict of interest.

GPT-4



Write a synopsis of 20 min lecture in a radiologic conference, topic is artificial intelligence in the prostate imaging



Title: Harnessing the Power of Artificial Intelligence in Prostate Imaging: Advancements and Applications

Synopsis:

In this 20-minute lecture, we will explore the transformative role of artificial intelligence (AI) in prostate imaging and its potential to revolutionize the field of radiology. The presentation will cover recent advancements, practical applications, and future directions in AI-driven prostate imaging, focusing on the following aspects:

1. Introduction to Prostate Imaging (3 minutes)

- The importance of accurate prostate imaging in early detection, diagnosis, and treatment of prostate-related conditions, including prostate cancer.
- Overview of traditional imaging techniques (e.g., transrectal ultrasound, MRI, and CT scans) and their limitations.

2. The Emergence of AI in Radiology (3 minutes)

- Brief history of AI in radiology.
- The role of machine learning and deep learning algorithms in image analysis.
- The potential of AI to address challenges in prostate imaging, such as improving accuracy, reducing interpretation time, and minimizing inter-reader variability.

3. AI Applications in Prostate Imaging (8 minutes)

- Computer-aided detection (CAD) systems for identifying suspicious lesions.
- AI-driven image segmentation for more precise delineation of prostate boundaries and tumor regions.
- Advanced radiomics for extraction of quantitative imaging biomarkers.
- The role of AI in improving prostate biopsy guidance and targeting.
- Integrating AI into the PI-RADS framework for more accurate and consistent assessment of prostate MRI exams.

4. Clinical Implementation and Validation (3 minutes)

- The importance of rigorous validation and standardization of AI algorithms in clinical practice.
- Current research efforts and multi-institutional collaborations.

GPT-4



Write a synopsis of 20 min lecture in a radiologic conference, topic is artificial intelligence in the prostate imaging



Title: Harnessing the Power of Artificial Intelligence in Prostate Imaging: Advancements and Applications

Synopsis:

In this 20-minute lecture, we will explore the transformative role of artificial intelligence (AI) in prostate imaging and its potential to revolutionize the field of radiology. The presentation will cover recent advancements, practical applications, and future directions in AI-driven prostate imaging, focusing on the following aspects:

1. Introduction to Prostate Imaging (3 minutes)

- The importance of accurate prostate imaging in early detection, diagnosis, and treatment of prostate-related conditions, including prostate cancer.
- Overview of traditional imaging techniques (e.g., transrectal ultrasound, MRI, and CT scans) and their limitations.

2. The Emergence of AI in Radiology (3 minutes)

- Brief history of AI in radiology.
- The role of machine learning and deep learning algorithms in image analysis.
- The potential of AI to address challenges in prostate imaging, such as improving accuracy, reducing interpretation time, and minimizing inter-reader variability.

3. AI Applications in Prostate Imaging (8 minutes)

- Computer-aided detection (CAD) systems for identifying suspicious lesions.
- AI-driven image segmentation for more precise delineation of prostate boundaries and tumor regions.
- Advanced radiomics for extraction of quantitative imaging biomarkers.
- The role of AI in improving prostate biopsy guidance and targeting.
- Integrating AI into the PI-RADS framework for more accurate and consistent assessment of prostate MRI exams.

4. Clinical Implementation and Validation (3 minutes)

- The importance of rigorous validation and standardization of AI algorithms in clinical practice.
- Current research efforts and multi-institutional collaborations.

"Classical" Tasks for AI

- Detection
- Segmentation
- Classification

AI in prostate MRI based on clinical questions

Q. What is the size of the prostate gland?

Segmentation of prostate gland

Q. Is there prostate cancer?

Detection or Classification
(cancer or normal)

Q. Where is tumor?

Localization, segmentation

Q. What is the likelihood of prostate cancer?

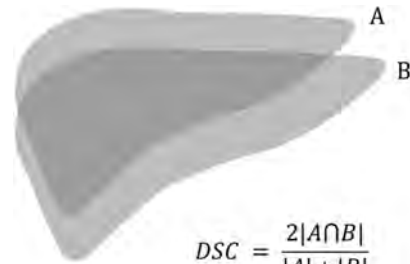
Probability map
Classification (PI-RADS)

Q. Gleason Grade?

Radiomics

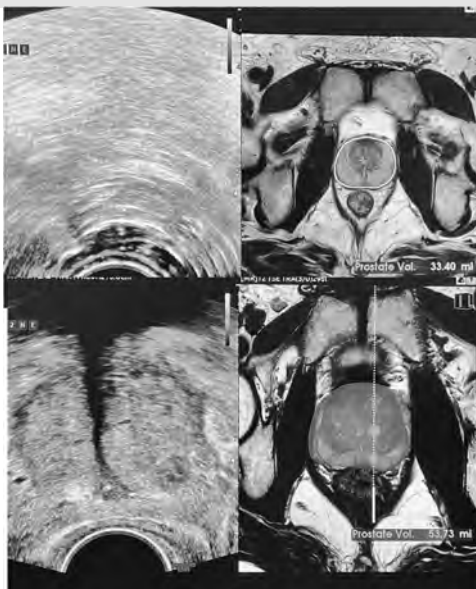
Segmentation Tasks

- Replacing time consuming manual delineation job
- Fusion biopsy guidance and radiotherapy planning
- 2D/3D Unet, Transfer learning
- DSC (Dice Similarity Coefficient):
0.88-0.94



DSC: Dice similarity coefficient

Incorporation with AI system



- FDA approval tools
Prostate MR: Siemens
Quantib Prostate: Quatib
OnQ Prostate: Cortechs.ai
PROView: GE
qp-Prostate: Quibim

Detection Tasks

- CNN, U-Net and derivatives
- AUC from 0.64 to 0.86
- High sensitivity/ Low specificity

TABLE 1: Currently Available Commercial Prostate MRI Artificial Intelligence (AI) Solutions in the United States and Europe

AI Product	Company	AI Application		Regulatory Status	
		Prostate Gland Segmentation	Lesion Detection	Approved by U.S. FDA	Passed Conformity Assessment per Regulation (EU) 2017/745
Prostate MR	Siemens Healthineers	Yes	Yes	Yes	Yes
Quantib Prostate	Quantib	Yes	Yes	Yes	Yes
OnQ Prostate	Coretechs.ai	Yes	No	Yes	No
PROView	GE Healthcare	Yes	Yes	Yes	Yes
Qp-Prostate	Quibim	Yes	No	Yes	No
JPC-Q1 K	JLK	No	Yes	No	Yes

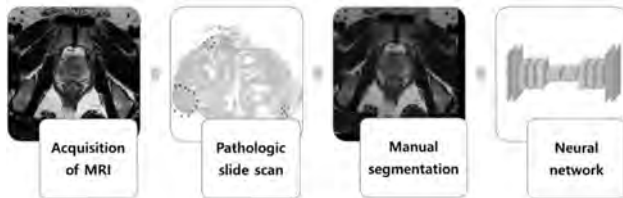
Turkbey B AJR 2022

Limitations

- Require large-scaled, diverse and well-annotated training and independent testing data set. (< 1000 Cases)
- Construction of a large, multicenter and resultantly diverse data sets: **Regulations** from the government or institution.
- Alternate solutions for developing robust AI model without data sharing but with model sharing, such as **federated learning**, enabling greater generalizability in clinical use without actual data sharing.
- Currently reported performance metrics are mostly based on cross-validation **and do not include an actual radiologist vs AI interaction**, and these far from representative of a real-world setting.

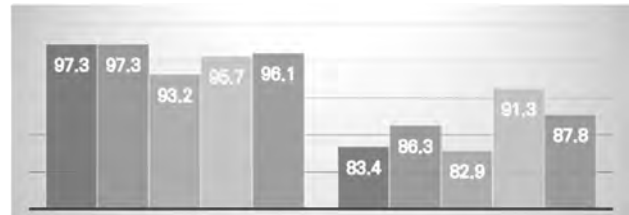
Turkbey B BJR 2022

Development of AI detection system



OVERALL Workflow

	FCN model	UNET model
AUROC	0.890	0.928
Accuracy	0.850	0.849
Sensitivity	0.688	0.824
Specificity	0.912	0.851

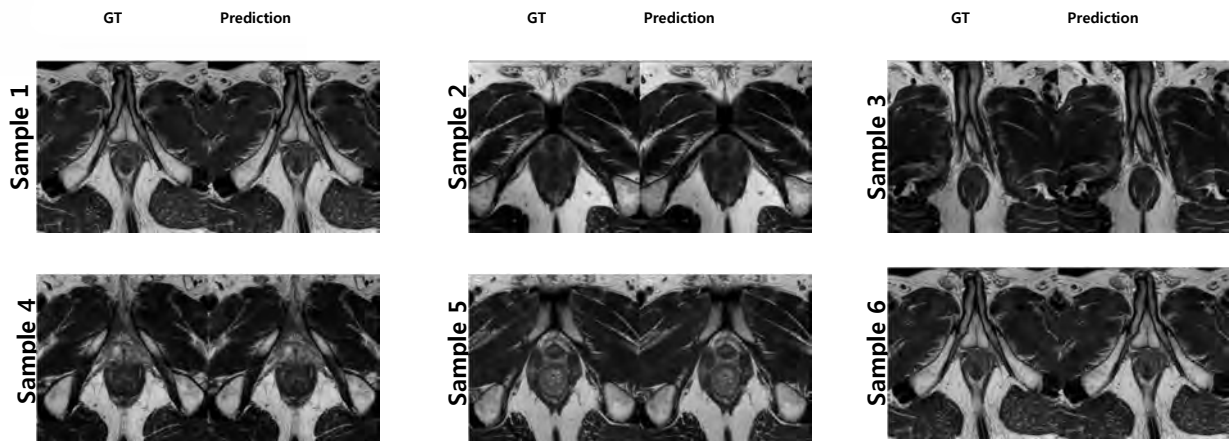


Accuracies and DSCs compared to human expert external validation in four centers

KFDA (Korean FDA) approval

식약처 인준 획득일	2020. 12. 23	등급	2
품목명	의료영상분석소프트웨어	제품명	PROMISE-I
제품 사용 목적	자기공명영상장치(MRI)로 촬영된 전립선 MR 영상을 자동으로 분석하여 저신호강도(low signal intensity)의 영역을 표시하여 의료진의 전립선암 진단에 도움을 주는 소프트웨어 의료기기		

Qualitative Analysis



MR-US fusion biopsy of the prostate assisted by deep learning based automatic segmentation

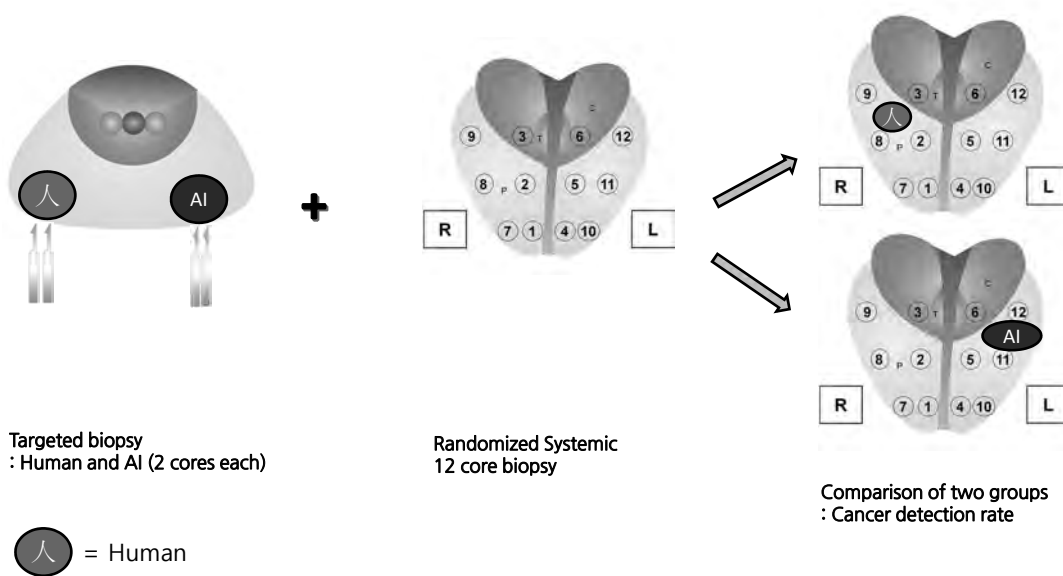
- Prospective, explorative study performed in a single institution
- Korean National Clinical Trial Registry (CRIS No. KCT0006421)
- From Oct 2021 to Feb 2022
- A total of 100 patients who requested for the fusion biopsy of the prostate

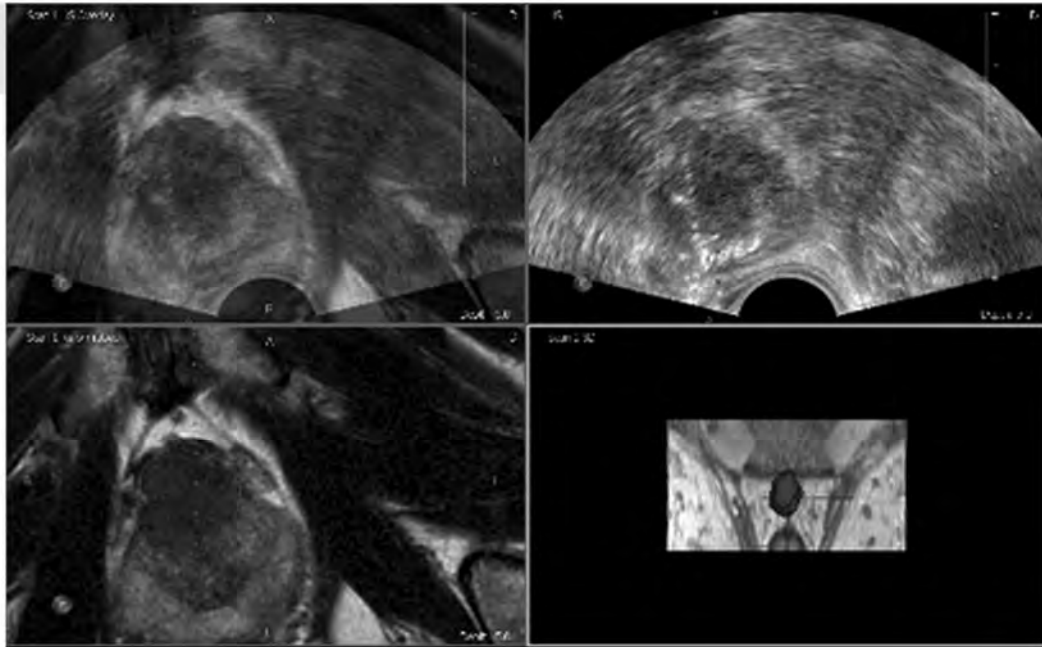
Exclusion Criteria

- (1) Patients who are contraindicated for the biopsy of the prostate
- (2) Patients who did not undergo prostate MRI before the biopsy
- (3) Patients whose fusion images are not technically produced
- (4) Patients who did not undertake prophylactic antibiotics
- (5) Patients who did not undertake prebiopsy enema

Hwang SI RSNA 2022

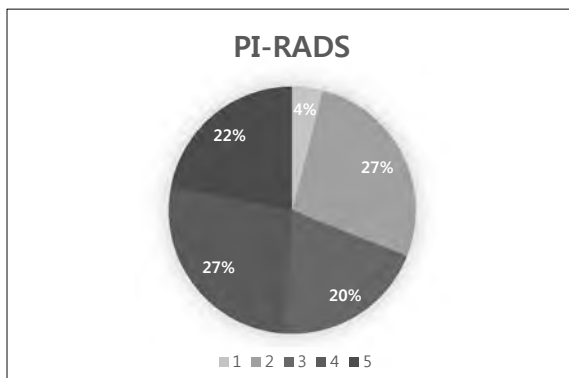
Bx Scheme: 2 core target per lesion +12 core random





Results: Patients and PI-RADS

- Age 66.9 ± 8.8 years old (Range: 36-85)
- PSA 10.2 ± 23.5 mg/dL (Range: 0.6-214)



Number of patients with index lesion (N=100)

No index lesion: 4	→ 12 core Bx
One index lesion: 82	→ 14 core Bx
Only Human index: 3	
Only AI index: 27	
Both: 52	
Two index lesions: 14	→ 16 core Bx

Results: CSC for TB

- CSC for targeted biopsy: 33/96



csCDR (55.6%)
29/52



csCDR (33.3%)
1/3 (PIRADS 4)



csCDR (0%)
0/27



csCDR (21.4%)
3/14
AI only: 1 (PIRADS 4)
Both: 2

Results

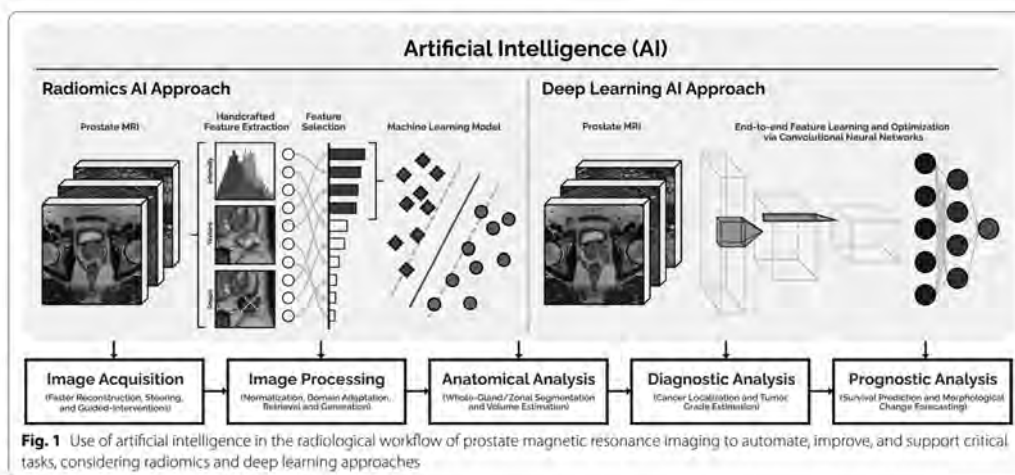
- csCDR from human index lesion was 46.3% (32/69) and csCDR from AI index was 34.4% (32/93) ($p < 0.05$).
- In a subgroup analysis of excluding PI-RADS score 2 lesions (N=27) from AI index lesions, csCDR rose to 48.9% (32/66).
- False positive detection from AI was the main problem, necessitating expert PI-RADS scoring after automatic segmentation.

PI-RADS Classification

- Very few studies
- ResNet-based CNN
- AUC 0.73 for PI-RADS 4 over lesion
- Kappa 0.4 (AI) vs 0.34 (radiologist) to independent radiologist

Zhong T Abd Radiol 2019
Sanford T JMRI 2020

Radiomics

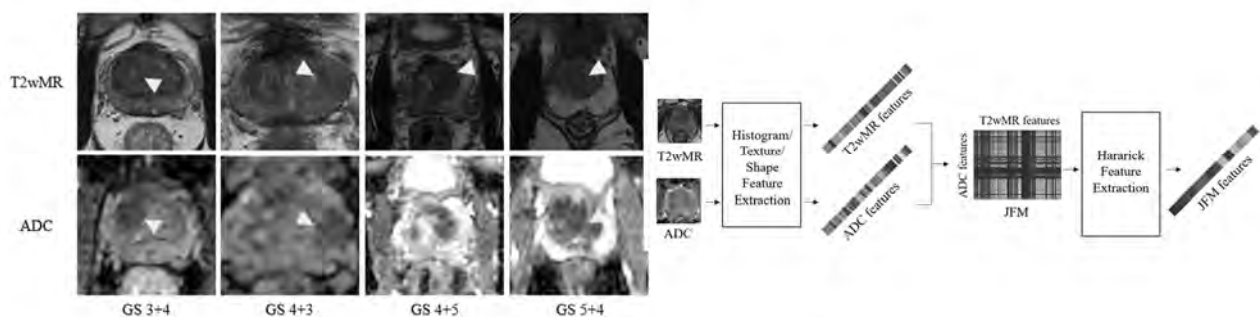


Sunoqrot Eur Radiol Exp 2022

Radiomics for the prostate

- Predicting Gleason Score
- DDx with CS cancer and nCS cancer
- Risk Straification
 - Assess the likelihood of cancer progression:
Low/Intermediate/High-risk prostate cancer
 - Combination of clinical/PET data
 - Prediction of low vs high, BCR

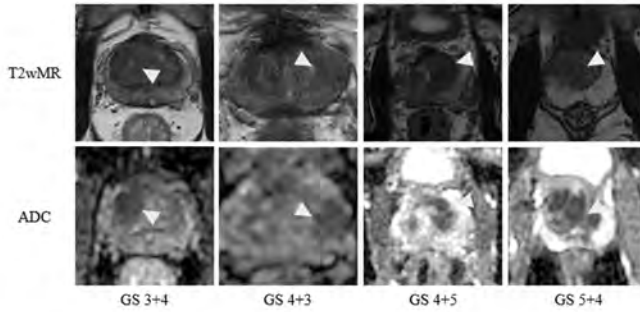
Prediction of Prostate Cancer Aggressiveness by Considering Feature-Level Correlation in Multi-parametric MRI



The JFM is defined as the co-occurrence matrix of the T2wMR and ADC features, where each row represents a uni-modal feature in ADC, and each column represents a uni-modal feature in T2wMR/

Jung J 2020 SPIE proceedings
2023 JDI submitted

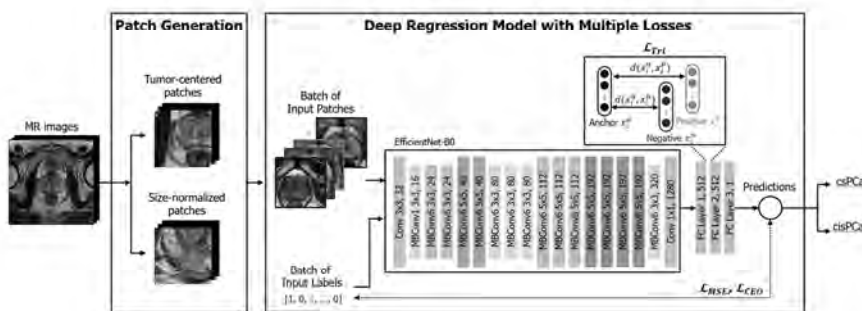
Prediction of Prostate Cancer Aggressiveness by Considering Feature-Level Correlation in Multi-parametric MRI



Feature Type	Accuracy	Sensitivity	Specificity	PPV	NPV	AUC
T2wMR	67.22	52.52	78.10	69.01	64.75	0.68
ADC	66.12	46.23	80.95	67.14	64.52	0.67
Concatenated	68.30	48.13	83.33	68.52	68.77	0.67
Averaged	64.22	46.88	77.14	66.37	60.00	0.66
Multiplied	67.50	51.31	79.52	68.95	64.81	0.67
JFM	68.32	49.42	82.38	68.77	68.32	0.69
Concatenated JFM	69.13	50.02	83.33	69.32	69.53	0.71

Jung J 2020 SPIE proceedings
2023 JDI submitted

Deep Regression Model with Ordinal and Triplet Loss for the Prediction of Prostate Cancer Aggressiveness in Multi-parametric MR Images



Methods	Input Patches	Accuracy(%)	AUC
Model with MSE Loss (Baseline)	Tumor-centered T2w	75.00	0.74
	Tumor-centered ADC	61.54	0.60
	Size-normalized T2w	67.31	0.67
	Size-normalized ADC	71.13	0.70
Model with MSE+CEO Losses	Tumor-centered T2w	75.00	0.73
	Tumor-centered ADC	65.38	0.61
	Size-normalized T2w	71.13	0.70
	Size-normalized ADC	75.00	0.75
Model with MSE+CEO + Triplet Losses (Ours)	Tumor-centered T2w	73.08	0.75
	Tumor-centered ADC	57.69	0.51
	Size-normalized T2w	71.13	0.71
	Size-normalized ADC	78.85	0.77
	Tumor-centered T2w + Size-normalized ADC	78.85	0.79

Kim Y 2023 SPIE proceedings

Open Datasets

Sunoqrot Eur Radiol Exp 2022

1	PROSTATE-MRI	TNO	MRI (tripolar T2W, DWI, pre-contrast T1W, DCE)	MRI cases (n = 26), pathology images (n = 26)	7	Prostate-MRI-US-Biopsy	UCCUC	MRI (axial T2W), ultrasound	MRI cases (n = 842), ultrasound cases (n = 1,151), glanc and lesions segmentations (n = 1,150)	10	SPIE - AAPM-NCI PROSTATEx Challenges	RUMC	MRI (tripolar T2W, DWI, DCE, ADC, PDW)	MRI cases (n = 346), Kinans images (n = 345), thumb-nails images (n = 345)
2	Prostate-Fused-MRI-Pathology	WRHRC, HUP	MRI (tripolar T2W, DWI, pre-contrast T1W, DCE)	MRI cases (n = 28), pathology images (n = 16)										
3	Prostate-IT	RUMC	MRI (axial T2W)	MRI cases (n = 64), SV and NVB segmentations (n = 15)						11	NCI-ISBI 2013 ASP5 Challenge	BMC, RUMC	MRI (axial T2W)	MRI cases (n = 80), zones segmentations
4	ICCB	Not reported	MRI (axial T2W, DWI, DCE, ADC)	MRI cases (n = 12)						12	PROMISE12 Challenge	HUP, BIDMC, UCL, RUMC		
5	TCGA-PRAD	UPMC, WHS, LHM	MRI (axial T2W, DWI, pre-contrast T1W, DCE, ADC, CT, PET)	MRI cases (n = 10), CT images (n = 4), PET images (n = 4), pathology images (n = 14), genomics data (n = 14)	8	QIN PROSTATE	BWH	MRI (axial T2W, DWI, pre-contrast T1W, DCE, ADC)	MRI cases (n = 22)	13	Medical Segmentation Decathlon	RUMC		
6	PROSTATE-DIAGNOSIS	BMC	MRI (axial and coronal T2W, DWI, pre-contrast T1W, DCE)	MRI cases (n = 92), SV and NVB segmentations (n = 15), zones and lesions segmentations	9	QIN-PROSTATE-Repeatibility	BWH	MRI (axial T2W, DWI, DCE, ADC)	MRI cases (n = 15) zones and lesions segmentations (n = 15)	14	QUBIO21 Challenge	Not reported		
										15	NCIGT-PROSTATE	BMWH		
										16			PI-CAI Challenge	RUMC, UMCg, ZGT
										17			ProstateIS8	CUB
													MRI (axial T2W, DWI, ADC)	MRI cases (n = 1,500), lesions segmentations (n = 1,295)



Invitation to Participate in the PI-CAI 22: Reader Study

From:
Jasper Twilt, Arinda Sahu, Joran S. Bosma,
Matin Hossainzadeh, Ike Slagboom,
Jurgen Fütterer, Maarten de Rooij, Henkjan Huisman
Department of Medical Imaging, Radboudumc

Brief Overview

Prostate cancer (PCa) is one of the most prevalent cancers in men worldwide. One million men receive a diagnosis and 300,000 die from clinically significant PCa (cSPCa) each year worldwide. Multiparametric magnetic resonance imaging (mpMRI) of cSPCa is playing an increasingly important role in the early diagnosis of prostate cancer, and has been recommended by the [European Association of Urology \(EAU\)](#) prior to biopsies. However, current guidelines for reading prostate mpMRI (i.e. [PI-RADS v2.1](#)) follow a semi-quantitative assessment that mandates substantial expertise for proper usage. In the absence of experienced radiologists this can lead to low inter-reader agreement (50%) and sub-optimal interpretation.

Modern **artificial intelligence (AI)** algorithms have paved the way for powerful computer-aided detection and diagnosis (CAD) systems that rival human performance in medical image analysis ([Edwards et al., 2017](#); [Moshirpour et al., 2020](#)). While clinical trials are the gold standard for assessing new medications and interventions in a controlled and comparative manner, the equivalent for AI algorithms is international competitions or **"grand challenges"**, where algorithm developers compete against each other using common training + testing datasets. Present-day public benchmark of cSPCa detection/diagnosis is the [ProstateX Challenge](#) from 2016-2017, which uses a testing set of 140 mpMRI exams to evaluate and compare AI algorithms. However, its small sample size and weak evaluation format (with publicly available as opposed to truly "unseen" testing images), limits the ability to reliably draw out definitive conclusions.

The **Prostate Imaging: Cancer AI Challenge (PI-CAI)** is an upcoming grand challenge with thousands of carefully curated mpMRI exams of biopsy-naïve men with elevated levels of prostate-specific antigen (PSA), and tools to upload, run and validate AI in a secure environment for bias-free performance estimation. The 2022 edition of PI-CAI will focus on developing AI for automatic patient-level cSPCa diagnosis and approximate lesion-level cSPCa localization in bpMRI.

The challenge consists of two parts:

- Evaluate state-of-the-art AI algorithms for automated cSPCa detection in bpMRI on a common benchmark cohort of 1000 unseen, multi-center, multi-vendor testing scans.
- Train the 5 top-ranking AI algorithms on a large multi-center, multi-vendor cohort of around 5000-7500 unseen scans and **benchmark their performance against a consensus of 20+ radiologists on 200 patient studies from the testing cohort** (whose imaging quality, cohort characteristics and ground-truth standard will be established in conjunction with an international board of scientific advisors).

PI-CAI Challenge

- **1,500 (of 12,500) cases** with a much stronger reference standard than that of the PROSTATEX challenge.
- Additionally, PI-CAI reserves a **hidden testing cohort of 1,000 cases**, with histopathology-confirmed positives (Gleason grade > 1) and histopathology (Gleason grade < 2) or follow-up confirmed negatives.
- Data will be **multivendor** (3-T scanners from Phillips and Siemens) and **multicenter** (Radboudumc, Ziekenhuis Groep Twente, University Medical Center Groningen, Norwegian University of Science and Technology).
- **Patient age, PSA density, PSA level and prostate volume** will be provided for all cases.
- **Expert-derived lesion delineations** are provided for approximately 80% of all cases, and **AI-derived lesion delineations** (pseudo-labels) are provided for all cases, using a state-of-the-art cSPCa detection developed at Radboudumc.

Conclusion

- Commercial Softwares
- Potential to standardize detection, clinical efficacy
- Limitations: biases in validation, heterogeneity
- Large scale multicenter study/Real world data
- Prospective validation